Towards Modeling Climate Effects
of Energetic Particle Precipitation

Katharina Meraner

Hamburg 2017

Towards Modeling Climate Effects
of Energetic Particle Precipitation

Dissertation with the aim of achieving a doctoral degree
at the Faculty of Mathematics, Informatics and Natural Sciences
Department of Earth Sciences of Universität Hamburg
submitted by

Katharina Meraner

Hamburg 2017

Katharina Meraner

Max-Planck-Institut für Meteorologie
Bundesstrasse 53
20146 Hamburg

Tag der Disputation: 30.01.2017

Folgende Gutachter empfehlen die Annahme der Dissertation:

Prof. Dr. Stefan Bühler
Dr. Hauke Schmidt

Abstract

Energetic particles enter Earth's atmosphere at the poles. The charged particles are either from solar or magnetospheric origin and alter the chemistry of the middle and upper atmosphere. Most importantly, they enhance the production of nitrogen oxides (NO_x) and hydrogen oxides (HO_x) in the winter mesosphere and lower thermosphere. Both components are powerful ozone destroyers. The impact of HO_x on ozone is limited to the mesosphere, because HO_x has a short chemical lifetime (up to hours). In contrast, NO_x can persist up to several months in the winter polar middle atmosphere and can be transported downward to the stratosphere. Models covering the middle and upper atmosphere underestimate this downward transport. This may lead to an underestimation of potential climate effects from energetic particle precipitation.

This thesis investigates the polar winter transport from the lower thermosphere to the stratosphere. Several observational studies confirmed the downward transport (e.g., Randall et al. 2009; Semeniuk et al. 2005). However, it remains unclear which processes cause the transport from the lower thermosphere to the mesosphere. This thesis quantifies, for the first time, the contribution of advection, eddy diffusion and molecular diffusion for the transport through the mesopause. Advection and molecular diffusion dominate the transport through the mesopause. Eddy diffusion has a negligible impact on the transport. However, if eddy diffusion is enhanced as suggested by observations, it can significantly contribute to the transport. This leaves advection being responsible for the underestimation of the downward transport. Gravity waves are the key driver for the advective downwelling in the polar winter mesosphere. This thesis shows that weakening gravity waves enhances the mesospheric transport bringing it close to satellite observations. The altitude of the mesospheric momentum deposition is identified to be key for the polar downwelling.

In addition to the analysis of the winter polar downward transport, climate effects of energetic particles are studied. Energetic particle precipitation reduces significantly ozone in the mesosphere and stratosphere. An ozone loss potentially influences the atmospheric temperature and the strength of the polar vortex. It has been shown that large variations in the polar vortex strength can propagate from the stratosphere down to the surface and force the surface temperature (Baldwin and Dunkerton 2001). This thesis presents the climate impact of a mesospheric and of a stratospheric ozone loss. No statistically significant changes in atmospheric winds are found neither for a mesospheric ozone loss nor for a stratospheric ozone loss. Hence, the influence of energetic particles is too weak to force significantly changes in the surface temperature.

In summary, this thesis advances the understanding of energetic particle precipitation. Processes relevant for the winter polar downward transport from the lower thermosphere to the stratosphere are identified. Two novel findings are the importance of advection in the thermosphere and the impact of weaker gravity waves on the dynamics of the middle and upper atmosphere. Based on this thesis, large climate effects of energetic particles seem unlikely.

Zusammenfassung

Die vorliegende Dissertation untersucht in den ersten beiden Kapiteln den Transport von Stickstoffoxiden, die durch energetische Partikel gebildet werden. Im dritten Teil wird auf ihre Auswirkungen auf das Klima eingegangen.

Energetische Partikel, welche entweder von der Sonne oder von der Magnetosphäre der Erde kommen und über den Polen in die Erdatmosphäre eindringen, verändern die Chemie der mittleren und oberen Atmosphäre. Eine bekannte Folge davon sind die Polarlichter. Außerdem steigern sie die Produktion von Stickstoffoxiden (NO_x) und Wasserstoffoxiden (HO_x) in der polaren Wintermesosphäre und -thermosphäre. Beide Gasverbindungen sind wirksame Faktoren für den Ozonabbau. Der Einfluss von HO_x auf Ozon ist auf die Mesosphäre beschränkt, da seine Lebensdauer nur wenige Stunden beträgt, NO_x hingegen kann sich auch mehrere Monate halten. Während der Polarnacht kann NO_x daher von der unteren Thermosphäre in die Stratosphäre transportiert werden. Dieser Transport ist jedoch in den globalen Zirkulationsmodellen zu schwach.

In dieser Dissertation wird der Transport von Stickstoffoxiden, ausgelöst von energetischen Partikeln, von der polaren, unteren Thermosphäre in die polare Stratosphäre untersucht, der schon in mehreren früheren Beobachtungen festgestellt wurde (Randall u. a. 2009; Semeniuk u. a. 2005). Bisher noch nicht gelöst waren jene Prozesse, die den Transport von der unteren Thermosphäre in die Mesosphäre bewirken. In dieser Dissertation konnte quantifiziert werden, welchen Beitrag Advektion, molekulare Diffusion und turbulente Diffusion zum Transport beitragen. Advektion und molekulare Diffusion dominieren den Transport durch die Mesopause. Der Einfluss der turbulenten Diffusion ist meist vernachlässigbar. Wenn jedoch die turbulente Diffusion, wie von Beobachtungen angedeutet, stärker ist, dann kann diese den Transport durch die Mesopause erheblich beeinflussen.

In dieser Dissertation wird gezeigt, dass die Defizite bezüglich des Abwärtstransportes in den Modellen vor allem auf einen zu geringen advektiven Transport zurückzuführen sind. Der advektive Transport in der Mesosphäre wird von Schwerewellen gesteuert, geringere Schwerewellen verstärken den Transport, so dass dieser mit den Beobachtungen stärker übereinstimmt. Die Ergebnisse belegen außerdem, dass es für den polaren Abwärtstransport entscheidend ist, in welcher Höhe in der Mesosphäre die Impulsdeposition erfolgt.

Im dritten Teil wurden die Auswirkungen der energetischen Partikel auf das Klima untersucht. Diese können signifikant zum Ozonabbau in der Mesosphäre und in der

Stratosphäre beitragen. Ein Ozonabbau wiederum verändert die stratosphärische Temperatur und die Stärke des Polarwirbels. Verschiedene Studien zeigten, dass große Veränderungen in der Stärke des Polarwirbels sich bis in die Troposphäre auswirken und dort die Oberflächentemperatur beeinflussen (Baldwin und Dunkerton 2001). Bei der Untersuchung des mesosphärischen und des stratosphärischen Ozonverlusts wurden keine statistisch signifikanten Veränderungen bezüglich der Stärke des Polarwirbels gefunden, weder für einen mesosphärischen noch für einen stratosphärischen Ozonverlust. Daher lässt sich folgern, dass der Einfluss der energetischen Partikel zu schwach ist, um die Oberflächentemperatur entscheidend zu beeinflussen.

Zusammenfassend kann man festhalten, dass die vorliegende Dissertation neue Erkenntnisse über die Bedeutung von energetischen Partikeln vorlegt, indem sie relevante Prozesse für den polaren Abwärtstransport von der unteren Thermosphäre in die Stratosphäre beschreibt. Dabei sind vor allem die Bedeutung der Advektion für den Transport in der unteren Thermosphäre und der Einfluss von geringeren Schwerewellen auf die Dynamik der mittleren und oberen Atmosphäre herausgearbeitet worden. Die Ergebnisse dieser Dissertation lassen erhebliche Auswirkungen von energetischen Partikeln auf das Klima als unwahrscheinlich erscheinen.

Contents

Introduction

<div style="text-align: right">1</div>

The Sun is the main source of energy for Earth's climate. The Sun warms our planet by heating the ground, oceans and atmosphere. In this sense, it is fundamental to all life on this planet. However, observations show that the Sun is a variable star. The term 'solar variability' describes different processes and denotes variations in total and spectral solar irradiance as well as variations in the strength of galactic cosmic rays and energetic particles.

Already in the beginning of the 19th century, Herschel (1801) speculated that the Sun's variability may cause Earth's climate to vary. Figure 1.1 gives an overview of processes that transfer solar variations to the Earth's surface, where they can affect our climate. The total solar irradiance (TSI) follows an 11-year solar cycle from sunspot minimum to sunspot maximum with a range of $1\,\mathrm{Wm^{-2}}$ (Gray et al. 2010). This causes a $0.17\,\mathrm{Wm^{-2}}$ (0.07 %) variation of the total solar irradiance available at the Earth ($239\,\mathrm{Wm^{-2}}$). Although the solar irradiance only varies slightly in total, it varies strongly within the solar spectrum. Variations up to 6 % occur at ultra-violet (UV) wavelengths altering the stratospheric temperature. This effect is modulated by a mechanism involving ozone production (Haigh 1994).

The other two processes that are modulated by the solar variability involve galactic cosmic rays (GCR) and energetic particles. The idea that GCRs may influence the climate was first introduced by Ney (1959). GCRs generate ions throughout the troposphere down to the surface increasing the amount of cloud condensation nuclei. The strength of GCRs is modulated by the solar wind, which is a stream of mainly electrons and protons that are able to escape the Sun's upper atmosphere. GCRs intensify during solar minimum and weaken during solar maximum. Recent studies suggested that the influence of GCRs on the cloudiness and on the atmosphere is weak (e.g., Jackman et al. 2016; Rawal et al. 2013). Finally, when the solar wind interacts with the Earth's magnetosphere, the magnetosphere can experience a loss of charged particles. A part of the lost energetic particles enter the Earth's atmosphere at high latitudes and alter the atmospheric composition through ionization and dissociation. This thesis aims to enhance the understanding of the climate effects of energetic particles.

Depending on their origin of acceleration, commonly, energetic particles are divided into two categories: Solar energetic protons (SEP) and magnetospheric energetic electrons (MEE). SEPs are associated with fast high-energy release phenomena of the Sun such as solar flares or coronal mass ejections. They occur as sporadic events and their energy reaches typically up to several MeV (Gray et al. 2010). Although the composition of SEPs changes for each SEP event, protons predominate (> 90 %). When SEPs
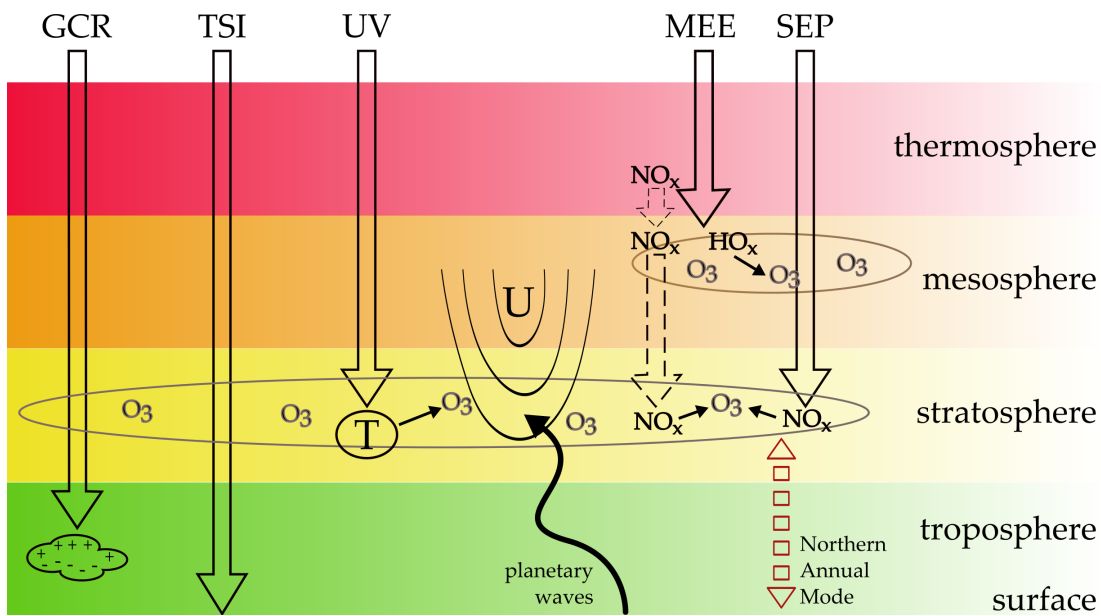
Figure 1.1. Schematic illustration of solar influence on Earth's climate. Shown are the effects of solar irradiance (TSI and UV) as well as the effects of galactic cosmic rays and energetic particles (MEE and SEP). Dashed arrows correspond to downward transport of NO_x inside the winter polar vortex. Modified from Gray et al. (2010).

hit the Earth's magnetosphere, they can penetrate into the middle atmosphere at the polar regions, where the magnetic field lines are open.

MEEs are associated with trapped electrons in the outer Van Allen radiation belt. During geomagnetic storms, the electrons are accelerated and lost to the atmosphere. In contrast to SEPs, which originate from the Sun, MEEs are not necessarily formed in the Earth's magnetosphere. Their name originates from the location of acceleration before they enter the atmosphere. MEEs are formed at different sources including the Sun and the magnetosphere of the Earth. MEEs can be classified according to their energy: low, medium and high energetic electrons. In general, the energy of charged particles is steadily absorbed by ionizing the surrounding matter. The higher the particle's energy, the deeper it penetrates into the atmosphere (Rodger et al. 2007). Low energetic electrons ($> 10\,\mathrm{keV}$) have their largest influence above 90 km, medium energetic electrons (30 to $300\,\mathrm{keV}$) between 70 - $90\,\mathrm{km}$ and high energetic electrons ($300\,\mathrm{keV}$ to several MeV) can even penetrate below $70\,\mathrm{km}$.

Most importantly, MEEs and SEPs alter the polar atmospheric chemistry due to a chain of processes starting with primary interactions of charged particles with matter. In the lower thermosphere and mesosphere, the primary interactions are dissociative ionization and ionization of the most abundant species – N_2, O_2 and O – resulting in N_2^+, O_2^+, N^+, O^+ and NO^+ (Rusch et al. 1981). In the stratosphere, only N_2 and O_2 need to be considered (Porter et al. 1976). Primary ions (N_2^+, O_2^+, N^+, O^+ and NO^+) are

the starting point of fast ion-chemistry reactions leading to the formation of nitrogen oxides (NO_x = N + NO + NO_2) and hydrogen oxides (HO_x = H + OH + HO_2) (Crutzen et al. 1975; Solomon et al. 1982). Ionization and dissociative ionization provide as well secondary electrons, which can interact with matter in a similar way. This causes a cascade of collision reactions, which ends when the kinetic energy of the primary and secondary electrons equals the average kinetic energy of the ambient air. In total, energetic particles enhance the production of NO_x and HO_x in the upper and middle atmosphere.

Acknowledging the fact that both components are powerful ozone destroyers (HO_x above and NO_x below 45 km), already in the 1980s, a possible climate impact of energetic particle precipitation (EPP) was suggested (Solomon et al. 1982). Ozone loss potentially influences stratospheric temperature and the polar vortex. The Northern Annual Mode (NAM) index is often used to describe the strength of the polar vortex, with positive NAM values indicating a strong polar vortex and negative NAM values indicating a weak polar vortex. Observations suggest that anomalous weather regimes associated with the NAM index can propagate from the stratosphere down to the surface (Baldwin and Dunkerton 2001).

The influence of SEPs on the atmosphere has extensively been discussed (e.g., Funke et al. 2011; Jackman et al. 2005; Sinnhuber et al. 2012; Weeks et al. 1972). During a very strong SEP event, high energetic solar protons reduce upper stratospheric ozone by about 30 % (Jackman et al. 2008). However, SEP events only occur sporadically and no long-term ozone changes due to SEPs are found (Jackman et al. 2009). In contrast, MEE events occur very frequently with a maximum occurrence during the declining phase of the solar cycle. During a very strong MEE event, low energetic electrons can reduce mesospheric ozone by more than 50 % (Kieser 2011). Several studies discussed whether medium and high energetic particles can have a significant influence on the middle atmosphere (e.g., Arsenovic et al. 2016; Baker et al. 1993; Callis et al. 2001; Semeniuk et al. 2011). So far, this remains unclear. However, observations suggest that if medium and high energetic particles have an influence below 70 km, it is rather small (Sinnhuber et al. 2012). Accordingly, the largest impact of MEEs on the middle atmosphere arises from low energetic electrons, which enhance the production of NO_x and HO_x in the polar mesosphere and lower thermosphere (MLT).

HO_x has a short chemical lifetime of only several seconds to hours in the mesosphere and is generated in-situ by energetic particles. Hence, the impact of HO_x on the ozone budget is of short duration. Outside the polar night, NO_x is quickly destroyed by photo-dissociation, whereas in the polar night, NO_x can persist up to several months. Hence, inside the winter polar vortex, NO_x can be transported downward from the polar lower thermosphere to the polar stratosphere (Funke et al. 2007;

Semeniuk et al. 2005). This transport can lead to significant accumulation of NO_x in the polar mesosphere and stratosphere causing large ozone losses. However, the impact is constrained to the winter high latitudes, (1) because of the short lifetime of NO_x in sunlit areas and (2) because large-scale polar downwelling can only occur during polar winter (Solomon et al. 1982). Satellite observations suggested an enhancement of the downward transport of NO_x after sudden stratospheric warming (SSW) events. Randall et al. (2009) showed that the NO_x amount descended from the thermosphere to the stratosphere was 50 times higher after the strong SSW in 2009 than during undisturbed conditions. However, general circulation models (GCM) underestimate the mesospheric descent of NO_x compared to observations (B. Funke, HEPPA-II model-measurement intercomparison project: EPP indirect effects during the dynamically perturbed NH winter 2008–2009, submitted to Atmospheric Chemistry and Physics). The effects of the downward transport of NO_x is called the 'indirect EPP effect', whereas the effects of the local production of NO_x and HO_x is called the 'direct EPP effect'. Using satellite data Sinnhuber et al. (2014) showed that the indirect EPP effect leads to higher NO_x concentrations above 40 km than the direct effect of even a very strong SEP event.

This thesis focuses on magnetospheric energetic electrons, which have been shown to have the largest influence on the atmosphere. In the chain of the processes related to MEEs, several questions are unresolved (Sinnhuber et al. 2011, B. Funke, HEPPA-II model-measurement intercomparison project: EPP indirect effects during the dynamically perturbed NH winter 2008–2009, submitted to Atmospheric Chemistry and Physics). The most important can be summarized in **two leading questions**:

(a) Which processes cause the too weak transport of NO_x in general circulation models compared to satellite observations?

(b) What is the climate impact of medium and low energetic electrons?

The thesis follows those two questions: Chapters 2 and 3 discuss the transport of nitrogen oxides from the lower thermosphere to the stratosphere. Chapter 4 determines the climate effects of energetic electrons.

A major part of this thesis studies the downward transport of NO_x, which is underestimated in GCMs covering the upper and middle atmosphere. Resolving the underestimation in mesospheric NO_x concentrations results in more realistic estimates of the ozone losses due to EPP. This topic is split into two chapters: Chapter 2 analyzes the transport through the mesopause and Chapter 3 analyzes the transport from the mesopause to the stratosphere. This division is reasonable because the dynamics of the upper atmosphere differ substantially from the dynamics of the middle atmosphere.

In the thermosphere, the mean free path of any molecule in air is greater than 1 km compared to 10^{-2} μm at the surface. The vertical transport in the thermosphere is

mainly governed by molecular diffusion, which mixes gases due to the large mean free path (Brasseur and Solomon 2005). Further, molecular diffusion separates molecules according to their molecular mass. As a result, lighter species such as H and He are transported upward (i.e., their concentrations increase with height), whereas heavier species such as N_2 and O_2 are transported downward (i.e., their concentrations decrease with height). In addition to molecular diffusion, turbulent mixing caused by gravity wave breaking contributes to the vertical transport below 100 km. This process is usually called eddy diffusion (Smith et al. 2011). The transition from the thermosphere to the mesosphere is unclear. Especially, it remains unclear how much each transport process contributes to the downward transport from the thermosphere to the mesosphere. **Chapter 2** separates the contributions of advection, eddy and molecular diffusion on the total transport by switching off processes for a passive tracer. Simulations with the atmospheric general circulation and chemistry model HAMMONIA (Hamburg Model of Neutral and Ionized Atmosphere; Schmidt et al. (2006)) are used.

The results obtained in Chapter 2 help us to understand which processes induce the underestimated NO_x concentrations in the mesosphere (B. Funke, HEPPA-II model-measurement intercomparison project: EPP indirect effects during the dynamically perturbed NH winter 2008–2009, submitted to Atmospheric Chemistry and Physics). In contrast to the thermosphere, the transport in the mesosphere is dominated by a large-scale meridional circulation which is largely produced by gravity waves. In the summer hemisphere, an eastward gravity wave drag acts on the zonal wind pulling the air equatorward. In the winter hemisphere, a westward gravity wave drag pulls the air poleward. By continuity, the flow is directed upward over the summer pole and downward over the winter pole (Brasseur and Solomon 2005). Siskind et al. (2015) suggested that a weak mesospheric descent is caused by an underestimation of gravity wave drag. **Chapter 3** discusses the impact of parameterized gravity waves on the transport of NO_x. Using simulations with HAMMONIA, differences in a homogeneous background gravity wave source and a source related to frontal activity are analyzed.

Considering the results from the Chapters 2 and 3, more realistic NO_x accumulations in the stratosphere and mesosphere due to energetic particles can be simulated. The increase in NO_x concentrations may lead to ozone destruction in the middle atmosphere potentially affecting our climate. Chapter 4 quantifies those climate effects. Several studies have analyzed the climate effects from low energetic particles (e.g, Baumgaertner et al. 2011; Rozanov et al. 2005; Seppälä et al. 2009). However, all of those studies used complex forcings and simulated only a few years. Instead of prescribing ozone loss, the EPP effects are considered by changing the production of NO_x and HO_x. This complicates the understanding of the atmospheric response due to energetic particles

as transport processes are involved and ozone depletion occurs at different altitudes and times. All studies reported a stratospheric cooling, although the radiative forcing of ozone suggests a warming. I concentrate on the indirect EPP effect and apply an idealized ozone forcing. Recently, Andersson et al. (2014) suggested a potential climate influence of a mesospheric ozone loss due to medium energetic electrons. They reported that HO_x causes long-term variability in mesospheric ozone up to -34 % between EPP maximum and EPP minimum in satellite observations. **Chapter 4** analyzes the climate impact of an idealized mesospheric and an idealized stratospheric ozone loss due to EPP using 150 years of simulations with the Max Planck Institute Earth System Model (MPI-ESM; Giorgetta et al. (2013)). The focus lies on the atmospheric responses, which are a precondition for a potential influence on the surface climate.

1.1 Outline and structure of the thesis

The Chapters 2, 3 and 4 of this thesis are written in the style of scientific journal contributions. They are motivated separately and have their own conclusions and can be read independently of one another. Nevertheless, Chapters 2 and 3 build upon each other by understanding the relevant processes for the transport of nitrogen oxides from the upper to the middle atmosphere. Chapters 2 and 3 are published in the *Journal of Geophysical Research - Atmospheres*. For consistency, some editorial changes and minor modification have been applied to those chapters. Finally, Chapter 4 is currently being prepared for submission. The thesis is structured in the following way:

Chapter 2 investigates the transport of nitrogen oxides through the winter polar mesopause. Several dynamical conditions ranging from undisturbed to disturbed stratospheric warming conditions are discussed. Based on the results, I identify the processes responsible for the downward transport from the thermosphere to the mesosphere.

Chapter 3 analyzes the transport of nitrogen oxides in the mesosphere and below. Following the results of Chapter 2, the sensitivity of the transport to parameterized gravity wave sources is presented. Both changes in a homogeneous background source and a source related to frontal activity are discussed. This chapter demonstrates how the underestimation of the NO_x transport in earlier modeling studies can be reduced.

Chapter 4 evaluates the climate impact of idealized mesospheric and stratospheric ozone losses due to EPP. This chapter discusses whether medium energetic electrons influence the surface climate.

Chapter 5 closes the thesis with a summary and conclusions of the results presented in the Chapters 2 to 4. It also provides an outlook discussing open questions.

1.2 Research questions

The goal of this thesis is to enhance the understanding of the climate effects of energetic particle precipitation (EPP). Before modeling the climate effects, I tackle open questions of the transport of nitrogen oxides, which leads to more realistic estimates of the ozone loss due to EPP. The two main questions mentioned earlier run like a thread throughout the whole thesis and are specified in more detail in the research questions:

Research questions:

- Which transport mechanisms are responsible for the downward transport of nitrogen oxides induced by energetic particle precipitation from the polar thermosphere to the polar mesosphere?

- How sensitive is the transport of nitrogen oxides to changes of the non-orographic gravity wave sources? How can the underestimation of the NO_x concentrations in the polar mesosphere be reduced?

- What is the climate impact of a mesospheric and a stratospheric ozone loss induced by energetic particles?

Transport of Nitrogen Oxides through the Winter Mesopause in HAMMONIA[1]

2

We analyze the importance of individual transport processes for the winter-polar downward transport of nitrogen oxides (NO_x) from the thermosphere to the mesosphere. The downward transport of NO_x produced by energetic particle precipitation induces chemical alterations in the middle atmosphere and influences ozone chemistry. However, it remains unclear how much each transport process contributes to the downward transport. We use simulations of the atmospheric general circulation and chemistry model HAMMONIA (Hamburg Model of Neutral and Ionized Atmosphere) for the extended winter 2008/2009 with a passive tracer. The model enables us to separate the contributions of advection, eddy and molecular diffusion on the total transport by switching off processes. The results show that molecular diffusion and resolved vertical mixing due to advection effectively transport NO_x to the mesosphere. While the impact of molecular diffusion on the transport rapidly decreases below 0.001 hPa, the impact of advection increases. Around the central date of the sudden stratospheric warming in January 2009, advection is strongly enhanced in the thermosphere and mesosphere and the downward transport through the mesopause region is almost entirely driven by advection. Eddy diffusion has limited impact on the transport in the upper mesosphere and negligible impact on the transport in the thermosphere. If eddy diffusion is enhanced as suggested by observations, it can potentially have a larger impact on transport through the mesopause than was previously assumed.

2.1 Introduction

Energetic particle precipitation (EPP) induces large chemical disturbances, mainly in the polar winter middle and upper atmosphere. Seppälä and Clilverd (2014) showed that the impact from EPP events on the northern-hemispheric stratosphere may be of the same magnitude as the impact from variability in solar UV irradiance.

Already in the 1970s and 1980s, it was discovered that EPP is a major source for nitrogen oxides (NO_x = N + NO + NO_2) and odd hydrogen (HO_x = H + OH + HO_2)

(Crutzen et al. 1975; Rusch et al. 1981; Solomon et al. 1981). Both chemical components catalytically deplete ozone in the middle atmosphere, NO_x mainly below and HO_x above about 45 km. However, HO_x is short-lived in the middle atmosphere and the impact of an EPP event on the HO_x budget is of short duration. In contrast, NO_x can persist up to several months in the polar-night stratosphere. Outside the polar night, NO_x is quickly destroyed by photo-dissociation, while inside the winter polar vortex, NO_x is transported downward from its original location in the polar upper mesosphere and lower thermosphere to the polar stratosphere (Funke et al. 2007; Sinnhuber et al. 2014). There NO_x contributes to ozone destruction. The effect of the downward transport of NO_x is called the indirect EPP effect, while the effect of the local production of NO_x and HO_x in the polar stratosphere and mesosphere is called the direct EPP effect (Randall et al. 2007; Randall et al. 2006).

Several observational studies have given evidence for the indirect EPP effect (e.g., Funke et al. 2005; Semeniuk et al. 2005). The downward transport of NO_x even exceeds the direct EPP impact of the large solar proton event in October and November 2003 on the NO_x budget above 60 km (Sinnhuber et al. 2014). However, it remains unclear which transport processes are responsible for the descent of NO_x from the thermosphere to the mesosphere.

In this study, we analyze the importance of individual transport processes for the winter-polar downward transport of NO_x from the thermosphere to the stratosphere using the extended winter 2008/2009 as an example. We use simulations of the general circulation and chemistry model HAMMONIA (Hamburg Model of Neutral and Ionized Atmosphere). Our results clarify which dynamical conditions favor the intrusion of thermospheric air to the mesosphere and indicate how potential trends in eddy diffusion, as discussed by Emmert et al. (2012) and Hoffmann et al. (2011), may change the transport characteristics.

At the winter polar mesospheric to the stratospheric altitudes, the downward transport is dominated by the residual circulation, which has an ascending branch over the summer pole and a descending branch over the winter pole (Brasseur and Solomon 2005). Hence, at these altitudes it has been shown that NO_x is dominantly transported by advection (Smith et al. 2011). The dominance of advection below the mesopause is highlighted in Figure 2.1 by the mass-stream function, which describes the net-trajectory of air parcels and is calculated using 6-hourly values from the Transformed Eulerian Mean (TEM) circulation. NO_x is frequently produced by EPP in the polar lower thermosphere, but the mass-stream function in Figure 2.1 shows no clear advective downward transport from the thermosphere to the mesosphere. Hence, this downward transport remains an open question, which we will tackle in this study. The only way to transport a tracer across the streamlines is either due to photochemi-
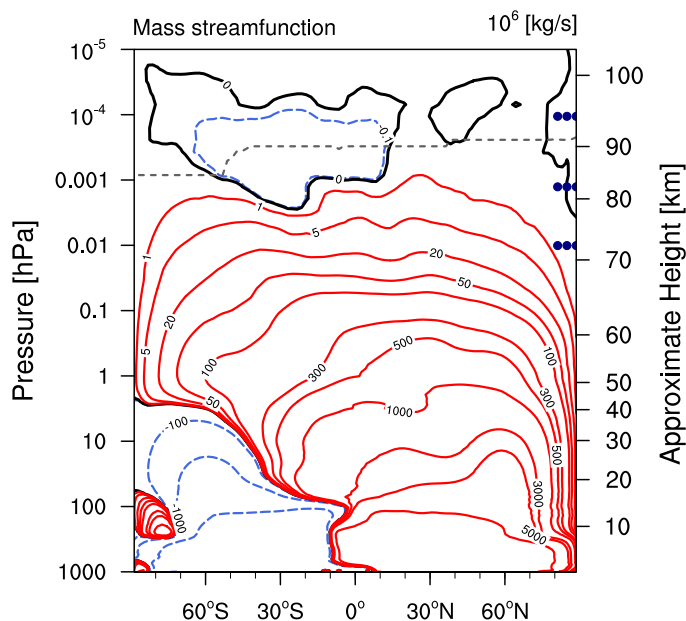
Figure 2.1. Zonal mean residual streamfunction for November and December 2008 calculated by HAMMONIA. Red, positive values correspond to a clockwise circulation and blue, negative values to a counter-clockwise circulation. The gray, dashed line above 0.001 hPa represents the height of the mesopause. The location and height of three emission areas used on the numerical experiments of this study are marked with blue dots.

cal processes or due to eddy or molecular diffusion. We do not consider photochemical processes and concentrate on the transport.

The total transport can be split into three processes: advection, eddy diffusion and molecular diffusion (Brasseur and Solomon 2005). Advection corresponds to the large-scale net-motion of air ("residual circulation") and includes also the resolved mixing. Eddy diffusion is transport by turbulence and implies the unresolved and irreversible vertical mixing. Its main source in the mesosphere and lower thermosphere is the breaking of gravity waves. Molecular diffusion is caused by molecular movement and is especially important above 90 km due to the increased path lengths at low densities. Additionally, gravitational settling redistributes molecules vertically according to their molecular mass and is commonly considered as a component of molecular diffusion.

Smith et al. (2011) analyzed the origin of particles in the polar stratosphere in the Whole Atmosphere Community Climate Model (WACCM) by calculating back trajectories from daily values of the Transformed Eulerian Mean circulation. They stated that in most winters, the stratospheric air at high latitudes originates in the upper mesosphere at lower latitudes, from where it was brought to the pole by the mesospheric circulation. Outside the polar vortex, NO_x is destroyed by sunlight, so the horizontal transport cannot explain the large enhancements in stratospheric NO_x con-

centration observed after times with high geomagnetic activity. Smith et al. (2011) also showed that eddy and molecular diffusion can transport high concentrations of thermospheric NO_x to the middle atmosphere, but the roles of the individual transport processes have not yet been quantified. This study aims, for the first time, to quantify the contribution of individual transport process.

Recent studies showed an enhancement of the descent of NO_x during sudden stratospheric warming (SSW) events (Holt et al. 2013; Randall et al. 2009). The major SSW event in January 2009 was the strongest and most prolonged on record (see Chandran et al. (2014) for more information on SSW and especially on the coupling between strato- and mesosphere). Anomalous wave-2 activity in the upper troposphere caused a reversal of the NH polar vortex westerlies (Manney et al. 2009). The stratopause warmed, displaced to a lower level and finally broke down. Contemporaneously with the warming of the stratosphere, the mesosphere cooled. In early February 2009, the stratopause reformed near 80 km. This reformation of the stratopause at an anomalously high altitude is called an elevated stratopause event (Chandran et al. 2013a). Connected to the SSW, the dynamical conditions changed due to modified gravity wave drag (Limpasuvan et al. 2012). This led to an unusually strong descent of NO_x to the stratosphere. The NO_x amount which descended from the thermosphere to the stratosphere was 50 times higher than during the average in 2005, 2007 and 2008 (Randall et al. 2009).

Over the last few years, several studies suggested that the atmospheric dynamics have been changed. Hoffmann et al. (2011) presented a positive trend in mesospheric gravity wave activity since 1990, which would lead to a positive trend in eddy diffusion. Emmert et al. (2012) showed that an increase in the eddy diffusion coefficient (K_{zz}) of 15% per decade brings the CO_x ($CO + CO_2$) trend of the NCAR global mean model very close to the trend of satellite observations. Hence, both studies suggested a secularly increasing eddy diffusion. Additionally, the magnitude of K_{zz} is not well constrained by observations (Collins et al. 2011; Liu 2009). A comparison of K_{zz} from the model and recent estimations from observations is provided in Section 2.2.1. In Section 2.3.3, we investigate the sensitivity of different transport processes to the value of the eddy diffusion coefficient.

This paper determines the transport processes responsible for the descent of NO_x from the thermosphere to the mesosphere for the extended winter 2008/2009 in HAMMONIA. We analyze four different dynamical cases: a) undisturbed winter conditions during November and December 2008, b) the sudden stratospheric warming event in January 2009, c) undisturbed conditions (November and December 2008) with enhanced eddy diffusion and d) the sudden stratospheric warming event in January 2009 with enhanced eddy diffusion. The model enables us to separate the contributions of

advection, eddy and molecular diffusion on the total transport by switching off the influence of the processes on the tracer. We implement an artificial, passive tracer (i.e., no impact on radiation and dynamics and no interaction with chemistry). Section 2.2 describes the model setup and evaluates the model by comparing the vertical profile of NO to satellite observations. Section 2.3 shows the contributions of advection, eddy and molecular diffusion on the total transport as well as the sensitivity of the transport to a SSW event and enhanced eddy diffusion. Finally, Section 2.4 summarizes and discusses the main outcomes and limitations of this study.

2.2 HAMMONIA: The Hamburg Model of the Neutral and Ionized Atmosphere

HAMMONIA (Schmidt et al. 2006) is a high-top model based on the ECHAM5 atmospheric general circulation model (Roeckner et al. 2006). The model treats atmospheric dynamics, chemistry and radiation interactively from the surface to approximately 250 km altitude. The dynamics and radiation are fully coupled to the chemical Model of Ozone and Related Tracers (MOZART3) (Kinnison et al. 2007).

To consider the effects of EPP, the HAMMONIA version used in this study is expanded to include the ion chemistry of the ionospheric E- and F-regions (Kieser 2011). The ion chemistry consists of 13 ion-neutral reactions and 5 ion-electron recombinations involving O^+, O_2^+, N^+, N_2^+, NO^+ and electrons. Five reactions directly involving precipitating energetic particles are considered. The ionization of O, O_2 and N_2 is calculated by using the particle-induced ion pair production rates provided by the Atmospheric Ionization Module Osnabrück (AIMOS - version 1.6) (Wissing and Kallenrode 2009). The explicit consideration of energetic particles is limited to the thermosphere, whereas in the middle atmosphere the production of atomic N and HO_x is parameterized following Jackman et al. (2005). The reaction rate coefficient of the 107 tri- and bi-molecular gas phase reactions used by Schmidt et al. (2006) are updated according to Sander et al. (2006).

Eddy and molecular diffusion are of central importance for the transport in the upper mesosphere and lower thermosphere. The parameterization of eddy diffusion describes the vertical mixing of air parcels not resolved by the model. In HAMONNIA, eddy diffusion near the mesopause region is almost exclusively caused by breaking of gravity waves, which is parameterized according to Hines (1997a) and Hines (1997b). Eddy diffusion is given by:

$$\frac{\partial X_i}{\partial t} = \frac{1}{\rho}\frac{\partial}{\partial z}\left(\rho K_{zz}\frac{\partial X_i}{\partial z}\right),$$ (2.1)
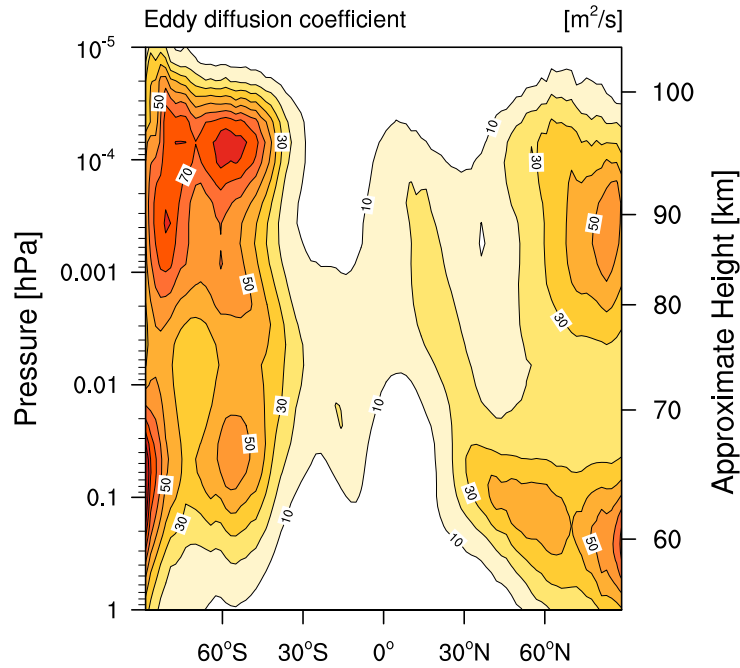
Figure 2.2. Zonal mean eddy diffusion coefficient from HAMMONIA for November and December 2008. Contour interval is $10\,\mathrm{m^2/s}$.

where ρ is the density (g/m^3), t and z describe the time and vertical dimensions (s and m), X_i is the mass mixing ratio of the constituent i (kg/kg) and K_{zz} is the respective eddy diffusion coefficient (m^2/s). $\mathrm{K_{zz}}$ is a product of the gravity wave parameterization depending on the total root-mean-square of the horizontal wind fluctuation, the rate of energy deposition and the buoyancy frequency. At altitudes where molecular diffusion is strong, eddy diffusion is limited as suggested by Akmaev et al. (1997).

The magnitude of eddy diffusion in the mesopause region is not well constrained by observations. However, several studies indicate that models may underestimate it. Figure 2.2 shows the zonal mean of $\mathrm{K_{zz}}$ from the default version of HAMMONIA for November and December 2008. The winter pole maximum ($53\,\mathrm{m^2/s}$) at $0.003\,\mathrm{hPa}$ corresponds to gravity wave breaking. Above $10^{-4}\,\mathrm{hPa}$ the eddy diffusion coefficient rapidly decreases to less than $1\,\mathrm{m^2/s}$. Smith (2012) showed a similar figure for WACCM but revealed much smaller values (about $25\,\mathrm{m^2/s}$ at $0.001\,\mathrm{hPa}$ at the winter pole). Grygalashvyly et al. (2011) calculated the diffusivity with a gravity wave-resolving model and estimated magnitudes for $\mathrm{K_{zz}}$ of several $100\,\mathrm{m^2/s}$. Liu (2009) measured the annual mean eddy diffusion coefficient by a lidar for the winters in 1998 - 2000 between 10 and $500\,^2/\mathrm{s}$. Collins et al. (2011) derived from lidar measurements a lower boundary of $\mathrm{K_{zz}}$ of $430\,\mathrm{m^2/s}$. The values from HAMMONIA are much smaller than any of those estimations. The large differences between different models and

observations are still unresolved.

Molecular diffusion is parameterized following the governing equation (Huang et al. 1998):

$$\frac{\partial X_i}{\partial t} = \frac{1}{\rho} \frac{\partial}{\partial z} \left(\rho D_i \frac{\partial X_i}{\partial z} \right) - \frac{1}{\rho} \frac{\partial}{\partial z} \left(\rho w_{D_i} X_i \right). \tag{2.2}$$

D_i is the respective molecular diffusion coefficient (m^2/s) and w_{D_i} is the vertical drift velocity, which separates the constituents of different molecular mass. D_i and w_{D_i} for NO$_x$ are taken from Banks and Kockarts (1973):

$$\rho D_i = 4.17 \times 10^{-6} \left(\frac{T}{273.15K} \right)^{0.5} \left(m_A + \frac{m_A^2}{m_i} \right)^{0.5}, \tag{2.3}$$

$$\rho w_{D_i} = \frac{\rho D_i g}{R^* T} \left(m_A - m_i \right). \tag{2.4}$$

T is the temperature (K), g the gravity acceleration (m/s^2), m_A is the molar mass of air (g/mol), m_i is the molar mass of the constituent i (g/mol) and R^* is the gas constant and is 8.31436 J/(mol K). As we analyze the transport of NO$_x$, we use its molecular mass. This implies that the difference between m_A and m_i in Equation 2.3 and 2.4 is small. From this follows that the influence of the vertical drift is negligible compared to molecular diffusion in Equation 2.2. Advection of tracers is performed using the flux form semi-Lagrangian scheme of Lin and Rood (1996).

As in the work by Schmidt et al. (2010), HAMMONIA is run with 119 vertical levels, but with a triangular truncation at wave number 63 (T63) instead of at wave number 31 (T31). This corresponds to a horizontal resolution of 1.9° in longitude and latitude. The vertical resolution is about 800 m in the upper troposphere and stratosphere and about 3 km in the mesopause region.

We carried out four sets of simulations: an ensemble of four simulations for undisturbed conditions running from October 2008 to May 2009 with slightly different initial conditions, a single run for SSW conditions running for January and February 2009, a single run for undisturbed conditions with enhanced eddy diffusion running from October 2008 to January 2009 and a single run for SSW conditions with enhanced eddy diffusion. For undisturbed conditions, the passive tracer is instantaneously emitted on the first time step of each month (e.g., 1 October 2008 - 00:00 am) and for SSW conditions, on the 20 January 2009 at 00:00 am. The passive tracer is emitted between 80° - 90° N at three different vertical levels: 10^{-2} hPa, 10^{-3} hPa and 10^{-4} hPa (as shown by the blue dots in Figure 2.1). The mesopause lays for all simulations near 0.0002 hPa.

Further simulations are created with unchanged dynamics, individual transport processes are switched off (i.e., the influence of the processes on the tracer is switched off). In all of those integrations, the surface pressure, the temperature, the divergence and

the vorticity are nudged (i.e., relaxed) from 850 hPa to 1 hPa with an upper and lower transition zone. The nudging data are 6-hourly values of the European Centre for Medium-Range Weather Forecasts (ECMWF) Interim Re-Analysis (ERA-interim) (Dee et al. 2011). The nudging assures that the model captures the tropospheric and stratospheric dynamics as observed during the extended winter 2008, including the major SSW event in January 2009. As the indirect effect of EPP – and hence the downward transport of NO_x – is most important at the winter polar cap, we concentrate our analysis on the high latitudes and show in all following figures polar cap averages (60° N - 90° N).

2.2.1 Evaluation of the Transport in the Model

Simulations of stratospheric and mesospheric chemistry and dynamics of HAMMONIA at resolution T31 have been compared to observations (e.g., Dikty et al. 2010; Schmidt et al. 2010) and to other models (Pedatella et al. 2014). The model performs well in simulating the climatological mean values of temperature, winds and most chemical species in the stratosphere and mesosphere. The High Energy Particle Precipitation in the Atmosphere (HEPPA) model versus Michelson Interferometer for Passive Atmospheric Sounding (MIPAS) (Fischer et al. 2008) data intercomparison study (Funke et al. 2011) provides a detailed evaluation on the ability of several general circulation models (including HAMMONIA) and chemistry-transport models to simulate EPP effects. HAMMONIA revealed too strong horizontal mixing across the polar vortex boundaries due to continuous wave-1 activity. The polar winter descent of CO is well reproduced in HAMMONIA. The strato- and mesospheric ozone response to the 'Halloween storms' in October and November 2003 is well simulated in terms of temporal evolution and latitudinal distribution. However, the mid-term ozone loss (between 16 and 26 November 2003) is too weak in HAMMONIA. Differences between our simulations at T63 horizontal resolution are small with respect to the previously used model version at T31 resolution (not shown).

Realistic transport of NO_x in the middle atmosphere is critical for our analysis. We compare the vertical profiles of NO in the mesosphere and lower thermosphere to MIPAS (see Figure 2.3). Several studies have shown the excellent agreement between MIPAS and other satellite observations - e.g., the Atmospheric Chemistry Experiment Fourier Transform Spectrometer (ACE-FTS) (Bender et al. 2015; Garcia et al. 2014). Hence, a comparison to ACE-FTS yields similar results as the comparison to MIPAS.

We interpolate 2-hourly gridded HAMMONIA data to the actual measurement times and locations of MIPAS. For the error estimates of MIPAS, we followed the approach of Garcia et al. (2014) and assume 10 % systematic error and use one sigma of the standard error, which is calculated from the averaging over the polar cap. The
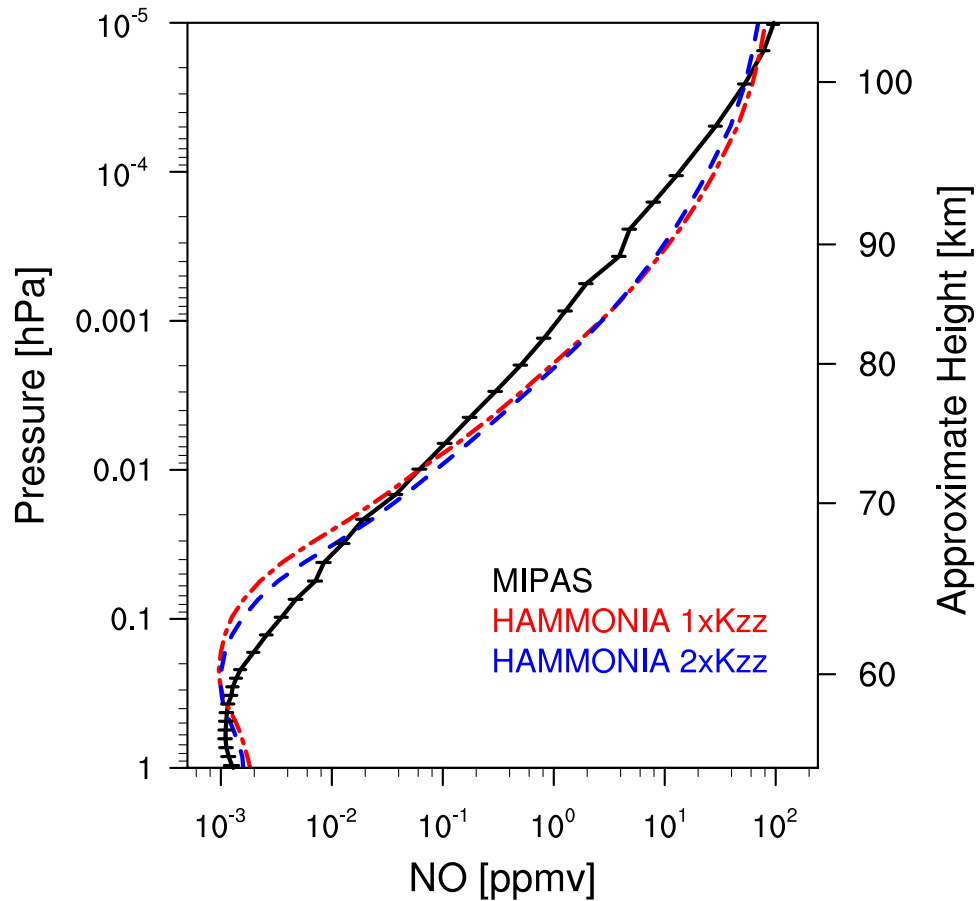
Figure 2.3. Vertical profiles of NO volume mixing ratio for November and December 2008 in HAMMONIA (colored lines) and in MIPAS (black line) averaged over the polar cap (60° - 90° N). Two experiments of HAMMONIA with different eddy diffusion coefficient are shown: $1 \times K_{zz}$ (dot-dashed, red) and $2 \times K_{zz}$ (dashed, blue). The error bars represent the total error (i.e., the sum in quadrature of the systematic error and the standard error of the area averaging).

total error is then the sum in quadrature of the systematic and standard error.

The NO profile simulated with HAMMONIA using the standard eddy diffusion coefficient ($1\times K_{zz}$) is denoted by the red line in Figure 2.3. The increase of NO in the mesosphere is well reproduced by the model, however we find some differences. HAMMONIA shows a local minimum near 0.2 hPa and the rate of increase of NO with increasing height is slightly higher in the model than in the observations. This implies too little NO around 0.2 hPa and too much NO above 0.01 hPa in HAMMONIA.

The underestimation at 0.2 hPa has also been found in other models covering this altitude region and may be related to an overestimation of NO photolysis, which is a major NO loss mechanism in the illuminated mesosphere (Funke et al. 2011). This is also supported by the fact that the underestimation shrinks if we average over 70° - 90° N, where the loss mechanism is weak (not shown). However, we can not exclude the influence of overestimated mixing of polar and mid-latitude air masses. The overestimation above 0.01 hPa may be related to the use of AIMOS, as it does not use the corrected medium energy electrons from the POES MEPED (Polar-orbiting Operational Environmental Satellites Medium Energy Proton/Electron Detector) instrument. This can result in an overestimation of ionization – and hence, NO – in the lower thermosphere and upper mesosphere (Peck et al. 2015; Rodger et al. 2010). There is an overall good agreement between MIPAS and HAMMONIA. Differences are between 10 % and 20 % below 0.1 hPa. The largest discrepancies emerge between 0.001 and 10^{-4} hPa, where the model overestimates the concentration of NO by 100 %.

2.3 Results

In the following, we analyze the transport of NO_x from the thermosphere to the mesosphere by switching on only individual transport processes for the passive tracer. We concentrate on four different dynamical cases: (1) undisturbed conditions (November and December 2008), (2) SSW conditions (January and February 2009), (3) undisturbed conditions with doubled eddy diffusion coefficient (November and December 2008) and (4) SSW conditions with doubled eddy diffusion coefficient (January and February 2009). For each case the same two subfigures are presented, which we introduce here briefly.

Figures 2.4a, 2.4c, 2.4e and 2.4g show the vertical distribution of the passive tracer 30 days after emission. Only individual transport processes are switched on (M = molecular diffusion, E = eddy diffusion, A = advection), while effects of the respective other processes on the tracer distribution are switched off. Figure 2.4a corresponds to undisturbed conditions, 2.4c to the SSW conditions, 2.4e to undisturbed conditions with $2\times K_{zz}$ and 2.4g to SSW conditions with $2\times K_{zz}$. In the model, molecular and eddy
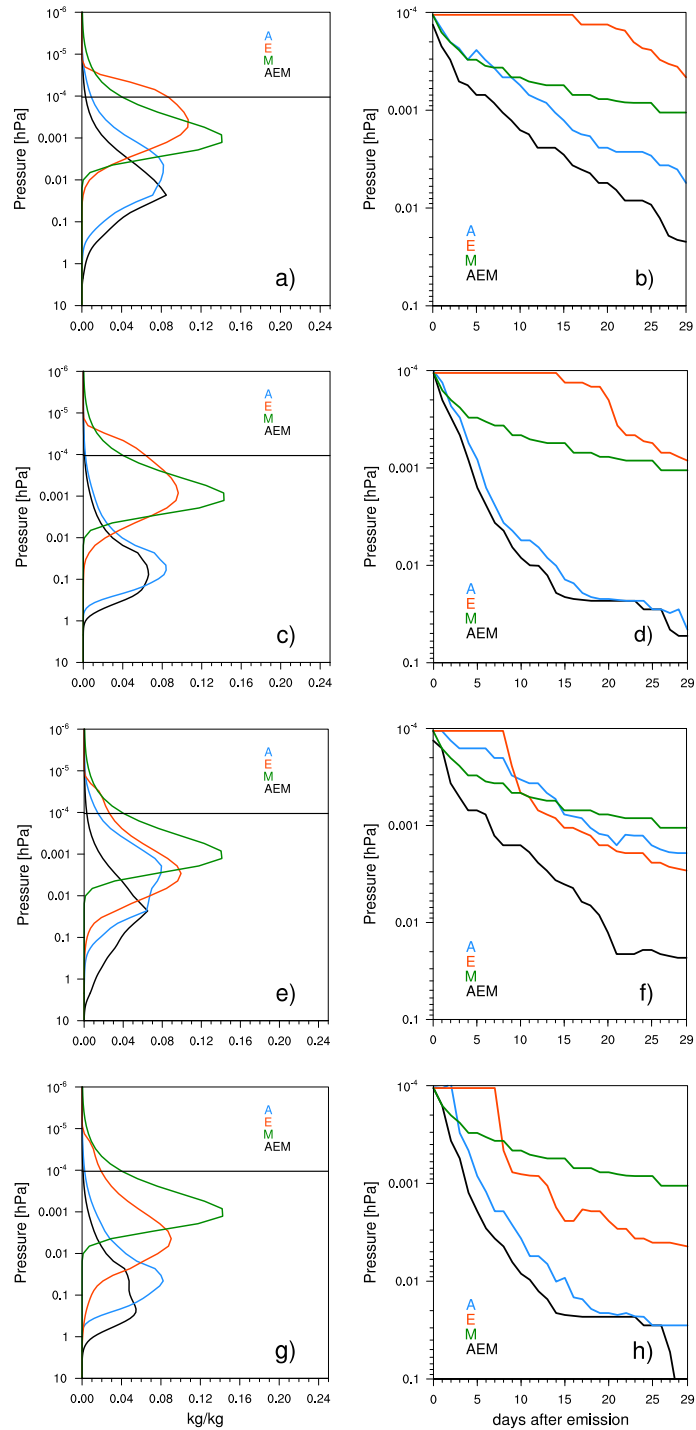
Figure 2.4. Left column: Normalized tracer mass 30 days after emission averaged over 60° - 90° N. The horizontal line is the emission height at 10^{-4} hPa. Right column: Vertical trajectory of the tracer maximum [kg/kg] over 60° - 90° N. Individual transport processes are switched on (A = advection, M = molecular diffusion, E = eddy diffusion, AEM = control simulation with all processes switched on. (a, b) For undisturbed conditions (November and December 2008), (c, d) for SSW conditions (January 2009), (e, f) as for (a, b) but with $2\times K_{zz}$, (g, h) as for (c, d) but with $2\times K_{zz}$. We use the ensemble mean for (a, b) and a single run for all others. The tracer is emitted on the 1st of each month, except for (c, d, g, h) where the tracer is emitted on the 20 January 2009.

19

diffusion only act in the vertical, while advection also transports horizontally. To consider that the processes transport the tracer over different latitudinal bands, the tracer mass $\tilde{\chi}$ is normalized against the total tracer mass between $60°$ - $90°$ N at day 30 after emission (t_{end}):

$$\chi(t,z,\phi) = \frac{\tilde{\chi}(t,z,\phi)}{\int\limits_{z=0}^{Z} \int\limits_{\phi=60°N}^{90°N} \tilde{\chi}(t_{end},z,\phi)}. \tag{2.5}$$

χ is the normalized tracer mass as function of time t, altitude z and latitude ϕ. A value of $1\,\text{kg/kg}$ would correspond to all mass being stored in a single layer after 30 days, hence no transport occurs. Note the normalized tracer mass provides no information on the actual transported tracer mass. Henceforward, we only use the normalized tracer mass but refer to it for simplicity as tracer mass.

Figures 2.4b, 2.4d, 2.4f and 2.4h show the vertical trajectory of the tracer maximum as a function of time and altitude. For each day the height of the maximum in the (normalized) tracer mass is estimated. Again, only individual transport processes are switched on (M = molecular diffusion, E = eddy diffusion, A = advection). Figure 2.4b corresponds to undisturbed conditions, 2.4d to SSW conditions, 2.4f to undisturbed conditions (as 2.4b) but with $2 \times K_{zz}$ and 2.4h to SSW conditions (as 2.4d) but with $2 \times K_{zz}$. As the tracer maximum is calculated with discrete model levels, this can create a step-function artifact (compare to the red line in Figure 2.4b). Additionally, we only show one aspect of the distribution (i.e., the level of the maximum). Hence, the distribution may spread even if the tracer maximum remains at one level.

2.3.1 Undisturbed Winter Conditions

In this section, we analyze the impact of different transport processes for undisturbed conditions. First, we explore the vertical distribution of the passive tracer 30 days after emission (see Figure 2.4a). We use the ensemble mean of four ensemble members and average over November and December 2008. Due to the nudging up to $1\,\text{hPa}$, the differences between the individual ensemble members are negligible. To prove this, we calculate the maximum deviation of the ensemble mean (maximum spread - minimum spread for all emissions levels and processes). The maximum spread is $0.03\,\text{kg/kg}$ at $0.01\,\text{hPa}$, which is smaller than the line thickness in Figure 2.4a. Analyzing November and December 2008 assures relatively undisturbed winter conditions. If the tracer is emitted on the first of each month, the months October 2008 to February 2009 show a similar behavior as November and December 2008. In Section 2.3.2 we analyze the transport during the SSW in January 2009 by emitting the tracer on the 20 January 2009.

If only molecular diffusion is switched on, most of the tracer mass emitted at 0.001
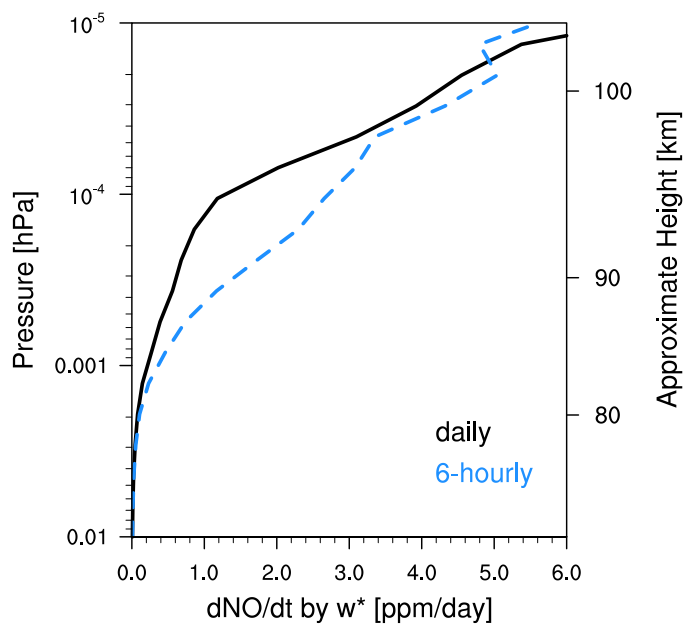
Figure 2.5. Tendency of NO concentration [ppm/day] due to advection by the residual vertical wind averaged over 60° - 90° N calculated from 6-hourly output (blue, dashed line) and from the daily mean as the average over the 6-hourly output (black, solid line). This is diagnostic variable computed by the TEM analysis.

hPa and 0.01 hPa is still located near the emission height after 30 days (not shown). The impact of molecular diffusion on the transport below the mesopause region is negligible. Eddy diffusion behaves similarly when the tracer is emitted at 0.01 hPa but not as extreme as molecular diffusion, i.e., advection is the dominant process at this altitude range. In the upper mesosphere, eddy diffusion is the second most important process, but the impact of advection is considerably larger. Hence, below the mesopause region, advection is the dominating transport process. This is in line with the results of Smith et al. (2011) and agrees well with our expectations, because at this altitude range the mesospheric circulation has a descending branch over the winter pole (see Figure 2.1).

However, for single events with large thermospheric NO_x source, e.g., an EPP event, the transport from the thermosphere to the mesosphere cannot be neglected. In the lower thermosphere, all three processes contribute to the transport (see Figure 2.4a), but the relative importance of the processes varies. While molecular diffusion and advection bring the tracer maximum down below the mesopause, most of the tracer transported by eddy diffusion remains above 0.001 hPa. The strong impact of advection disagrees with our expectations from Figure 2.1.

However, the shown streamfunction is the mean over two months, while on intradiurnal timescale (i.e., within a day) the variability is high. To illustrate this, we cal-

culate the intra-diurnal (from 6-hourly output) and day-to-day (from daily means of the 6-hourly output) standard deviation of the zonal mean residual vertical wind (w^*) averaged between 0.001 and 10^{-4} hPa and between $60°$ - $90°$ N for November and December 2008. The intra-diurnal variability (0.022 m/s) is three-times larger than the day-to-day variability (0.007 m/s). This behavior is also evident in the averages over individual universal times (i.e., the mean over all timesteps at 0, 6, 12 and 18 UT, respectively, in November and December 2008): The 6 UT-mean (-0.0127 m/s) and the 18 UT-mean (-0.0196 m/s) show strong descent, while the 0 UT-mean (0.0073 m/s) and the 12 UT-mean (0.0082 m/s) show ascent. The intra-diurnal variability strongly affects the downward transport of NO. Figure 2.5 shows the change in NO concentration due to the TEM residual vertical wind calculated from (a) the 6-hourly model output and (b) the daily mean as the average over the 6-hourly timesteps. In the lower thermosphere the impact of the residual vertical wind on the NO concentration is doubled when 6-hourly values are used. We speculate that the influence of the large intra-diurnal variability on the transport of NO is caused due to the dynamical transport by atmospheric tides as described in Jones et al. (2014) for lower latitudes. However, sensitivity studies with more idealized models would be needed to confirm this.

This resolved vertical mixing (as well as the mixing by molecular diffusion) balances the gradient of the mass-mixing ratio, which leads to a higher amount of mass below than above the emission level due to the decrease in density with increasing height. As mentioned above all three processes act on the tracer (i.e., transport the tracer maximum downward), but Figure 2.4a is only a snapshot, i.e., it shows the distribution of the tracer only at one time step (day 30 after emission). Hence, the initial impact of individual processes in the lower thermosphere is masked.

For a better understanding of the behavior in the lower thermosphere, we separate the impact of advection, eddy and molecular diffusion for single model levels. Figure 2.4b shows the vertical trajectory of the tracer maximum for different processes. In the highest model levels, transport by advection and by molecular diffusion have the same order of magnitude and the maximum concentration of the tracer is transported by advection and molecular diffusion within 8 days to $3.6 \cdot 10^{-4}$ hPa. The tracer maximum transported by eddy diffusion remains for 17 days at the emission level before it reaches the next lower level. Hence, eddy diffusion has a negligible impact on the transport in the lower thermosphere in this case. At altitudes below $4.6 \cdot 10^{-4}$ hPa, advection dominates the transport. While molecular diffusion is still second most important down to 0.001 hPa, its impact on the transport decreases below and eddy diffusion becomes the second largest process (not shown).

As mentioned above, the increasing influence of advection with decreasing height is not surprising because of the generally downward circulation in the high-latitude

winter mesosphere. The impact of molecular diffusion is very similar for all months and does not depend on dynamical conditions. The major source of eddy diffusion in the middle and upper atmosphere is the breaking of gravity waves in the upper mesosphere. The step-function of the trajectory due to eddy diffusion is associated with the strong gradient of the tracer at the emission level. As mentioned above Figure 2.4b shows only the level of the maximum, which can only have discrete model levels. A sudden height change in the tracer maximum may have been caused by a flat distribution of the tracer. A small vertical redistribution of the tracer mass then may lead to a rapid (vertical) displacement of the tracer maximum. The eddy diffusion coefficient is relatively small at 10^{-4} hPa (see Figure 2.2) and about 6 times smaller than the molecular diffusion coefficient (not shown). Hence, it takes 17 days until eddy diffusion mixes enough tracer from the emission level so that a new maximum develops below. We analyze this behavior more in detail in Section 2.3.3.

2.3.2 Impact of the Sudden Stratospheric Warming Event in January 2009

In the following, we investigate how the SSW in January 2009 influences the transport of NO_x from the thermosphere to the stratosphere. Figure 2.4c shows the vertical distribution of the passive tracer after 30 days. The passive tracer is emitted on the 20 January 2009, shortly before the SSW. We compare Figures 2.4a and 2.4c to determine whether transport processes act differently during a SSW vs. during undisturbed conditions.

Results shown here indicate that the downward transport of the tracer by eddy and molecular diffusion are similar to those during undisturbed winter conditions. While the maximum concentration of the tracer transported by eddy diffusion remains at roughly the same altitude, the distribution slightly broadens. The SSW has little influence on eddy and molecular diffusion. Advection strengthens in the lower thermosphere and upper mesosphere. Irrespective of the emission height, the maximum of the tracer transported by advection reaches 0.1 hPa. Under undisturbed winter conditions, the tracer emitted at 10^{-4} hPa is after 30 days at a much higher altitude (about 0.01 hPa), while the tracer emitted at 0.01 hPa reaches much further down (about 10 hPa - not shown) (see Figures 2.4a and 2.4c). Hence, during SSW conditions the descent rate of the tracer slows down below 0.1 hPa.

The analysis of the tracer maximum in Figure 2.4d confirms the small impact of eddy and molecular diffusion on the transport during the SSW. The tracer maximum transported by eddy diffusion reaches the next lower discrete model level slightly earlier (after 15 days compared to after 17 days during undisturbed winter conditions). Changes in eddy diffusion are due to the strong circulation changes, which affect the propagation conditions of gravity waves (Limpasuvan et al. 2012). However, eddy

Table 2.1. Inter-monthly spread of the endpoints of the trajectories of the tracer maximum [hPa] for undisturbed conditions (October 2008 - February 2009) and endpoints of the trajectories of the tracer maximum [hPa] for SSW conditions (January and February 2009), undisturbed conditions with $2{\times}K_{zz}$ (November and December 2008) and SSW conditions with $2{\times}K_{zz}$ (January and February 2009). Single transport processes are switched on (A = advection, E = eddy diffusion, AEM = control simulation with all processes switched on).

Case	AEM	A	E
undisturbed conditions (min - max)	0.0150 - 0.0254	0.0030 - 0.0222	0.0002 - 0.0012
SSW conditions	0.0530	0.0457	0.0008
undisturbed conditions with $2{\times}K_{zz}$	0.0231	0.0019	0.0029
SSW conditions with $2{\times}K_{zz}$	0.2178	0.0283	0.0044

diffusion is still the weakest process above 0.001 hPa. Advection is much stronger than under undisturbed winter conditions. In 8 days, the tracer maximum reaches 0.0024 hPa compared to $3.6 \cdot 10^{-4}$ hPa under undisturbed conditions. The deceleration in the downward transport below 0.1 hPa is confirmed by Figure 2.4d.

To evaluate the robustness of these results, we compare the inter-monthly spread of the endpoints of the trajectories for undisturbed winter conditions to the endpoints of the trajectories for SSW conditions (see Table 2.1). The inter-monthly spread (minimum and maximum of the endpoints over all months) describes how strongly the endpoints of each trajectory varies between the months in height. The comparison of the inter-monthly spread to the endpoints of each trajectory during SSW conditions shows how different the results for SSW conditions are from the results for undisturbed conditions. The inter-monthly spread is calculated for the control tracer (AEM - all processes switched on), the tracer transported by eddy diffusion (E) and the tracer transported by advection (A) using October 2008 to February 2009. We did not calculate the ensemble spread for the tracer transported by molecular diffusion as it does not depend on the dynamics and hence its trajectories are very similar for all months and all dynamical conditions. Table 2.1 shows that the endpoints for SSW conditions are outside the inter-monthly spread for the control tracer and the tracer transported by advection, which indicates a robustly different behavior under SSW conditions.

Figure 2.6 shows the temperature and residual vertical wind differences for January to mid-February 2009. The differences are calculated with respect to the mean of November and December 2008. The height of the stratopause (dashed, green line) is determined as the first local temperature maximum above the tropopause. The warming and displacement of the stratopause to a lower altitude is well reproduced. In early February, the stratopause reforms at high altitudes above 80 km. However, the reformation and the descent of the elevated stratopause happen too quickly, which is
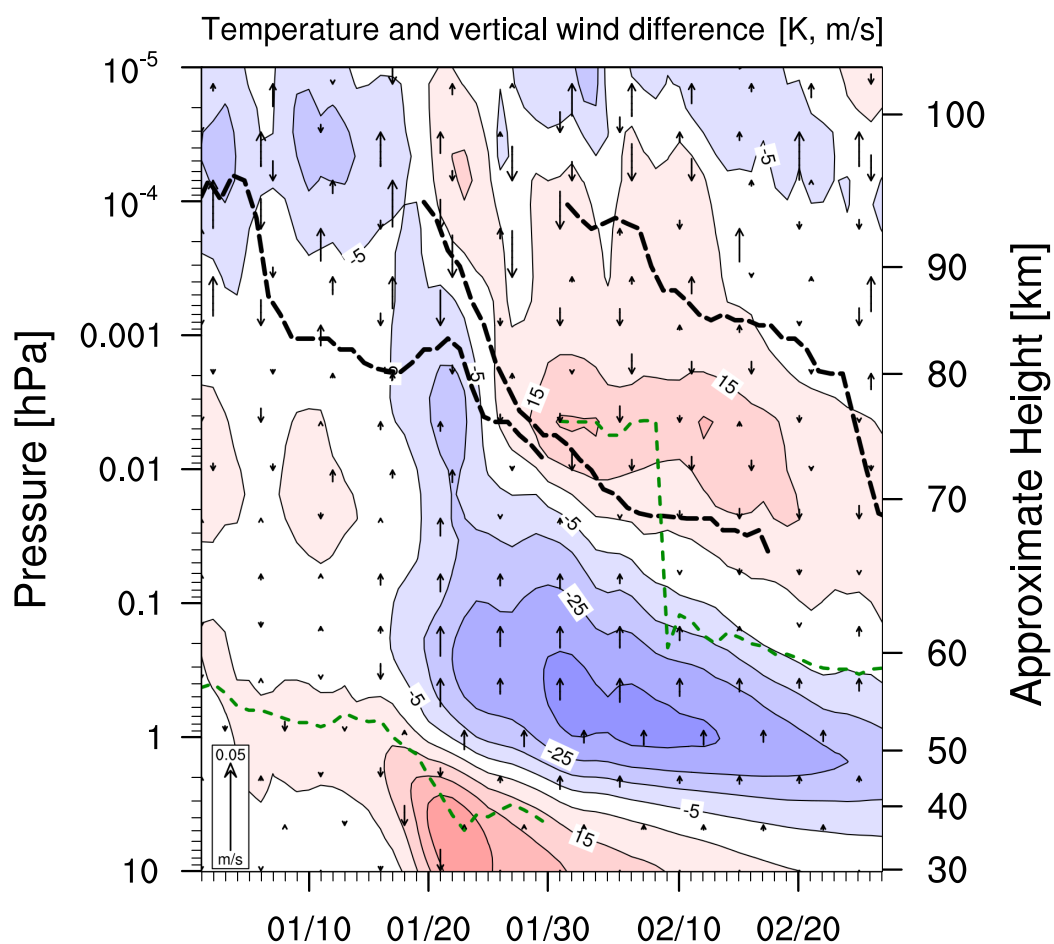
Figure 2.6. Temperature (colored contours) and residual vertical wind (vectors) differences [K, m/s] between January to March 2009 and the mean over November and December 2008. The dashed lines correspond to the vertical trajectory of the tracer maximum transported by advection only. Three emission times are shown: 1 January, 20 January and 1 February (from left to right). The dashed, green line represents the height of the stratopause. The contour interval is 10 K.

common in models covering this altitude range (Pedatella et al. 2014). The vertical residual wind differences explain well the trajectories of the tracer maximum (dashed lines). Note that only the tracer transported by advection is shown but for three different emission times. Strong downwelling occurs during the warming in the upper mesosphere, which is related to the elevated stratopause and its descent to its climatological altitude (Chandran et al. 2013a). Note that there is no net-upward flow between 10 and 0.1 hPa after the SSW, but just weakened downward flow. The weak descent of the tracer below 0.1 hPa seen in Figures 2.4c – 2.4d is caused by convergent winds at 0.03 hPa.

Direction and strength of advection are highly variable on the time scale of a few days during the period of the SSW. Holt et al. (2013) stated that the amount of stratospheric NO_x varies with the timing of a SSW event within a season. The earlier the event occurs in the winter, the more NO_x is transported to the stratosphere. The strong dependency of stratospheric NO_x on the timing of SSW has two main reasons: (1) the earlier the SSW occurs, the more negative (descent) is the vertical wind and (2) the earlier the SSW occurs, the longer the NO_x descends and the less NO_x is mixed laterally (due to the breakdown of the polar vortex) to latitudes, where it gets destroyed by sunlight. Holt et al. (2013) used a constant EPP forcing during the whole simulation, i.e., a continuous auroral electron EPP event. We find that the descent of NO_x varies in terms of velocity and mass over a few days during the SSW. Hence, the amount of stratospheric NO_x depends not only on the timing of the SSW within the winter season, but also on the timing of the EPP forcing (production of NO_x) and of the disturbed SSW dynamics on the timescale of a few days.

2.3.3 Impact of a Doubled Eddy Diffusion Coefficient

Garcia et al. (2014) suggested an underestimation of eddy diffusion in WACCM (version 4). They increased K_{zz} by halving the Prandtl number, which is inversely proportional to K_{zz}. For doubled K_{zz}, WACCM agrees better with the observations for CO_2. The default value of the Prandtl number used in HAMMONIA is 3, which is between the standard value used in WACCM (Pr = 4) and the tuned value (Pr = 2) used by Garcia et al. (2014). In the following, we investigate the effect of a stronger eddy diffusion on the downward transport. To estimate consequences of such an underestimation or of changes over time, we doubled the eddy diffusion coefficient ($2 \times K_{zz}$) in the gravity wave parameterization scheme (see Section 2.2 and Equation 2.1 for more details on the implementation of eddy diffusion in HAMMONIA).

As for $1 \times K_{zz}$, we investigate the vertical distribution of the passive tracer averaged over November and December 2008 (see Figure 2.4e), but for $2 \times K_{zz}$ we only use one ensemble member. The distribution of the tracer transported by advection slightly

changes compared to $1 \times K_{zz}$ (see Figure 2.4a), while eddy diffusion clearly strengthens at all altitudes but most in the lower thermosphere. For $1 \times K_{zz}$, the maximum of the tracer transported by eddy diffusion is at $3 \cdot 10^{-4}$ hPa for the emission level of 10^{-4} hPa and 0.003 hPa for the emission level of 0.001 hPa (not shown). For $2 \times K_{zz}$, the tracer maximum is transported further down: 0.003 hPa for the emission level of 10^{-4} hPa and 0.007 hPa for the emission level of 0.001 hPa (not shown). Below the mesopause region, advection is still the dominant process and eddy diffusion the second largest process (not shown).

Figure 2.4f shows the vertical trajectory of the tracer maximum for $2 \times K_{zz}$ for the mean over November and December 2008. Advection is much weaker than for $1 \times K_{zz}$ (see Figure 2.4b). A change in K_{zz} may influence advection, because non-resolved vertical mixing acts not only on composition but also on momentum. Further analysis of the relation between K_{zz} and advection is beyond the scope of this study. With a weaker advection, molecular diffusion is the leading process for the total transport down to about $5 \cdot 10^{-4}$ hPa. Note that, as mentioned before, molecular diffusion only weakly depends on the dynamics and its impact on the transport is, hence, the same as under undisturbed winter conditions. After 9 days the tracer transported by eddy diffusion develops a new maximum below the emission level. For $1 \times K_{zz}$, the tracer maximum transported by eddy diffusion remains 17 days at the emission level before building a new maximum below. Hence, the time until a new tracer maximum is developed below the emission level is almost halved for $2 \times K_{zz}$. Furthermore, the transport by eddy diffusion is strongly enhanced in the lower thermosphere and upper mesosphere. Between $5 \cdot 10^{-4}$ hPa and 0.003 hPa eddy diffusion is dominant, while advection takes over below 0.003 hPa (not shown). Eddy diffusion can potentially have a large impact on the transport to the mesosphere. However, the impact of eddy diffusion depends on K_{zz}, which bears large uncertainty.

To evaluate the robustness of our results, we compare the endpoints of each trajectory for $2 \times K_{zz}$ to the inter-monthly spread of the ensemble for $1 \times K_{zz}$ (see Table 2.1). This comparison describes whether the results of $2 \times K_{zz}$ are different from the inter-monthly changes of $1 \times K_{zz}$. A more detailed description on how the inter-monthly spread is calculated is provided in Section 2.3.2. Table 2.1 shows that the endpoints for $2 \times K_{zz}$ are outside the inter-monthly spread for the tracer transported by advection and by eddy diffusion, which indicates a robustly different behavior for $2 \times K_{zz}$.

To test, if the impact of an enhanced eddy diffusion changes during disturbed SSW dynamics, we have performed an additional experiment with $2 \times K_{zz}$ during SSW conditions (see Figures 2.4g – 2.4h). We find that the strengthening of advection due to SSW dynamics is larger than the strengthening of eddy diffusion due to doubled K_{zz}. The endpoint of each trajectory trajectory lies outside the inter-monthly spread of the
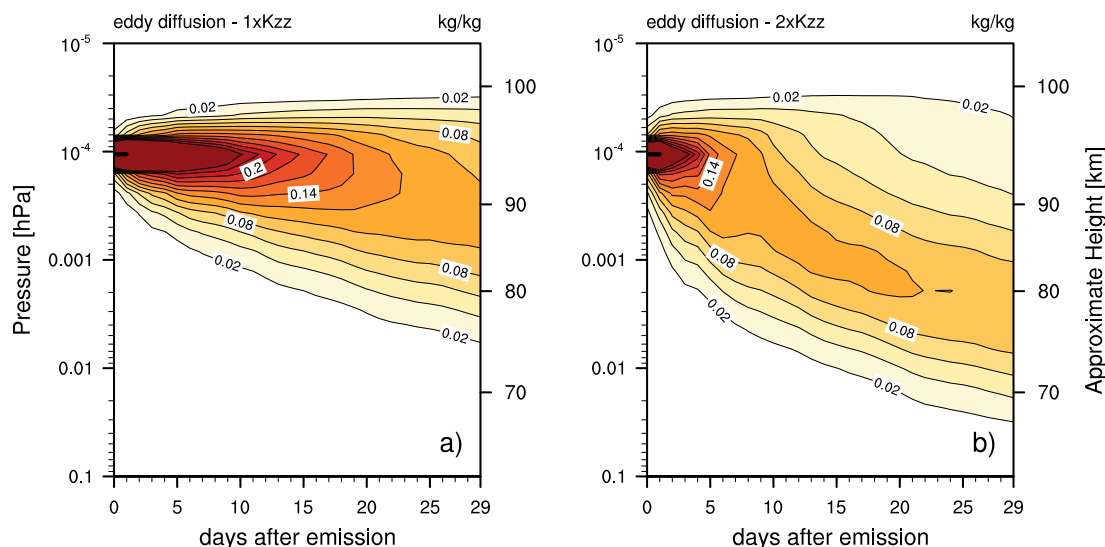
Figure 2.7. Normalized tracer mass transported only by eddy diffusion for undisturbed conditions with (a) $1\times K_{zz}$ and (b) $2\times K_{zz}$. The average of the simulations with emission dates on 1 November and 1 December 2008 are shown. We use the ensemble mean for (a) and a single run for (b). The tracer is emitted at the 1st of each month. The contour interval is $0.02\,kg/kg$.

ensemble for undisturbed conditions with $1\times K_{zz}$ (see Table 2.1).

Figure 2.7 shows the normalized tracer mass transported only by eddy diffusion as a function of altitude and time. Only the tracer emitted at $10^{-4}\,hPa$ is shown. The mean over November and December 2008 for two different K_{zz} values is used, (a) for $1\times K_{zz}$ and (b) for $2\times K_{zz}$. The tracer maximum remains for both K_{zz} values several days at the emission level, however, the distribution spreads. For both K_{zz} values, a flat distribution develops around the tracer maximum. If a small amount of mass is then transported downward from the emission level, a new maximum develops several levels below. This happens for $1\times K_{zz}$ at day 17 and for $2\times K_{zz}$ at day 9 and explains the sudden descent of the tracer maximum seen in Figures 2.4b and 2.4f. For $2\times K_{zz}$, eddy diffusion is much stronger and hence, the strong gradient at the emission level is weakened faster. This leads to the earlier descent of the tracer maximum for $2\times K_{zz}$.

To evaluate the influence of an enhanced eddy diffusion on the transport, we compare NO profiles simulated with $2\times K_{zz}$ to the MIPAS data (see Figure 2.3). As in the reference simulation, also the simulation with doubled K_{zz} underestimates the concentration of NO at $0.1\,hPa$ and overestimates it above $0.01\,hPa$. Doubling the eddy diffusion coefficient yields little to no improvement. The largest discrepancies emerge between 0.001 and $10^{-4}\,hPa$, where the model overestimates the concentration of NO by $100\,\%$. For CO the agreement between HAMMONIA and MIPAS worsens with

$2 \times K_{zz}$ (not shown), which has also been observed by Garcia et al. (2014).

2.4 Summary and Conclusion

In this study, we analyzed the role of advection, molecular diffusion and eddy diffusion for the transport of nitrogen oxides through the mesopause region. Simulations with HAMMONIA were carried out including a passive tracer and selected transport processes switched off. We found that molecular diffusion and advection are the dominant processes for the transport of NO_x in the lower thermosphere. The impact of molecular diffusion rapidly decreases with decreasing heights, while the impact of advection increases. Above the mesopause, the intra-diurnal variability associated with atmospheric tides strongly affects the transport of NO_x. The dominant impact of advection below the mesopause agrees well with the streamfunction-theory and other studies (Smith et al. 2011). In the default configuration of the model, eddy diffusion negligibly contributes to the total transport in the lower thermosphere and weakly contributes to the transport in the upper mesosphere. The weak influence of eddy diffusion on the transport in the thermosphere is caused by a strong gradient of the tracer at the emission level and a small eddy diffusion coefficient.

Besides undisturbed winter conditions, we also analyzed the transport during the sudden stratospheric warming (SSW) in January 2009. Shortly after the SSW, advection is strongly enhanced in the thermosphere and mesosphere, which agrees with the results of Randall et al. (2009). Hence, the downward transport through the mesopause region is dominantly driven by advection. Weak downward residual circulation related to a warming in the upper mesosphere hinders the further descent of the tracer below $0.1\,hPa$. Over a few days during the SSW advection strongly varies in terms of strength and direction. Hence, the stratospheric amount of NO_x depends strongly on the timing of thermospheric NO_x production due to EPP and disturbed vortex dynamics.

Smith et al. (2011) showed that most air in the polar stratosphere in WACCM originates in the mesosphere at lower latitude, instead of being advected from the thermosphere. Our study agrees on the importance of advection for the downward transport below the mesopause region. However, we did not consider the latitudinal transport and concentrated on the vertical transport. For single events with large thermospheric NO_x source, e.g., an EPP event, the transport from the thermosphere to the mesosphere cannot be neglected. Additionally, Smith et al. (2011) considered only daily means, while we have shown that more NO in the lower thermosphere is transported downward if 6-hourly values are taken into account. Thus, this paper extends the analysis of Smith et al. (2011) and identifies molecular diffusion and vertical advection as the

major drivers for transport in the lower thermosphere for undisturbed winter conditions.

Recent studies have suggested positive trends in eddy diffusion of 15 % on the decadal time scale (Emmert et al. 2012; Hoffmann et al. 2011). We conducted an experiment with doubled eddy diffusion coefficient ($2 \times K_{zz}$) to quantify the sensitivity of different transport processes to the value of K_{zz}. In this sensitivity study, eddy diffusion becomes the second largest process for the downward transport in the lower thermosphere and near 0.001 hPa eddy diffusion is dominant. The impact of advection on transport in the lower thermosphere decreases with doubled K_{zz}, leaving molecular diffusion the dominant process. If eddy diffusion is enhanced as suggested by observations or due to a positive trend in K_{zz}, eddy diffusion can potentially have a larger impact on transport through the mesopause region than was previously assumed.

This study is based on the extended winter 2008/2009 and on simulations with HAMMONIA. We evaluated the model with MIPAS observations and find that the model underestimates the vertical gradient of NO concentration in the MLT region, which leads to a slight overestimation of the NO concentration in the lower thermosphere. In the upper mesosphere and lower thermosphere, the simulated NO concentrations are outside of the error bars of the observations. The underestimation of NO in the upper mesosphere (at 0.2 hPa) may be related to an overestimation of the NO photolysis in the illuminated mesosphere. The overestimation of NO in the lower thermosphere (above 0.001 hPa) may be caused by the use of AIMOS, which does not use the corrected medium energy electrons from the POES MEPED instrument (Peck et al. 2015; Rodger et al. 2010). We believe that the transport is reasonably reproduced by the model. Enhancing eddy diffusion yields only slightly better agreement with MIPAS. Further work on the uncertainty concerning transport processes introduced by the uncertainty of eddy diffusion is needed.

More in general, it is clear that current models cannot reproduce perfectly the observed trace gas distributions indicating deficiencies in the implemented processes. But trace gas observations by satellite only provide insight in the integrated effects of production and transport processes. Estimates of the relative importance of the differences will therefore always rely on modeling efforts. To reduce the uncertainty left by our study we can imagine two pathways: (1) improving the understanding of the underlying processes and its representation and (2) using observations of specific events that may be more informative concerning transport processes. With respect to (1) observations of gravity wave breaking and the resulting turbulence may allow for improving the representation of both eddy-diffusive and advective transport in models. Gravity wave observation from satellite as suggested by Geller et al. (2013) may be one element of such a strategy. With respect to (2) observing the time evolution of

trace gas distributions after events of extreme geomagnetic activity may help to better evaluate and constrain numerical models. However, higher temporal and spatial resolution observations are required than currently exist.

Short summary of Chapter 2:

- Advection and molecular diffusion dominate the transport through the mesopause.

- Eddy diffusion has a negligible impact on the transport in the lower thermosphere and a limited impact on the transport in the upper mesosphere.

- After sudden stratospheric warming events, the transport is almost purely driven by advection.

Sensitivity of Simulated Mesospheric Transport of Nitrogen Oxides to Parameterized Gravity Waves [1]

3

Gravity waves strongly influence the circulation and transport processes in the middle atmosphere. We analyze the sensitivity of the simulated mesospheric transport of nitrogen oxides (NO_x) to differences in a parameterization of non-orographic gravity waves. After particularly strong sudden stratospheric warming (SSW) events as in January 2009, satellite instruments measured a strong mesospheric descent of NO_x. However, this downward transport is in general underestimated in models covering this altitude range. We use simulations of the atmospheric general circulation and chemistry model HAMMONIA (Hamburg Model of Neutral and Ionized Atmosphere) to discuss both differences in a homogeneous background gravity wave source and a source related to frontal activity. The results show that the transport of NO_x is highly sensitive to such differences. With a stronger gravity wave source, less NO_x is transported after the SSW to the mesosphere and the elevated stratopause descends more rapidly to its climatological altitude. We observe the opposite by weakening the gravity wave sources yielding a better agreement with the observations. The amount of the transported NO_x is controlled by the altitude at which momentum is deposited in the atmosphere. The higher the altitude where the momentum is deposited in the upper mesosphere, the stronger is the descent of NO_x. A small wave amplitude favors the transition to turbulence at a higher altitude due to the exponential increase of the amplitude with height.

3.1 Introduction

The large scale circulation of the middle atmosphere is strongly influenced by the momentum deposition from gravity waves that propagate upward from tropospheric sources. The momentum deposition is the main driver for the mesospheric mean meridional circulation with upwelling in the summer and downwelling in the winter hemisphere (Alexander et al. 2010; Haynes et al. 1991; Holton et al. 1995). The latter enables the transport of tracers from the mesopause to the stratosphere and is there-

fore a key process for the potential influence of thermospheric nitrogen oxides (NO_x) produced by energetic particle precipitation on stratospheric ozone and subsequently stratospheric circulation and surface climate (Baumgaertner et al. 2011; Randall et al. 2007; Rozanov et al. 2005; Seppälä et al. 2009).

Recent satellite observations measured an enhancement of the downward transport of NO_x after sudden stratospheric warming (SSW) events. Randall et al. (2009) showed that the NO_x amount which descended from the thermosphere to the stratosphere after the SSW in 2009 was 50 times higher than during undisturbed conditions. However, the assessment of mesospheric descent of NO_x and CO after the 2009 SSW in observations and general circulation models covering this altitude range, currently being conducted within SPARC's SOLARIS-HEPPA project, indicates that the modeled descent is generally too weak. This underestimation is speculated to be due to deficiencies in the representation of either advective or diffusive mesospheric transport (Holt et al. 2013; Smith et al. 2011), which are both largely caused by dissipating gravity waves. In a study with the Hamburg Model of Neutral and Ionized Atmosphere (HAMMONIA) which is also used here, Meraner and Schmidt (2016) showed that after a SSW event NO_x is predominantly transported by advection from the polar thermosphere downward. The contribution of molecular diffusion is limited to the thermosphere, and eddy diffusion only contributed marginally. Changes of the circulation could, hence, have a strong impact on the descent of NO_x.

In this study, we analyze the sensitivity of the simulated transport of NO_x to differences in the gravity wave parameterization in the general circulation and chemistry model HAMMONIA. Due to the small horizontal wavelength of gravity waves their effects on the circulation need to be parameterized in most general circulation models of the middle atmosphere.

McLandress et al. (2013) stated that after a SSW advection is strongly forced by non-orographic gravity waves. They carried out simulations with the Canadian Middle Atmosphere Model (CMAM) with sources of either the orographic or the non-orographic gravity waves switched off for the dynamically perturbed Northern winters of 2006 and 2009. They found that without orographic gravity waves, the upper mesospheric downwelling under undisturbed conditions is twice as strong as in the control run. Furthermore, the relative importance of the two types of gravity waves depends on the time with respect to the central date of the SSW. After the SSW when the westerlies are too weak to allow much vertical propagation of the orographic gravity waves to the mesosphere, the non-orographic gravity waves drive the circulation and thereby the descent of tracers (e.g., CO and NO_x) from the thermosphere. Moreover, Siskind et al. (2015) showed that models have deficits in simulating the non-orographic gravity wave forcing and suggested that a weak mesospheric descent is caused by an under-

estimation of the non-orographic gravity wave drag.

However, due to the small spatial scale of large parts of the gravity wave spectrum, constraining gravity wave drag from global satellite observation remains a challenge (e.g., Alexander 2015; Geller et al. 2013). The resulting uncertainty makes it necessary to tune gravity wave parameterizations in general circulation models (GCMs) and in particular the gravity wave sources to reproduce available macroscale observations. Common constraints are to simulate realistic climatological zonal winds or a realistic quasi-biennial oscillation (e.g., Richter et al. 2010; Scaife et al. 2000). In a similar sense, McLandress et al. (2013) suggested that also observations of the downward transport of NO_x data may be used to provide additional constraints for gravity wave sources in numerical models.

Following McLandress et al. (2013) this paper determines the impact of the non-orographic gravity wave parameterization on simulations of the NO_x transport. We use simulations with the general circulation and chemistry model HAMMONIA, in which we either modify the homogeneous background source of gravity waves or a source related to tropospheric fronts. The simulations are evaluated against observational data taken by MIPAS/Envisat. We concentrate on the winter 2009, because the major SSW event in January 2009 was the strongest and most prolonged on record (Manney et al. 2009). Additionally, after the final break-down of the recent stratopause the new stratopause reformed in early February near 80 km. This reformation of the new stratopause at an anomalously high level is called an elevated stratopause event and is an indicator of enhanced descent in the mesosphere and lower thermospher (Siskind et al. 2007).

Our study aims at a better understanding of the role of gravity waves for the downward transport of NO_x during the Northern Hemisphere winter in relation to SSWs and thereby to allow for a better estimation of potential geomagnetic effects on climate. (Baumgaertner et al. 2011; Seppälä et al. 2009). Furthermore, we discuss to what extent the observed mesospheric downward transport in nudged simulations may be used to further constrain gravity wave sources as suggested by McLandress et al. (2013). Our study extends the sensitivity analysis by Charron and Manzini (2002), who used a model with a top of 0.1 hPa, while HAMMONIA treats the dynamics up to 10^{-7} hPa. Moreover, our study sheds light on the importance of anomalous gravity wave filtering for the disturbed mesospheric dynamics observed during SSWs, e.g., the cooling of the lower mesosphere (e.g., Limpasuvan et al. 2012; Siskind et al. 2005) or the occasional occurrence of an elevated stratopause (e.g., Tomikawa et al. 2012). Additionally, the possible interaction between resolved waves and gravity waves as reported e.g., by Chandran et al. (2013b) and Sigmond and Shepherd (2014) is discussed. Especially, after a SSW the effect of non-orographic gravity waves is amplified by resolved waves

(Limpasuvan et al. 2016). Manzini and McFarlane (1998) reported compensation of resolved and gravity waves in the lower mesosphere in the northern hemisphere.

This paper is organized in the following way: Section 3.2 describes the model setup and the observations. Section 3.3 shows the impact of the background source and the frontal source on the transport and explains the importance of the altitude of momentum deposition for the strength of the transport. Finally, Section 3.4 summarizes and discusses the main outcomes as well as the limitations of the study.

3.2 Model and Observational Data

3.2.1 HAMMONIA: The Hamburg Model of the Neutral and Ionized Atmosphere

HAMMONIA is an upward extension of the ECHAM5 GCM (Roeckner et al. 2006) coupled to the MOZART3 chemistry model (Kinnison et al. 2007). Atmospheric dynamics, radiation and chemistry are treated interactively from the surface to the thermosphere (approximately 250 km altitude). A detailed description of the model is given in Schmidt et al. (2006). To include the electron impact on NO production, we enhanced the model to incorporate the ion chemistry of the ionospheric *E* and *F* region as described in Kieser (2011) and Meraner and Schmidt (2016). Siskind et al. (2015) stated that an additional source of NO from high energetic particle precipitation is not needed. In this study, HAMMONIA is run with a triangular truncation at wave number 63 (T63), corresponding to a resolution of about 1.9° in latitude and longitude, and with 119 vertical layers. The vertical resolution varies between 800 m in the upper troposphere and 3 km in the lower thermosphere. Sea surface temperature and sea ice cover are taken from the Atmospheric Model Intercomparison Project 2 (AMIP2) climatology. Present-day conditions of greenhouse gas concentrations are used. EUV-related thermospheric NO production corresponding to solar minimum is parameterized as function of the F10.7 solar flux ranging from 64 to 74 10^{-22} Wm^{-2} Hz^{-1} for the period under investigation. Total and spectral solar irradiance are as well specified for the 2009 solar minimum. The particle-induced ion pair production rates are provided by the Atmospheric Ionization Module Osnabrück (AIMOS - version 1.6) (Wissing and Kallenrode 2009).

Two parameterizations are used to describe gravity wave processes. Orographic waves and surface blocking are parameterized according to Lott and Miller (1997), while non-orographic gravity waves are parameterized according to the Doppler-spread theory from Hines (1997a) and Hines (1997b). As stated above, we concentrate on studying the sensitivity of the tracer transport to non-orographic gravity waves and, hence, the parameterization of the orographic gravity waves remains unchanged. The Hines parameterization considers a broadband and continuous spectrum arising

from a variety of forcing mechanisms (e.g., shear instability, convective activity). It is assumed that all sources are located in the troposphere and that the generated gravity waves exclusively propagate vertically. In this study, we use a geographically uniform isotropic gravity wave source spectrum with a constant root-mean-square (rms) wave wind-speed launched at 830 hPa (σ). The rms wind speed describes the strength of the gravity wave source (i.e., the amplitude of the waves). The default value is 0.8 m/s.

While the homogeneous background source of gravity waves is independent of the actual simulated meteorology, HAMMONIA additionally offers the option to include tropospheric fronts as a gravity wave source following Charron and Manzini (2002). The parameterization assumes that frontogenesis occurs when a strong deformation of the wind field increases the horizontal temperature gradient. If the threshold of $0.1 \, \text{K}^2 \, (100 \, \text{km})^{-2} \, \text{h}^{-2}$ is reached, a gravity wave spectrum is emitted but with an rms wave wind-speed of 2 m/s instead of 0.8 m/s. Hence, at the location of fronts the homogeneous source is replaced by the frontal source of Charron and Manzini (2002) and no gravity waves are emitted from the background. The homogeneous source with an rms wind speed of 0.8 m/s is only used in at grid points where no frontal source is used. Gravity waves excited by fronts are emitted in the two cross-front directions (perpendicular to the tropospheric winds associated with the fronts).

As gravity waves propagate upward, the wave action is conserved until the gravity wave spectrum as a whole becomes unstable and waves at high vertical wave numbers break down into turbulence. The transition to turbulence is parameterized according to Hines (1997a) and Hines (1997b) to occur at a specific wave number, called the cut-off wave number. It is assumed that waves with a wave number larger than the cutoff wave number are removed from the spectrum and the momentum they carried is deposited into the background flow. This, in turn, influences the middle atmospheric dynamics and thereby the advection, which dominates the transport of tracers below the mesopause (Meraner and Schmidt 2016).

We analyze the sensitivity of the tracer transport to two modifications of gravity sources: (1) switching on/off the emission of gravity waves from fronts and (2) varying the strength of the homogeneous background source. We carried out four experiments running from January to April 2009, which are summarized in Table 3.1. Compared to the control simulation, two experiments consider a strengthening of gravity wave sources (i.e., an increase of the wave amplitude), either by switching on the emission of gravity waves from fronts (front on) or by increasing σ from 0.8 to 1.0 m/s (strong background). In the fourth experiment gravity wave sources are weakened via a reduction of σ to 0.6 m/s (weak background). Note that by switching on the emission of gravity waves from fronts not only the wave amplitude (i.e., the rms wave wind-speed) but also the orientation of the phase speed are modified. In earlier studies of

Table 3.1. List of nudged experiments with gravity waves from fronts (lfront) either switched on (true) or switched off (false) and different rms wave wind-speeds (σ) of the background source. Note that the frontal source is launched with a rms wave wind-speed of 2 m/s.

Experiment	lfront	σ [m/s]
Control	False	0.8
Front on	True	0.8
Weak Background	False	0.6
Strong Background	False	1.0

HAMMONIA either the 'front on' - configuration (e.g., Funke et al. 2011) or the 'strong background' - configuration (e.g., Pedatella et al. 2014) is used.

In all four simulations, surface pressure, temperature, divergence and vorticity are nudged (i.e., relaxed) from 850 hPa to 1 hPa with an upper and lower transition zone. The nudging data are 6-hourly values of the European Centre for Medium-Range Weather Forecasts (ECMWF) Interim Re-Analysis (ERA-interim) (Dee et al. 2011). The nudging assures that the model captures the tropospheric and stratospheric dynamics as observed during the winter 2009, including the major SSW event in January 2009. As long as the critical-level filtering of gravity waves in the troposphere and stratosphere is captured, the upper atmosphere is strongly constrained through the nudging without the need of explicitly nudging the mesospheric temperature (Ren et al. 2011). Temperature and NO_x of these experiments are compared to MIPAS (Michelson Interferometer for Passive Atmospheric Sounding), and thereby averaging kernel filtering is applied. For temperature, the simulations are filtered based on the average diagonal element of the averaging kernel matrix with a threshold of 0.03. For NO_x, latitudinal bins are rejected when the average of the averaging kernel diagonal element is larger than 0.03.

In addition to the nudged simulations, we performed two free-running simulations lasting 49 years. To make them comparable to the nudged simulations, we used the same boundary conditions as for the nudged simulations (fixed SST, greenhouse gases, solar and energetic forcing from June 2008 to May 2009). The only difference between the nudged and the free-running simulations, hence, is the nudging. To explore the sensitivity of the transport of NO_x to extreme cases, two experiments were carried out, which correspond to the 'front on' and 'weak background' experiments. We concentrate our analysis on the high latitudes. Therefore, all following figures show polar cap averages (60° N - 90° N) unless otherwise stated.

3.2.2 MIPAS: Michelson Interferometer for Passive Atmospheric Sounding

MIPAS is a mid-infrared Fourier transform limb emission spectrometer (Fischer et al. 2008) onboard of the European Environmental Satellite (ENVISAT). The instrument measured atmospheric trace species from March 2002 to April 2012. The retrieval of the gas and temperature profiles has been performed using the level 2 processor developed by the Institute of Meteorology and Climate Research of the Karlsruhe Institute of Technology and the Instituto de Astrofísica de Andalucía. Here we use temperature (V5_220 and V5_521) (García-Comas et al. 2014) and NO_x (V4_220 and V4_501) (Funke et al. 2005) data from January to April 2009. The data are derived from the nominal below 0.02 hPa and from the middle and upper atmosphere observation mode above 0.02 hPa. The nominal observational mode measured regularly on an almost daily basis and covered an altitude range from 7 - 70 km. MIPAS measured in the middle and upper atmosphere mode only between 1 to 12 days per month and covered an altitude range of 20 - 102 km. We interpolate 2-hourly gridded HAMMONIA data to the actual measurement times and locations of MIPAS.

MIPAS temperature and NO_x agree very well with other satellite measurements (e.g., the Atmospheric Chemistry Experiment Fourier Transform Spectrometer (ACE-FTS) observation) and ground-based observations (Bender et al. 2015; García-Comas et al. 2014). Meraner and Schmidt (2016) showed that the MIPAS vertical NO profile is reasonably reproduced by HAMMONIA.

3.3 Results

3.3.1 Sensitivity of Temperature and NO_x Transport to Gravity Wave Sources in Nudged Simulations

In the following, we analyze the changes in the temperature and transport of NO_x due to variations in the gravity wave parameterization. We discuss differences in the homogeneous background source and in the source related to frontal activity. All HAMMONIA experiments are compared to MIPAS observations. First, we explore the changes in the temperature and in NO_x due to switching on / off the emission of gravity waves excited by fronts. Note that at the locations where frontal gravity waves are excited no additional background source is considered.

Figures 3.1a, 3.1c and 3.1d show the temperature for January to April 2009 including the major SSW event in late January. On 24 January 2009, a reversal of the northern polar vortex westerlies occurred due to anomalous wave-2 activity in the upper troposphere (Manney et al. 2009). Subsequently, the stratopause warmed, dropped below 30 km and finally broke down in late January. At the same time, the mesosphere

cooled. In mid-February the elevated stratopause reformed at an anomalously high altitude (near 80 km) and descended thereafter to its climatological altitude.

The stratopause is determined as the first local temperature maximum above the tropopause and is located near 0.3 hPa during undisturbed conditions (see Figure 3.1a). Compared to MIPAS the stratopause under undisturbed conditions (early January) is about 11 K too warm in the experiment 'front on'. The control experiment produces a colder stratopause that agrees better with MIPAS (only 6 K too warm). The warming and displacement of the stratopause to a lower altitude after 24 January is well reproduced in both HAMMONIA simulations. Note that the model is nudged up to 1 hPa to the ERA-Interim reanalysis data. Hence, the HAMMONIA experiments only slightly differ below 1 hPa and are similar to the MIPAS observations. Simultaneously with the warming of the stratosphere, the mesosphere cooled. However, the cooling is too weak in the 'front on' experiment (about 20 K too warm compared to MIPAS). The reformation of the elevated stratopause and its descent happen too quickly in HAMMONIA, which is common in models covering this altitude range (Pedatella et al. 2014). However, in the control experiment the new stratopause stays longer at a higher altitude and reaches its approximate climatological altitude later than for the experiment with gravity waves emitted from fronts (see Figure 3.1b).

Figures 3.2a – 3.2c show a comparison of the NO_x mixing ratio observed by MIPAS to those in the two HAMMONIA experiments, with and without gravity waves excited from fronts. Prior to the SSW both model simulations show similar NO_x concentrations in the stratosphere and mesosphere. The SSW is characterized by the decrease of NO_x on 24 January 2009, which is caused by enhanced lateral mixing following the split of the polar vortex (Salmi et al. 2011). Qualitatively, the decrease in NO_x is reproduced in both HAMMONIA simulations, however, weaker than in MIPAS. This deficiency is caused by a too weak horizontal NO_x gradient in HAMMONIA (not shown).

The reformation of the new stratopause led to a strong descent of NO_x and to a development of a tongue-like structure (see Figure 3.2a). High NO_x amounts were transported to the mesosphere leading to 4 times higher values of NO_x concentrations at 0.1 hPa after the SSW than before the SSW. In early March the NO_x concentrations decreased and dropped even below the pre-SSW level above 0.1 hPa. Hence, at the end of March the amount of NO_x is more than 2 times higher at 1 hPa than at 0.04 hPa. This enhanced descent is associated with the recovery of the polar vortex (Randall et al. 2009).

Both HAMMONIA experiments (front on and control) show the enhancement of the NO_x concentrations after the SSW and a development of a tongue. However, the tongue is not as pronounced in HAMMONIA as it is in MIPAS. This is especially true for the experiment with gravity waves emitted from fronts (see Figure 3.2b). For this
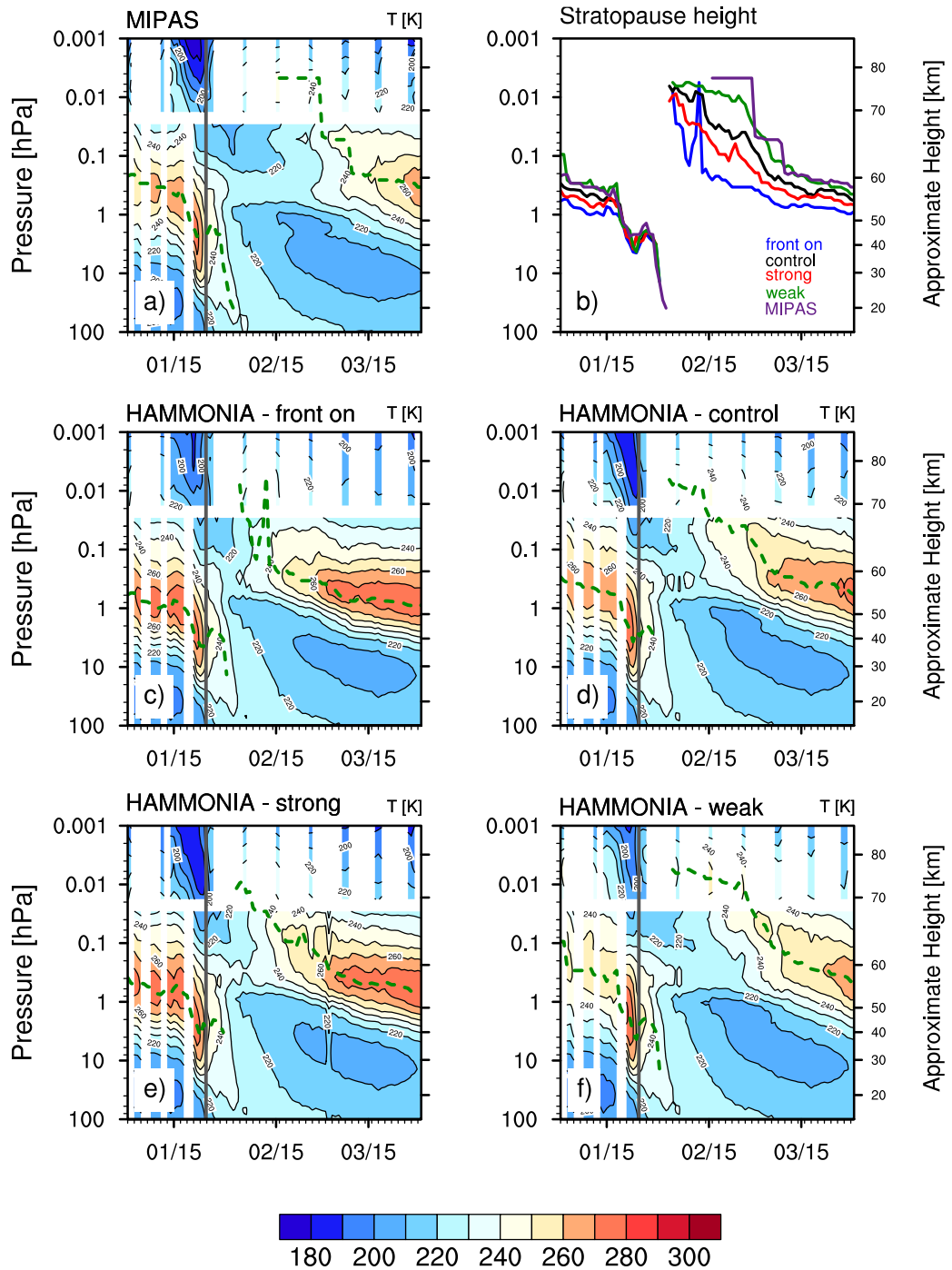
Figure 3.1. Temperature averaged over the polar cap (60° N - 90° N) for January to April 2009 in (a) MIPAS and four HAMMONIA simulations: (c) with gravity waves induced by fronts, (d) control experiment (σ = 0.8 m/s), (e) with a strong background source (σ = 1.0 m/s), (f) with a weak background source (σ = 0.6 m/s). For (d) – (f) gravity waves from fronts are switched off. The contour interval is 10 K. (b) The height of the stratopause for MIPAS and all four HAMMONIA experiments. The gray solid line corresponds to the central date of the SSW (24 January 2009). The height of the stratopause of MIPAS (a) and the individual experiments (c to f) is marked by the green dashed line.
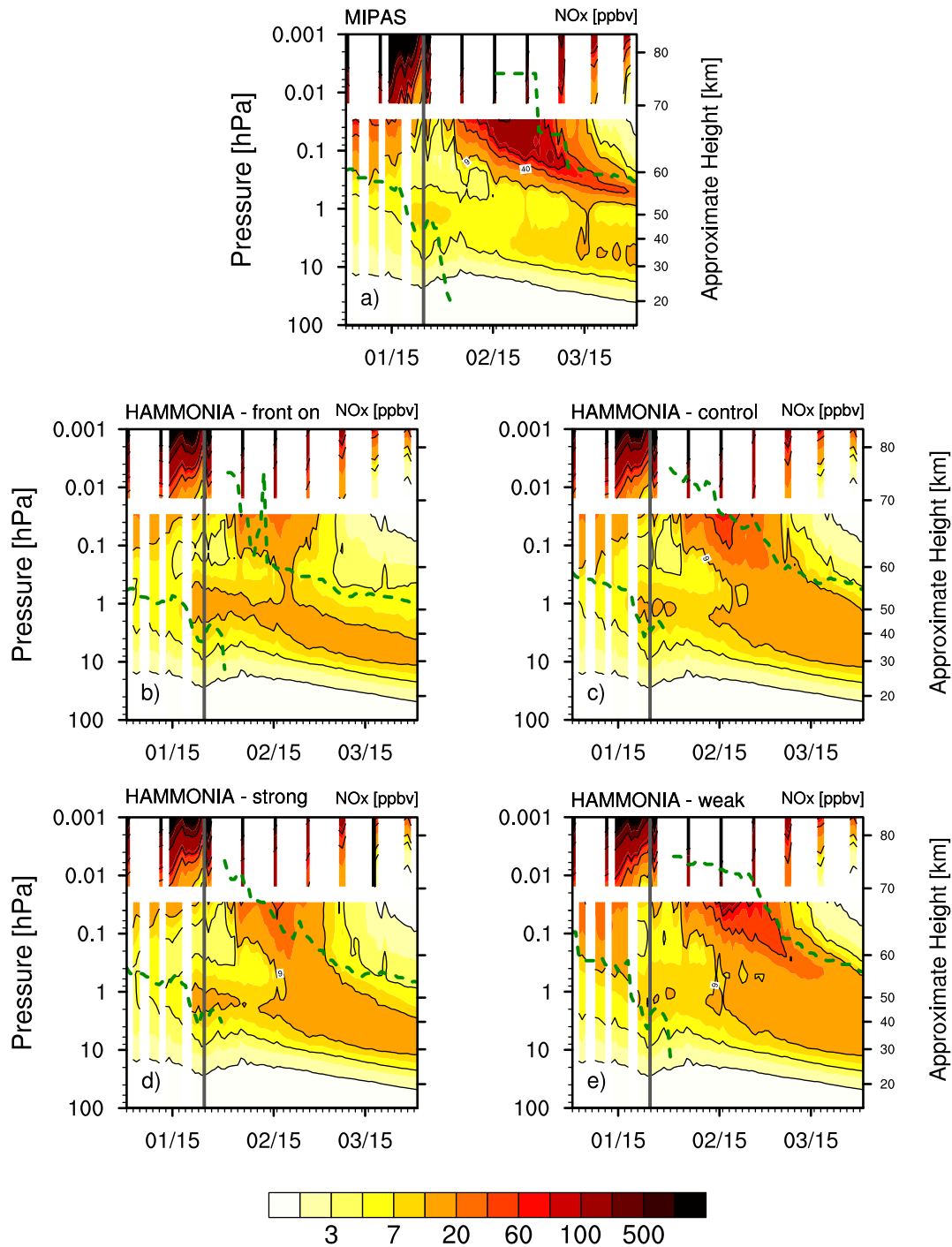
Figure 3.2. NO_x volume mixing ratio over $60°$ N - $90°$ N for January to April 2009 in (a) MIPAS and four HAMMONIA simulations: (b) with gravity waves induced by fronts, (c) control experiment ($\sigma = 0.8$ m/s), (d) with a strong background source ($\sigma = 1.0$ m/s), (e) with a weak background source ($\sigma = 0.6$ m/s). For (c), (d) and (e) gravity waves from fronts are switched off. The gray solid line corresponds to the central date of the SSW (24 January 2009). The height of the stratopause of MIPAS (a) and the individual experiments (b to e) is marked by the green dashed line.

experiment, the NO_x concentrations decreased already on 16 February, while for the control experiment the tongue is still evident until 4 March. Hence, the descent lasts longer in the control experiment resulting in a better agreement with MIPAS than in the experiment with gravity waves emitted from fronts.

In the following, we explore the changes in temperature and in NO_x due to the background source by varying σ (see Figures 3.1d – 3.1f and 3.2c – 3.2e). In those experiments the emission of gravity waves by fronts is switched off. The control experiment corresponds to a wave wind-speed of 0.8 m/s. Starting from this default background source, we either weaken the background source ($\sigma = 0.6$ m/s) or strengthen the background source ($\sigma = 1.0$ m/s).

Figures 3.1d – 3.1f show the temperatures from the three HAMMONIA experiments. The main characteristics of the displacement and the reformation of the elevated stratopause are reproduced in all simulations. However, some differences emerge. Compared to the MIPAS observations (see Figure 3.1a), the stratopause is under undisturbed conditions about 12 K too warm for a strong background source and about 6 K too cold for a weak background source. The cooling of the mesosphere around the central date of the SSW agrees well for a strong background source with MIPAS. With a weak background source, the mesospheric cooling is too weak. All three simulations show an elevated stratopause in early February. However, the descent of the new stratopause is too fast with a strong background source, while the experiment with a weak background source agrees better with the MIPAS observations. With a strong background source, the new stratopause reaches its climatological altitude on 14 March, while for a weak background source this is delayed for 4 days.

Analyzing again the NO_x concentrations of MIPAS and HAMMONIA, the SSW is characterized by the decrease in NO_x on 24 January (see Figures 3.2a, 3.2c – 3.2e). HAMMONIA reproduces the decrease in NO_x but again much weaker than MIPAS (see above). In the experiment with a weak background source the NO_x concentrations in early January are increased around 0.04 hPa compared to the control experiment.

Along with the reformation of the new stratopause at an unusually high altitude, high NO_x concentrations are transported downward in all simulations. However, the duration and the actual amount of transported NO_x varies. With a strong background source, less NO_x is transported to 0.04 hPa compared to the default background source (control experiment). Already on 18 February the NO_x concentrations decrease at 0.04 hPa and the tongue becomes indistinguishable from the background NO_x. This occurs earlier than in the control experiment (24 February). With a weak background source, more NO_x is transported to 0.04 hPa compared to the control experiment. The tongue is more elongated than with a strong background source and becomes only indistinguishable from the background NO_x on 18 March (at 0.4 hPa).

Until now we have discussed how temperature and NO_x concentrations change due to variations of two gravity wave sources. We either decreased the background source or increased the sources in two different ways: either (a) by allowing the emission of gravity waves from fronts or (b) by strengthening the background source. Compared to the control experiment, both ways of increasing the gravity wave sources show a similar behavior: The undisturbed stratopause is slightly too warm, the elevated stratopause descends too fast to its climatological altitude and the descent of high NO_x amounts stopped too early. However, some differences emerge, e.g., the tongue in NO_x is more pronounced in the experiment with a strong background than in the experiment with gravity waves emitted from fronts. On the whole, the experiment with a weak background shows the best agreement with MIPAS in terms of temperature and NO_x concentration. In Section 3.3.2 we will link the seen changes in NO_x and temperature to an upward shift of the altitude of the momentum deposition in the upper mesosphere.

3.3.2 Linking NO_x Transport and Gravity Wave Drag

In this section, we explain the simulated effects on NO_x concentrations by analyzing the resulting residual vertical wind and the wave forcing. Figure 3.3 shows the changes in vertical wind and temperature caused by increasing the gravity wave sources (due to the frontal or background source) or by decreasing the gravity wave sources. Both strengthening experiments show similar characteristics (see Figures 3.3a – 3.3b): The stratopause in early January (i.e., under undisturbed conditions) is too warm. The descent of the elevated stratopause happens too quickly highlighted by the dipole structure from February to April 2009 (also compare to Figures 3.1 – 3.1c and 3.1 e). However, some differences also emerge between Figure 3.3a and Figure 3.3b. The stratopause in 'front on' is in March warmer than in the experiment with a strong background source. Along with the relative cooling of the upper mesosphere, the downwelling weakens as can be seen by the vertical vectors. Note that there is no net-upward flow between 10 hPa and 0.001 hPa after the SSW but just weakened downward flow. The strongest weakening of the downwelling occurs in both experiments at different time and altitude: at 0.004 hPa on 26 February for the 'front on' - experiment and at 0.0008 hPa on 1 February for the 'strong background' - experiment. The weakened vertical wind explains well the lower NO_x concentrations at 0.01 hPa after the SSW in both experiments compared to the control experiment.

If we decrease the gravity wave sources, the above mentioned differences change in sign (see Figure 3.3c). The stratopause in early January is cooler and the elevated stratopause remains longer at a higher altitude (see again the dipole structure from February to April 2009 and compare to Figure 3.1b). Along with the reformation of the
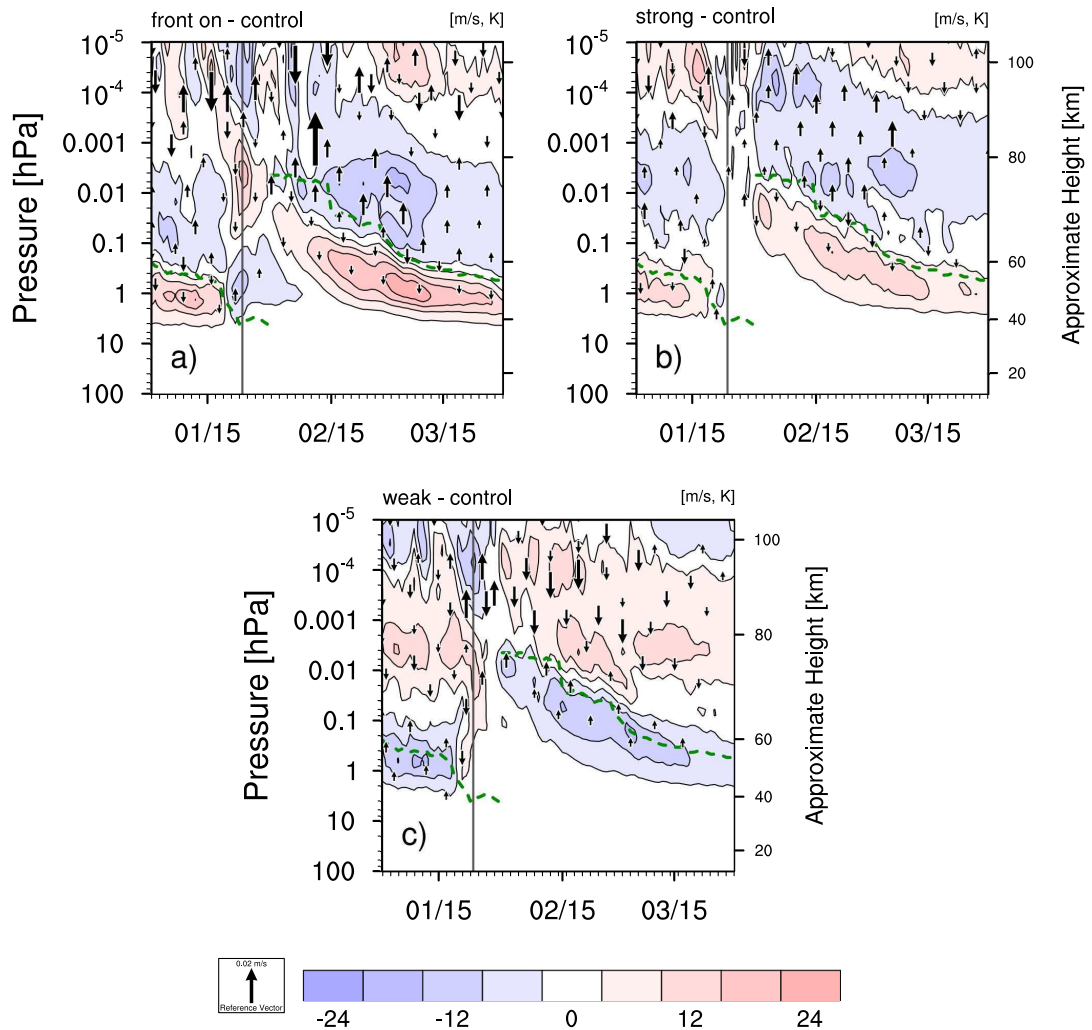
Figure 3.3. Temperature (colored contours) and residual vertical wind (vectors) differences [K, m/s] for January to April 2009. Anomalies to the control experiment are given for (a) front on, (b) strong background and (c) weak background. The contour interval is 6 K. The gray solid line corresponds to the central date of the SSW (24 January 2009). The height of the stratopause of the control experiment is marked by the green dashed line. Wind arrows smaller than 0.005 m/s are not shown.

45

new stratopause, the downward vertical wind enhances. The strongest downwelling occurs at a similar time and altitude as the weakened downwelling in the 'strong background' - experiment (at 10^{-4} hPa on 6 February). The enhanced downwelling explains well the higher NO_x concentrations after the SSW at 0.01 hPa compared to the control experiment.

In the following, we analyze the influences of the parameterized gravity wave drag and the resolved wave drag on the circulation. The component of gravity wave drag shown describes the forcing of the zonal wind due to momentum deposition of dissipating gravity waves. With decreasing density the drag from momentum deposition increases with height. Thus, the maximum gravity wave drag may not describe the altitude at which most wave breaking is occurring and most momentum is deposited. Note that if we refer to gravity waves, we mean non-orographic gravity waves. The changes in the orographic gravity drag are minimal, likely due to modified propagation conditions caused by changed non-orographic gravity waves.

Figure 3.4a shows the zonally averaged non-orographic gravity wave drag (per unit mass) for the control experiment. The drag is averaged over 10 February to 12 March 2009. This period is chosen to include the strongest change of the vertical wind in Figure 3.3. The gravity wave drag is in general negative in the polar winter stratosphere and mesosphere, which means that westward momentum is deposited.

Figures 3.4b and 3.4c show the change in the non-orographic gravity wave drag caused by strengthening the gravity wave sources (due to the frontal or background source). If we increase the gravity wave sources, the altitude of the maximum gravity wave drag drops. However, the actual altitude of the maximum differs between both experiments and is slightly higher for the 'strong background' - experiment (0.06 hPa) than for the 'front on' - experiment (0.1 hPa). In contrast, if we weaken the background source, the altitude of the momentum deposition is shifted upward compared to the control experiment to 10^{-4} hPa (see Figure 3.4d). This result agrees well with the enhanced downwelling near 10^{-4} hPa in Figure 3.3c. The upward shift of the gravity wave drag maximum for a weak background source remains valid also under undisturbed conditions (not shown).

Analogous to the gravity wave forcing, we now analyze the resolved wave forcing as diagnosed by the Eliassen-Palm (EP) flux divergence (see Figure 3.5). Several studies highlighted the strong interplay of gravity waves and resolved waves, especially after a SSW (e.g., Limpasuvan et al. 2016). Hence, the transfer of momentum from resolved waves to the mean circulation should be taken into account. Resolved waves exert an easterly force on the zonal mean flow throughout most of the winter middle atmosphere (see Figure 3.5a). The strongest westward force occurs in the mid-latitudes in the upper mesosphere. Above the mesopause a strong deposition of eastward mo-
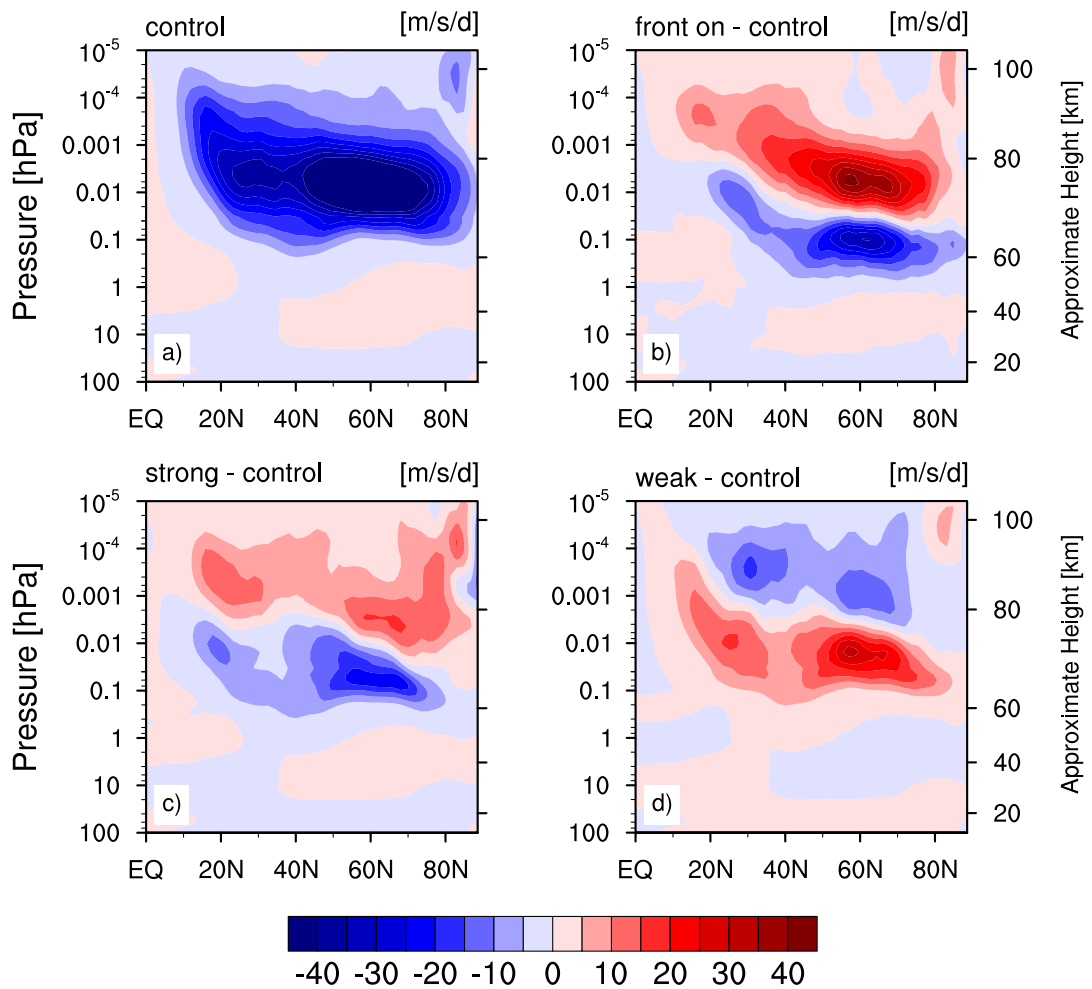
Figure 3.4. Non-orographic gravity wave drag [m/s/d] for 10 February to 12 March 2009 for (a) control experiment. Differences to the control experiment are given for (b) front on, (c) strong background and (d) weak background. The contour interval is 5 m/s/d.
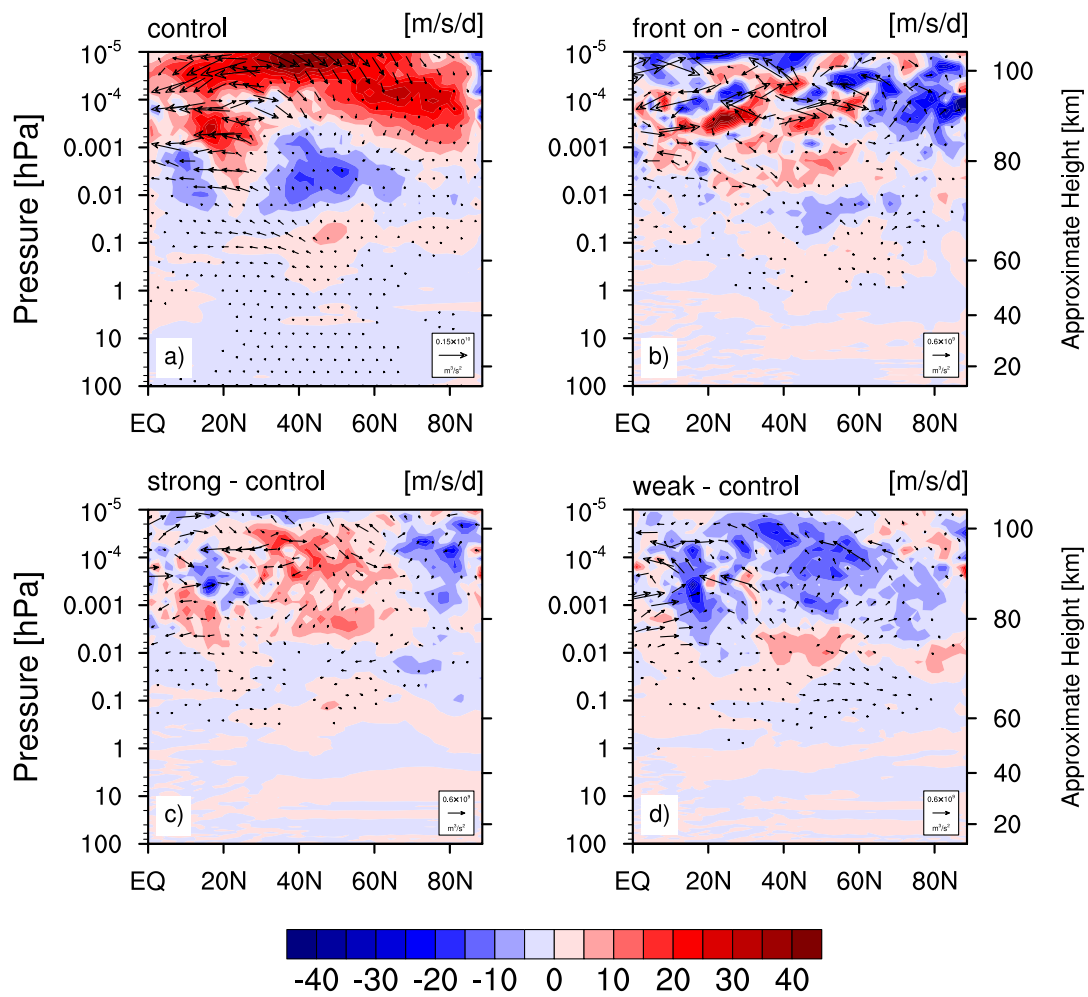
Figure 3.5. As in Figure 3.4 but for the resolved wave drag associated with the Eliassen-Palm (EP) flux divergence (contours) [m/s/d]. The EP flux [m^3/s^2] scaled by density is depicted by arrows. The contour interval is 5 m/s/d. Arrows smaller than 1.7×10^7 m^3/s^2 are not shown.

mentum is evident. Figures 3.5b and 3.5c show the changes in the EP-flux divergence by strengthening the gravity wave sources. In those cases, the EP-flux divergence is reduced in the high latitudes near 10^{-4} hPa, while at mid-latitudes near the mesopause resolved waves tend to reduce the deceleration. In contrast, by weakening the gravity wave sources, the EP-convergence is enhanced above 0.001 hPa (see Figure 3.5d). This is at a similar height, at which the gravity wave forcing peaks for the 'weak background' case.

Figure 3.6a shows vertical profiles of the vertical residual wind (w^*). The height of the strongest downwelling is shifted upward to the upper mesosphere for a weaker background source, while for the 'front on' case the vertical wind peaks in the lower mesosphere. Via the downward control principle (Haynes et al. 1991),we split w^* into contributions of different wave forcings (see Figures 3.6b and 3.6c). The overall agreement between the directly computed w^* (black line) and the estimate for w^* from the total wave forcing (green line) demonstrates the validity of the downward control estimates. The individual contributions reveal that the downwelling is almost entirely driven by the non-orographic gravity waves, which is consistent with McLandress et al. (2013). If we weaken the gravity background source, the downwelling in the upper mesosphere (up to 10^{-4} hPa) strengthens compared to the control experiment (see Figure 3.6c). Again, the differences between the control experiment and the 'weak background' experiment are mainly due to differences in the non-orographic gravity waves. However, in the upper mesosphere and lower thermosphere resolved waves contribute equally to the strengthening of the vertical wind. Hence, resolved waves amplify the enhanced downwelling caused by gravity waves.

We conclude that the altitude at which momentum is deposited by gravity waves in the upper mesosphere has a strong impact on the mesospheric transport. Resolved waves amplify the gravity wave forcing in the recovery phase of a SSW. Even if most momentum is deposited at a much lower altitude (not shown), the momentum deposited in the upper mesosphere is crucial for the mesospheric transport. A deposition of momentum at a higher altitude extends the downwelling branch of the meridional circulation to a higher level (see Figure 3.6a). Then advection may become the dominant transport process in the lower thermosphere (Meraner and Schmidt 2016), where NO_x is frequently produced by energetic particle precipitation. The downwelling extends upward to the height of the strongest NO_x gradient, and hence, more thermospheric NO_x is transported downward to the lower mesosphere and upper stratosphere. Differences in the gravity wave sources may also influence the contribution of eddy diffusion for the transport to the mesosphere. However, Meraner and Schmidt (2016) showed that during a SSW the downward transport through the mesopause region is dominantly driven by advection. Even with a doubled eddy diffusion coef-
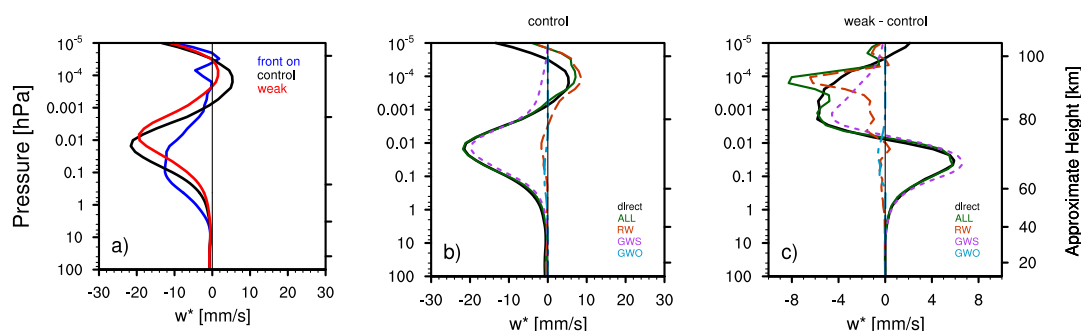
Figure 3.6. (a) Vertical profile of the residual vertical velocity (w^*) [mm/s] averaged between 60° N and 90° N for 10 February to 12 March 2009 for three experiments: control (black), front on (blue), and weak background (red). (b) Corresponding downward control estimates of the residual vertical velocity in the control experiment computed by using the total wave forcing (green, solid line), only the orographic wave drag (cyan, dash-dotted), only the non-orographic wave drag (purple, short-dashed) and only the resolved wave drag (orange, long-dashed). (c) Differences of the downward control estimates of w^* between the weak background and control experiments are given.

ficient, eddy diffusion has limited impact on the thermospheric transport after a SSW in their experiments. Here, changing the gravity wave sources leads to an increase of the eddy diffusion coefficient by only up to a factor of 1.2 (1.7) compared to the control (front on) experiment.

The deposition of horizontal momentum by gravity waves can be modulated by two factors: changes in gravity wave source parameters and changes in the characteristics of the environment in which the waves propagate. Gravity waves break either because the wave amplitude becomes too big and unstable or because the phase speed matches the actual wind speed (critical-level filtering). Without changes in the gravity waves, the atmospheric conditions (i.e., the characteristics of the medium) would be very similar for all experiments due to the nudging. However, the gravity wave sources are substantially modified in our experiment by changing the total wind variance (i.e., σ^2).

To understand the changes of the gravity wave drag, we analyze the total wind variance (i.e., the wave amplitude) averaged over the polar cap (60° N - 90° N) for three HAMMONIA experiments: control (black), front on (blue), and weak background (red) (see Figure 3.7). Note that we averaged over the polar cap, thus, locally the total wind variance might be bigger. Substantial filtering by tropospheric winds between the launching height and 500 hPa can explain the relatively small total wind variance at 100 hPa (Charron and Manzini 2002).

The wave amplitude of gravity waves strongly increases from the launching level until 0.1 hPa. This can easily be explained by the fact that without dissipation, the
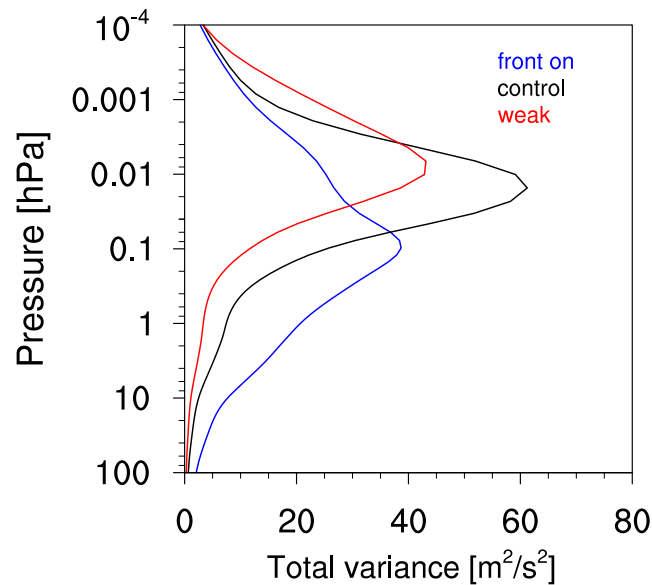
Figure 3.7. Total gravity wave wind variance [$m^2\ s^{-2}$] on 18 February 2009 averaged between $60°$ N and $90°$ N for three experiments: control (black), front on (blue), and weak background (red).

wave amplitude is inversely proportional to the density. The initial total wind variance of gravity waves excited from fronts is greater than the amplitude of gravity waves from the background. Hence, the altitude at which the gravity wave spectrum becomes unstable and breaks into turbulence is lower with gravity waves emitted from fronts than in the control experiment. This conforms to the results of Charron and Manzini (2002). Gravity waves emitted from fronts are parameterized in a way that their propagation direction is perpendicular to the tropospheric wind associated with the front. This reduces the critical-level filtering in the troposphere and facilitates the penetration of gravity waves emitted from fronts in the stratosphere (Charron and Manzini 2002). The total variance of the gravity waves emerging from fronts is small at 0.001 hPa, because most of the transported horizontal momentum is already deposited at a lower altitude.

A similar reasoning applies if we weaken the background source. The total variance at the launching level is reduced compared to the control experiment. Hence, the altitude at which the wave amplitude becomes unstable is higher for a weak background source than in the control experiment. The total variance peaks in this experiment at the highest level of all four experiments. Thus, the small wave amplitude at launching level facilitates the penetration of gravity waves to a higher altitude in the upper mesosphere, where they deposit their momentum, which in turn enhances the mesospheric

descent. However, we cannot exclude an impact of the critical-level filtering, because changes in the breaking conditions feed back on the propagation conditions of gravity waves.

We strengthen the gravity wave sources in two ways by either increasing the background or the frontal source. Compared to the control experiment, both cases show a qualitatively similar behavior (e.g., momentum deposition at a lower level in the upper mesosphere). Even if the mean strength of the gravity wave forcing may be the same, it turned out that the momentum flux reaching the middle atmosphere is larger when gravity waves from fronts are present (Charron and Manzini 2002). This is caused by the reduced critical-level filtering in the troposphere for gravity waves induced by fronts. Additionally, fronts depend on the actual dynamical conditions in the troposphere, and hence, the impact of gravity waves excited by fronts may vary with season and geography.

3.3.3 Sensitivity of Zonal Wind and NO$_x$ Transport to Gravity Wave Sources in Free-Running Simulations

In the following, we analyze the impact of differences in the gravity wave parameterization in a free-running model. Modifying the gravity wave sources, of course, affects not only the tracer transport but also the mean circulation. However, tropospheric and stratospheric dynamics are constrained to reanalysis data in the nudged simulations. The free-running simulation enables us (1) to estimate the influence of differences in the gravity wave sources on the mean circulation and (2) to assess to which extent the effects on the tracer transport may be specific for the meteorological condition of 2009. We performed two simulations which correspond to the nudged experiments 'front on' and 'weak background'. Those extreme cases are chosen to obtain a large signal to noise ratio. Note that we set up the free-running simulations in a way which facilitates the comparison with the nudged simulations (i.e., we annually repeat boundary conditions valid for the period from June 2008 to May 2009). This setup favors the generation of SSWs, which are in total 61 for the 'front on' and 50 for the 'weak background' experiment.

Figure 3.8 shows the zonal mean zonal wind of both simulations compared to Modern-Era Retrospective Analysis for Research and Applications (MERRA) (Rienecker et al. 2011) reanalysis data. An average of 37 years (1979–2015) is used for the reanalysis data and of 49 years for the HAMMONIA simulations. The main characteristics (e.g., the subtropical jets) are well reproduced in both simulations. However, some differences emerge between the model simulations and MERRA. For the 'front on' experiment, the stratospheric maximum of the eastward wind in the Northern Hemisphere is confined between the Equator and 60° N, while in the reanalysis data
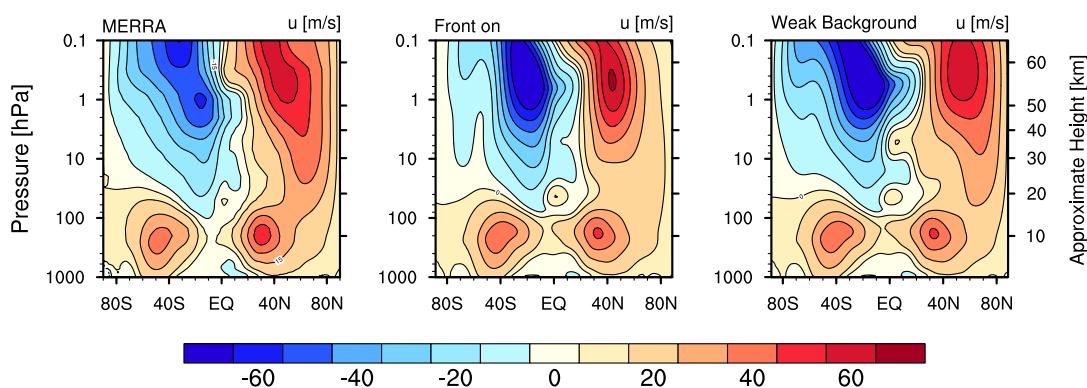
Figure 3.8. Zonal mean zonal wind averaged over December–February (DJF) for (a) MERRA reanalysis and two free-running simulations (b) with gravity waves from fronts and a medium background ($\sigma = 0.8$ m/s) and (c) with a weak background ($\sigma = 0.6$ m/s) and no frontal source. The mean over 1979–2015 is used for MERRA and the mean over 49 years for both HAMMONIA simulations. The contour interval is 10 m/s.

the maximum in the eastward wind extends to the winter pole. Similarly, the westward wind in the Southern Hemisphere is limited to lower latitudes compared to MERRA. For the 'weak background' experiment, the maximum in the eastward wind expands from the Equator to the winter pole and reaches near the pole to a lower altitude than the 'front on' experiment. Both characteristics are consistent with the reanalysis data. The westward wind in the Southern Hemisphere is tilted toward the summer pole spanning from the Equator to the pole, which agrees very well with MERRA. Considering the large number of SSW in the 'weak background' experiments, the magnitude of the eastward wind in the Northern Hemisphere agrees surprisingly well with the reanalysis data. However, HAMMONIA tends to overestimate the strength of the lower meospheric eastward jet during quiet times (i.e., months without a SSW) (not shown). The large number of SSW weakens the eastward wind bringing it closer to the wind magnitude simulated by MERRA. Overall, the 'weak background' experiment reproduces a more realistic structure of the zonal mean zonal wind and shows a better agreement with MERRA reanalysis data than the 'front on' experiment.

Now we evaluate if changes in NO_x transport persist in the free-running simulations (see Figure 3.9). In the Southern Hemisphere, differences in NO_x amounts are small between both free-running HAMMONIA simulations. While the Northern Hemispheric meridional gradient is weak in the 'front on' experiment, the polar NO_x concentrations in the 'weak background' experiment increases by more than 200% near 0.1 hPa compared to the 'front on' experiment. The increase of NO concentration in the mesosphere results from enhanced downwelling near 0.001 hPa (not shown). The higher NO_x concentrations in the mesosphere for a weak background and no frontal source is consistent with the changes in the nudged simulations. This result agrees also with
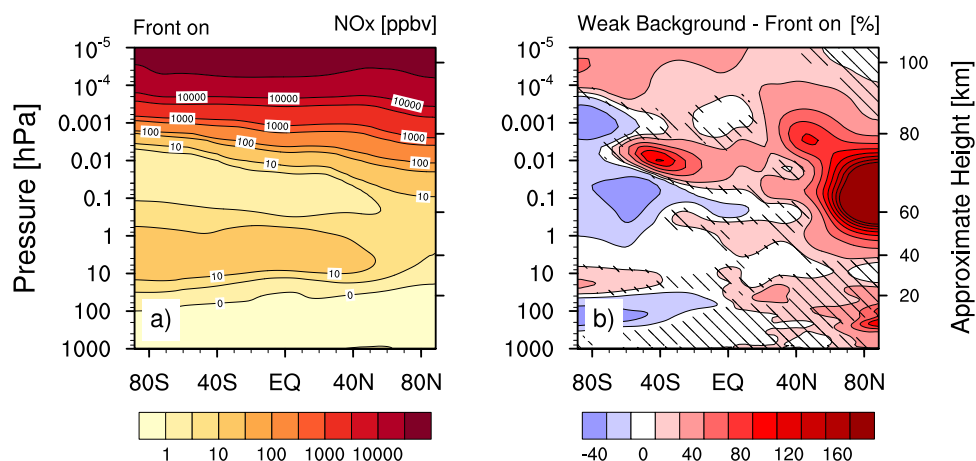
Figure 3.9. (a) Zonal mean NO_x volume mixing ratio averaged over December–February (DJF) for the free-running simulation 'front on'. (b) Difference in zonal mean NO_x volume mixing ratio (DJF) between two free-running simulations (weak background - front on). Shaded areas are not significant at the 95% confidence interval. The mean over 49 years is used.

McLandress et al. (2013), who found that non-orographic gravity waves cause a strong descent of CO under undisturbed conditions.

Both simulations produce different dynamical responses, e.g., number of SSWs. Thus, one may ask if the simulated effects on the NO_x transport is related to the vertical extension of the downwelling as in the nudged simulations or could be influenced by the higher frequency of major SSWs in the 'front on' experiment. We tested this by comparing the NO_x transport excluding all months in which a major SSW occurs (not shown). The increase in NO_x concentrations occurs similarly for this subset of months and we conclude that the effects of changed gravity wave sources on the tracer transport are not only specific for the meteorological condition of 2009. Additionally, we have only looked at a subset of climatological changes (i.e., zonal wind and NO_x concentrations), while other aspects may also vary. For example, the winter (summer) mesopause warms (cools) by about 5 K in the 'weak background' experiment compared to the 'front on' experiment (not shown). Compared to the lidar measurements of Lübken and Zahn (1991), the winter (summer) mesopause in HAMMONIA is general too cold (warm). However, the changes induced by weakening the background source bring the mesopause in HAMMONIA closer to the observations.

3.4 Summary and Conclusion

In this study, we analyzed the impact of parameterized non-orographic gravity wave sources on the simulated transport of nitrogen oxides (NO_x) in the polar winter meso-

sphere. Simulations with the general circulation and chemistry model HAMMONIA were carried out in both nudged and free-running simulations mode. We analyzed differences in a homogeneous background source and in a source related to frontal activity.

Recent studies showed that parameterized non-orographic gravity waves drive the middle atmospheric dynamics after a sudden stratospheric warming (SSW) event (e.g., the descent of the elevated stratopause, the downward transport of tracers) (McLandress et al. 2013; Ren et al. 2011; Siskind et al. 2010). Following their analysis we found that the transport of NO_x is highly sensitive to differences in non-orographic gravity waves. Compared to a control simulation, we either strengthen the gravity wave sources (i.e., an increase of the wave amplitude) by switching on the emission of gravity waves from fronts or by increasing the background source or weaken the background source. Strengthening the gravity wave sources (frontal or background source) reduces the transport of NO_x to the mesosphere after the SSW and leads to a quicker descent of the elevated stratopause to its climatological altitude. If we weaken the background source, the transport of NO_x after the SSW is enhanced and the elevated stratopause stays longer at a higher altitude. This result may seem counterintuitive as gravity waves are considered as the key driver of downwelling in the winter mesosphere. One might assume that more wave activity would strengthen the downwelling and, hence, the tracer transport. However, in our experiments the amount of NO_x transported downward is controlled by the altitude of the largest gravity wave drag and hence by the vertical extent of downwelling. In the upper mesosphere and lower thermosphere resolved waves strongly contribute to the strengthening of the vertical wind. In other words, resolved waves amplify the enhanced downwelling originally caused by gravity waves. With weaker gravity waves the maximum in the gravity wave drag is shifted upward leading to the strongest transport in all of our simulations. This results from the smallest total variance at launching level used in all simulations, because the level at which the wave amplitude becomes unstable is then highest. Our findings extend the diagnosis of the sensitivity of the circulation to the breaking height to the upper mesosphere, as discussed in the context of the gravity waves from fronts by Charron and Manzini (2002). Our results agree with McLandress et al. (2013), who showed that the downwelling under undisturbed conditions in an experiment with only non-orographic gravity waves (i.e., with weak gravity wave sources) is two times stronger than in a control run.

In line with Siskind et al. (2015) we show that simulations with a free-running mesosphere have among others deficits in simulating a realistic gravity wave drag in the upper mesosphere. They suggested that a weak mesospheric transport is produced by an underestimated non-orographic gravity wave drag. However, our main result

is that not only the magnitude of the drag but also its altitude distribution are key to transporting NO_x downward. Both parameters can be manipulated via tuning the gravity wave sources. We have shown that a reduction of the gravity wave amplitude at source level leads to an increased momentum deposition in the upper mesosphere and, hence, to an increased (and in our case a fairly realistic) downward transport of NO_x.

We now briefly discuss the implications of our study. First, for the proper estimation of the indirect effect of energetic particle precipitation, i.e., circulation effects of NO_x produced in the lower thermosphere and transported downward during polar night, a realistic simulation of this transport is necessary in addition to a realistic representation of energetic particle sources. The underestimation of the transport in earlier modeling studies may be reduced through a reduction of parameterized gravity wave sources.

Second, due to the high uncertainty in observed momentum flux the gravity wave parameterization cannot be constrained by direct observations. The need to adjust parameters in the models may provide the opportunity for an indirect constraint of gravity wave sources. McLandress et al. (2013) have suggested simulations of the downward transport for this purpose, as used here. Our simulations suggest that the magnitude of gravity wave sources may be less than assumed in earlier simulations. However, we cannot exclude that the vertical shift of the gravity wave maximum which influences strongly the downward transport of NO_x may be reached by other ways of tuning the parameterization, e.g., the launching level or cutoff wave number. In a similar sense, parameters of the frontal gravity wave source may be tuned, which may lead to a higher momentum deposition in the mesosphere. We are not implying that more realistic gravity wave parameterizations (e.g., including effects from fronts) lead to less realistic simulations of mesospheric transport in general. It is possible that in our case the exclusion of specific frontal sources leads to an improvement via compensation of errors. More complex gravity wave parameterization (e.g., considering lateral propagation of waves) may have a different impact on the simulated transport. Improved attempts to observe gravity waves from satellite as suggested by Geller et al. (2013) seem still key for a better quantification and a more realistic parameterization of their effects.

Finally, this study concentrated on the Northern Polar winter, but changing gravity waves affects, of course, also other regions (e.g., Tropics or Southern Hemisphere). In our first set of simulations, the dynamics of the troposphere and stratosphere were prevented to strongly drift apart by the nudging. Free-running simulations show a substantial change in the zonal wind due to differences in gravity wave sources. For an experiment with a weak background and no frontal source, the stratospheric zonal

wind extends in both hemispheres further to the pole, which is consistent with MERRA reanalysis data. Furthermore, higher NO_x concentrations in the polar mesosphere for this experiment agree with the results of the nudged simulations. Hence, nudged and free-running simulations highlight the importance of momentum deposition in the upper mesosphere for a realistic NO_x transport.

Short summary of Chapter 3:

- Weakening non-orographic gravity waves enhances the mesospheric transport of NO_x.

- The strengthening of the vertical wind is amplified by resolved waves.

- The altitude at which momentum is deposited is crucial for the downward transport.

Climate Impact of a Mesospheric and Stratospheric Ozone Loss due to Energetic Particle Precipitation

4

Energetic particles enter the polar atmosphere and enhance the production of nitrogen oxides and hydrogen oxides in the winter stratosphere and mesosphere. Both components are powerful ozone destroyers. Recently, Andersson et al. (2014) showed that the direct effect of energetic particle precipitation(EPP) causes significant long-term mesospheric ozone variability. Satellites observe a decrease in mesospheric ozone by up to 34 % between EPP maximum and EPP minimum. Here, we analyze the climate impact of a mesospheric and a stratospheric ozone loss due to EPP in the coupled climate model MPI-ESM. To rule out potential additional forcings, the boundary conditions are fixed to preindustrial conditions. Using radiative transfer modeling, we find that the radiative forcing of a mesospheric ozone loss is negligible. Hence, the climate effects of a mesospheric ozone loss due to energetic particles proposed by Andersson et al. (2014) seem unlikely. A stratospheric ozone loss due to energetic particles cools the winter polar stratosphere and subsequently weakens the polar vortex. However, those changes are small, and no statistically significant changes in the air surface temperature are found.

4.1 Introduction

Energetic particles enter the Earth's atmosphere at the pole altering the chemistry of the middle and upper atmosphere. Energetic particle precipitation (EPP) is the major source of nitrogen oxides (NO_x) and hydrogen oxides (HO_x) in the polar middle and upper atmosphere (Crutzen et al. 1975; Solomon et al. 1981). Both chemical components catalytically deplete ozone; NO_x mainly below and HO_x mainly above 45 km.

Whereas HO_x is short-lived in the middle atmosphere, NO_x persists up to several months in the polar winter middle atmosphere. Inside the polar vortex, NO_x can be transported downward from its origin region in the lower thermosphere to the stratosphere where it affects ozone (Funke et al. 2007; Sinnhuber et al. 2014). Ozone loss potentially influences stratospheric temperature and the polar vortex. The Northern Annual Mode (NAM) index is often used to describe the strength of the polar vortex, with positive NAM values indicating a strong polar vortex and negative NAM

values indicating a weak polar vortex. Observations suggest that anomalous weather regimes associated with the NAM index can propagate from the stratosphere down to the surface (Baldwin and Dunkerton 2001). Hence, energetic particle precipitation may provide a link from space weather to the surface climate.

Commonly, the effects of EPP are classified into a direct and an indirect effect (Randall et al. 2007; Randall et al. 2006). The direct effect is the effect of the local production of NO_x and HO_x, whereas the indirect effect is the effect of the NO_x transport from the thermosphere to the stratosphere. As the local production of NO_x below 45 km is small, the direct effect is usually associated with the local production of HO_x in the mesosphere. Sinnhuber et al. (2014) showed that the indirect EPP effect in satellite observations exceeds the direct effect of even a very strong EPP event as the 'Halloween storms' in October and November 2003.

Here, we study the climate impact of an ozone loss due to EPP. Discussed are both a mesospheric and a stratospheric ozone loss.

The climate influence of ozone has been intensively studied. Shortly after the discovery of the ozone hole, it was realized that ozone has an impact on the stratospheric radiative equilibrium (e.g., Lubis et al. 2016; Randel and Wu 1999; Shine 1986). Most studies concentrated on the climate impact of the ozone hole during austral spring and reported a cooling in the Southern Hemispheric stratosphere and a strengthening of the polar vortex. In contrast, our study concentrate on an ozone loss during the Northern Hemispheric polar night. During polar night reduced ozone slightly decreases the longwave cooling of the polar stratosphere (i.e., a net stratospheric warming) (Graf et al. 1998; Langematz et al. 2003).

Several studies suggested a significant influence of EPP on the surface air temperature. Seppälä et al. (2009) analyzed surface temperature changes in reanalysis data for years with various strength of energetic particle precipitation. They found a warming over Eurasia and a cooling over Greenland, but could not physically link those changes to EPP. Moreover, they could not rule out that the estimated changes are induced by the NAM variability.

Other studies relied on atmospheric chemistry models (e.g., Arsenovic et al. 2016; Baumgaertner et al. 2011; Rozanov et al. 2005). Their estimated surface warming pattern is similar to Seppälä et al. (2009). Merely, they reported a cooling in the winter stratosphere due to EPP, whereas the radiative forcing of ozone suggests a warming(Graf et al. 1998). Baumgaertner et al. (2011) discussed that the stratospheric cooling is attributed to a dynamical heating induced by a decrease of the mean meridional circulation. A weaker meridional circulation affects the vertical wind leading to a weakened descending and, hence, an adiabatic cooling (Langematz et al. 2003). However, the dynamical heating has to our knowledge not been addressed for a latitudinal

confined ozone decrease before. All model studies have few simulation years and complex forcings in common. Instead of prescribing ozone, those studies considered EPP by changing the production of NO_x and HO_x (only Arsenovic et al. (2016)). This complicates the understanding of the atmospheric response due to the EPP induced ozone loss as transport processes are involved and ozone depletion occurs at different altitudes and times. Furthermore, Baumgaertner et al. (2011) and Rozanov et al. (2005) overestimated the NO_x production (Bailey et al. 2014; Randall et al. 2007). We use an idealized ozone forcing and a long simulation period.

Whereas most of the above mentioned studies discuss a mainly stratospheric ozone loss due to the indirect EPP effect, Andersson et al. (2014) suggested a potential climate influence of a mesospheric ozone loss due to the direct EPP effect. By using satellite observations they showed that HO_x causes long-term variability in mesospheric ozone up to -34 % between EPP maximum and EPP minimum. Arsenovic et al. (2016) were the first to include the direct effect of HO_x local production due to EPP in a chemistry-climate model. They found a similar mesospheric ozone loss as Andersson et al. (2014) and ultimately, reported a cooling over Greenland and a warming over Eurasia. Arsenovic et al. (2016) also considered the indirect effect of the NO_x descent. Hence, the impact of a mesospheric ozone loss only due to the direct EPP effect as suggested by Andersson et al. (2014) remains unclear.

This paper studies the climate impact of a mesospheric and a stratospheric ozone loss due to EPP. We use simulations with the Max Planck Institute Earth System Model (MPI-ESM) applying an idealized ozone forcing in either the mesosphere or the stratosphere. Additionally, we use a radiative transfer model to quantify the radiative forcing of ozone on different altitudes and months. Ultimately, we show whether an ozone loss in the middle atmosphere due to EPP has the potential to significantly alter the surface climate. Section 4.2 describes the MPI-ESM as well as the radiative transfer model. Section 4.3 links a mesospheric and stratospheric ozone loss to changes in the atmospheric temperature and wind changes. Finally, Section 4.4 summarizes and discusses the main outcomes and limitations of this study.

4.2 Models

4.2.1 MPI-ESM: The Max Planck Institute Earth System Model

The Max Planck Institute Earth System Model (MPI-ESM; Giorgetta et al. (2013)) consists of the coupled atmospheric and ocean general circulation models, ECHAM6 (Stevens et al. 2013) and MPIOM (Jungclaus et al. 2013) as well as of the land and vegetation model JSBACH (Reick et al. 2013) and of the model for marine bio-geochemistry HAMOCC (Ilyina et al. 2013). We use the 'mixed-resolution' configuration of the

model (MPI-ESM-MR). The ocean model uses a tripolar quasi-isotropic grid with a nominal resolution of $0.4°$ and 40 vertical layers. ECHAM6 is run with a triangular truncation at wave number 63 (T63), which corresponds to $1.9°$ in latitude and longitude. The vertical grid contains 95 hybrid sigma-pressure levels resolving the atmosphere from the surface up to $0.01\,\mathrm{hPa}$. The vertical resolution of $700\,\mathrm{m}$ is nearly constant from the upper troposphere to the middle stratosphere and less than $1000\,\mathrm{m}$ at the stratopause. The time steps in the atmosphere and ocean are 450 and $3600\,\mathrm{s}$, respectively.

The model has been used for many simulations within the CMIP5 (Coupled Model Intercomparison Project Phase 5) framework (Taylor et al. 2012). An overview of the dynamics of the middle atmosphere in these simulations is given by Schmidt et al. (2013). In this study, the preindustrial CMIP5 simulation (piControl) is used. The forcing is constant in time and uses pre-industrial conditions (1850 AD) for the greenhouse gases. Solar irradiance and ozone concentrations are averaged over a solar cycle (1844-1856 for the solar irradiance and 1850-1860 for ozone concentrations). No volcanic forcing is applied. A period of 150 years of this simulation is used.

In order to analyze the impact of ozone changes on the model climate, two additional experiments with reduced ozone concentration are carried out. In one experiment, the mesospheric ozone is reduced by $40\,\%$ between $0.01\,\mathrm{hPa}$ and $0.1\,\mathrm{hPa}$ and between $60°$ and $90°\,\mathrm{N/S}$ constant over time. In the other experiment, stratospheric ozone is reduced by $20\,\%$ between $1\,\mathrm{hPa}$ and $10\,\mathrm{hPa}$ and between $60°$ and $90°\,\mathrm{N/S}$ constant over time. In the following, we call the first experiment "meso-O_3" and the second "strato-O_3". Both experiments are forced by the same conditions as the piControl experiment. Moreover, the simulations are restarted from the piControl experiment. This ensures that the ocean is in phase for all three experiments and no additional forcing from the internal variability of the ocean is induced. For both simulations 150 years are simulated. Note that the applied ozone losses are larger than observations reported. We use the stronger forcing to obtain a clear signal from which to diagnose the sensitivity of the climate to an ozone loss due to EPP. However, this implies a potentially overestimated climate response.

4.2.2 The radiative transfer model PSrad

Additionally to the earth system model, the radiative transfer model PSrad (Pincus and Stevens 2013) is used to study the impact of ozone on the temperature. PSrad is a two-stream model that originates from the RRTM for GCMs (RRTMG) codes (Iacono et al. 2008; Mlawer et al. 1997). The shortwave and longwave components are organized in parallel. Optical properties for gases, clouds and aerosols are computed separately and then combined to compute heating rates.

PSrad expects profile of gases (H_2O, N_2O, CH_4, CO, O_3), profile of clouds as well as additional parameter (e.g., albedo and zenith angle) as input. For gases, we use multi-year monthly means representative for the late 20th century provided by the atmospheric and chemistry model HAMMONIA (Hamburg Model for Neutral and Ionized Atmosphere; Schmidt et al. (2006)). For the albedo and cloud properties (e.g., cloud fraction, cloud water/ice content), multi-year monthly means from the piControl experiment are used. The zenith angle is calculated for 12 UTC at $75°$ N $0°$ E for the 15th of each month. All quantities are extracted for $75°$ N. This latitude is chosen as it represents a mean polar latitude. The results are insensitive to the actual latitude, the main difference is the length of the polar night.

To quantify the impact of ozone on the temperature, we perform multiple runs in which for each single layer the ozone concentration is set to 0 once. The differences to a control run are then summed up.

4.3 Results

4.3.1 Climate Effects of a Mesospheric Ozone Loss

In the following, we analyze the climate effect of an idealized mesospheric ozone loss, while in Section 4.3.2 we analyze the climate effect of an idealized stratospheric ozone loss. Large variations in the stratospheric wind can propagate downward and affect the surface climate. We, first, study the middle atmospheric changes due to an ozone loss, which are a precondition for a potential climate impact of EPP.

Figures 4.1a – 4.1c show the zonal mean temperature simulated for boreal winter (December - February). The absolute values for piControl and meso-O_3 are shown in Figures 4.1a and 4.1b. Both experiments reproduce the main characteristics of the zonal mean temperature, e.g., the rising of the stratopause from the summer towards the winter pole. In most regions, the difference between both experiments is very small (see Figure 4.1c). The summer mesosphere is cooler in meso-O_3 than in piControl. However, the cooling is confined to the upper mesosphere, i.e., the region where ozone is reduced. A mesospheric ozone loss in summer, hence, does not influence lower altitude regions. At the winter pole, a mesospheric ozone loss has a different influence on the temperature. A dipole structure emerges with a warming in the stratosphere and a cooling in the lower mesosphere. However, those differences are not significant at the 95 % confidence interval. Moreover, no change is evident in the region where ozone is actually lost (0.01 - 0.1 hPa). In austral winter, the changes are even smaller and not significant (not shown).

Note that with fewer simulation years apparently very different results can be obtained. Using different simulation periods the mesosphere significantly cools or

warms. Particularly, we found a statistically significant weakening of the polar vortex if we only use 80 simulation years. The reason therefore is that the winter stratosphere exhibits a high degree of internal variability. The most dramatic demonstration of this variability are sudden stratospheric warmings (SSW), which occur on average about 6 times per decade in the Northern Hemisphere (see Chandran et al. (2014) for more information on SSW). A short simulation period may lead to a over-representation or under-representation of SSWs. We would like to raise the awareness to be cautious with few simulation years. Over our whole simulation period (150 years) the number of SSWs is balanced in all three experiments. In total, there are 102 events in piControl, 103 events in meso-O_3 and 105 events in strato-O_3.

Figures 4.1d – 4.1f show the zonal-mean zonal wind for boreal winter. The climatological structure of easterlies in the summer middle and upper atmosphere and westerlies in the winter middle and upper atmosphere is simulated by both experiments. In the summer mesosphere, the zonal wind statistically significantly strengthens (see Figure 4.1f). This change is confined to the altitude and latitude region in which the ozone forcing is applied (60° S - 90° S and 0.01 - 0.1 hPa). No influence to lower altitudes is seen. However, we would not expect the signal to reach the surface in summer. At the winter pole, the polar vortex weakens; however, this difference is not significant. As stated above, large variation in the winter polar vortex can propagate to the surface influencing the surface climate. However, the changes reported here are too small to propagate downward. Indeed, the surface temperature reveal no statistically significant change (not shown).

Signals are not statistically significant even after 150 simulated years. Nevertheless, it makes sense to analyze if the signals could have a physical explanation and not be purely accidental. Therefore we now study the applied ozone forcing. By reducing ozone in the mesosphere, we induce a direct temperature forcing. Figure 4.2 shows the difference in the heating rates between meso-O_3 and piControl. The heating rates are taken for the first time step of the model at which the radiation is updated (1 January). Hence, the changes in the heating rates describe the direct radiative forcing induced by the ozone loss excluding any feedbacks occurring only at later time steps. The absolute difference is shown in Figures 4.2a – 4.2c and the relative difference in Figures 4.2d – 4.2f.

In the shortwave part of the spectrum, ozone strongly absorbs solar radiation and heats the atmosphere. A loss in ozone leads to reduced heating of the summer mesosphere by up to 0.5 K/day (15%) (see Figures 4.2a and 4.2d). This agrees very well with the cooling of the summer mesosphere seen in Figure 4.1c. In the winter hemisphere, only a small part is sunlit. The cooling induced by reduced shortwave absorption vanishes poleward of the terminator. The radiative effect of ozone in the longwave
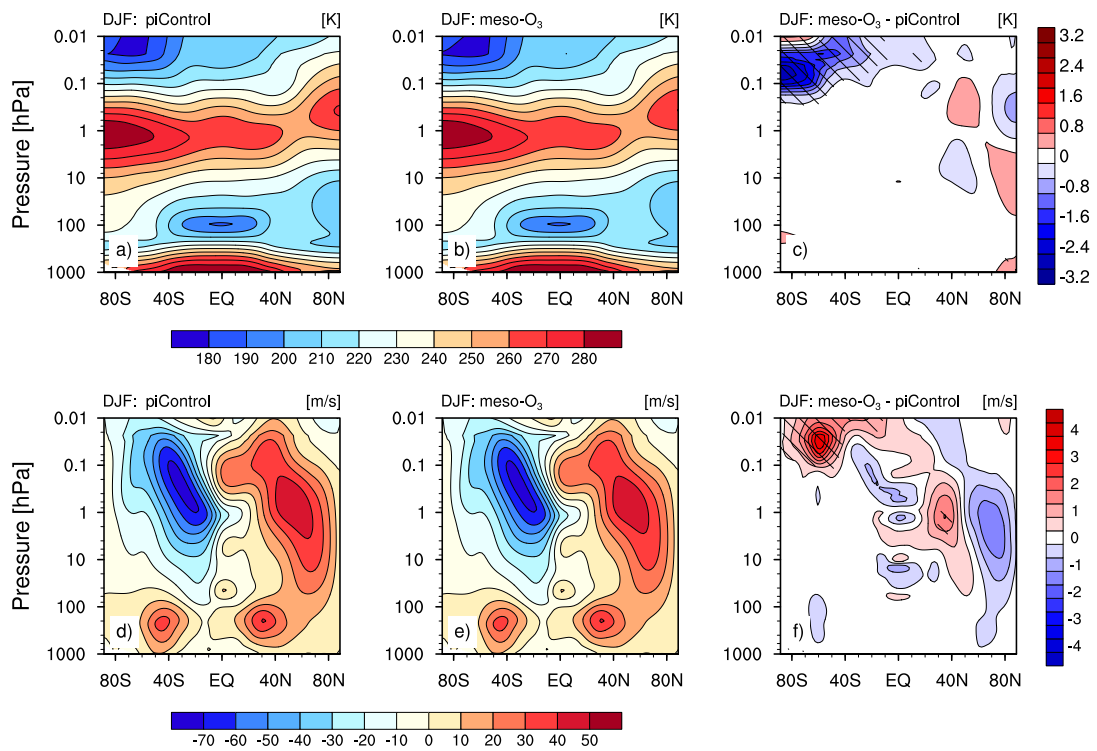
Figure 4.1. (upper row) Zonal mean temperature [K] and (lower row) zonal mean zonal wind [m/s] averaged over December - February (DJF) for the simulations (a,d) piControl, (b,e) meso-O$_3$ and (c,f) their difference. Shaded areas are statistically significant at the 95 % confidence interval.
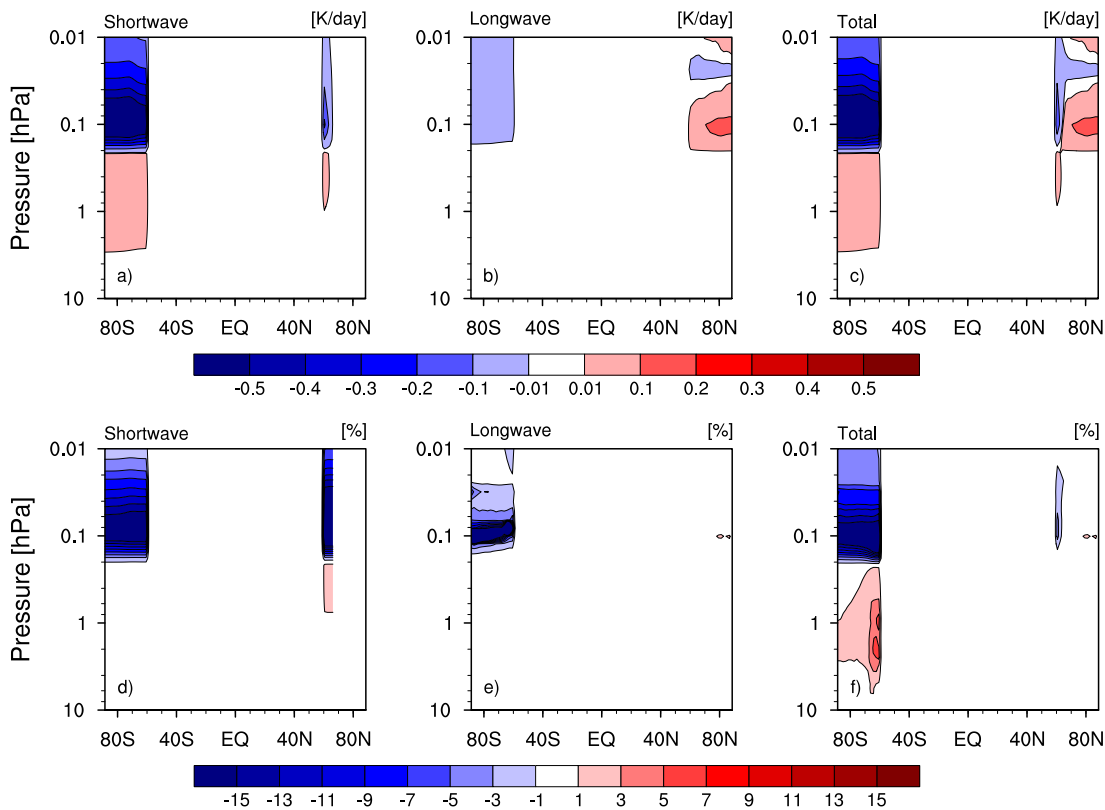
Figure 4.2. Zonal mean heating rates [K/day] for the first timestep of the simulation (1 January) for (a,d) shortwave, (b,e) longwave and (c,f) total (shortwave + longwave). The difference between meso-O_3 and piControl is shown. Upper row shows absolute difference and lower row shows relative difference.

part of the spectrum is highly temperature dependent. In the summer mesosphere, where temperature are very low, an ozone loss leads to a cooling (see Figures 4.2b and 4.2e). Generally, in this region, ozone absorption exceeds ozone emission heating the summer mesosphere. Less ozone, hence, leads to less longwave absorption and to a relative cooling. However, this cooling is very small (below 0.01 K/day) compared to the shortwave cooling. In total, the net radiative heating in the summer mesosphere is dominated by the shortwave cooling due to reduced absorption (see Figures 4.2c and 4.2f). In the warmer winter mesosphere, ozone generallyhas a net cooling effect due to longwave emission. Hence, an ozone loss results in a relative warming in the winter mesosphere. As the shortwave net cooling only affects the small, sunlit part of the high latitudes, the longwave net heating dominates the net total heating rate in the winter mesosphere. However, in the climatological mean the mesosphere cools (see Figure 4.1c). Indeed, compared to the heating rates of piControl the radiative forcing in the winter mesosphere is very small (below 2%). This also explains the low significance of the polar winter temperature and wind responses (see Figures 4.1c and 4.1f).

Figure 4.2 describes only the changes in the heating rate for 1 January, whereas ozone depletion due to energetic particle precipitation may occur during all the winter. This may change the radiative forcing. We use the radiative transfer model PSrad to analyze the radiative forcing of ozone throughout the year for 75° N (see Figure 4.3). This latitude was chosen as it represents a mean polar latitude. The results are insensitive to the actual latitude, the main difference is the length of the polar night (see Section 4.2.2 for more details how the radiative forcing of ozone is calculated). While Figure 4.2 describes the influence of an ozone loss, Figure 4.3 describes the influence of ozone on heating rates (i.e., where ozone heats or cools the atmosphere).

As expected, in the shortwave, ozone heats the atmosphere via absorption of solar radiation (see Figure 4.3a). The strongest heating occurs at the altitudes of the ozone maximum. An ozone loss would, hence, result in a relative cooling due to reduced heating. This agrees with Figure 4.2a. However, while Figure 4.2 only shows the shortwave cooling due to an ozone loss in the mesosphere, we can now argue that this is also true for the whole atmosphere (including the stratosphere). In the longwave, ozone cools the atmosphere via longwave emission in the stratosphere and in the mesosphere below 0.1 hPa (see Figure 4.3b). The strongest cooling occurs at the stratopause, i.e., the region where the atmospheric temperature is highest. In the troposphere, the absorption of outgoing radiation exceeds the longwave emission leading to a heating of the atmosphere. Above 0.1 hPa, the radiative forcing of ozone is divided into a winter and a summer response. Whereas in summer ozone heats the atmosphere, in winter ozone cools the atmosphere. As the stratopause rises towards the winter, the longwave emission exceeds the longwave absorption because the longwave radiation is highly temperature dependent. An ozone loss above 0.1 hPa would lead to a cooling in the summer and a warming in the winter. This again agrees with Figure 4.2b.

In total, the shortwave heating dominates all sunlit months. During polar night, the atmosphere cools due to ozone from 0.1 to 100 hPa. In November and February, the net influence of ozone is more complex: At some altitudes ozone heats and at some it cools the atmosphere. The net radiative forcing of an ozone loss depends on when and where ozone is reduced. A late winter mesospheric ozone loss leads to a mesospheric cooling, whereas an early winter mesospheric ozone loss leads to a mesospheric warming (not shown). However, both effects are small (± 1 K at 0.1 hPa) and cancel each other out resulting in a very small (not significant) change in boreal winter (see Figure 4.1c).

4.3.2 Climate Effects of a Stratospheric Ozone Loss

In this section, we analyze the climate effect of an idealized stratospheric ozone loss. On the basis of Figure 4.3 we can study the radiative forcing of ozone in the strato-
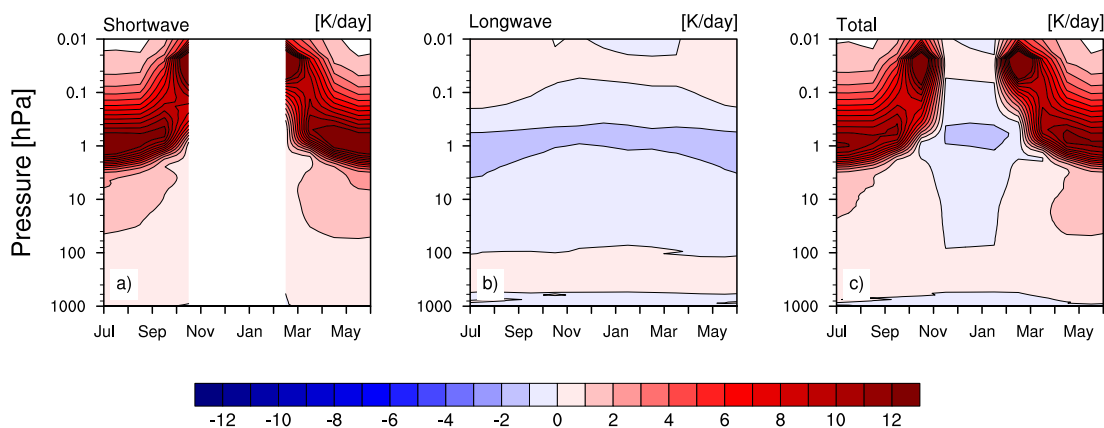
Figure 4.3. Monthly mean heating rates [K/day] for 75° N calculated by the radiative transfer model PSrad for (a) shortwave, (b) longwave and (c) total (shortwave + long-wave).

sphere. Stratospheric ozone heats the atmosphere in the shortwave and cools it in the longwave for all months. In total, ozone cools the stratosphere during polar night, while in all other months ozone mainly heats the stratosphere. Hence, an ozone loss would result in a warming during polar night and in a cooling in all other months. However, the forcing in the winter stratosphere is small (about 10% of the total heating rate) (not shown).

Figure 4.4 shows the zonal mean temperature and zonal wind simulated for boreal winter (December - February) for piControl, strato-O_3 and their difference. The winter stratosphere warms due to an ozone loss as expected from Figure 4.3. While the stratospheric warming is not significant in boreal winter, the warming is slightly significant in austral winter (not shown). Consequently, the polar vortex weakens. The mesospheric cooling may result from enhanced westward momentum deposition from gravity waves (not shown).

In summer, the stratosphere significantly cools in both hemispheres as expected due to the reduced shortwave heating. The mesospheric temperature response may again be dynamically induced; an enhanced eastward momentum deposition from gravity waves may lead to an adiabatic warming in the mesosphere.

Figure 4.4 shows only changes for the mean over December to February, while the radiative transfer model suggests that the monthly variability is large. To study whether the impact of a stratospheric ozone loss differs over the course of the winter, we analyze the monthly means of temperature and zonal wind (see Figure 4.5). An ozone loss during polar night leads to a stratospheric warming, whereas in all other months it leads to a cooling. This agrees with the calculations of the radiative transfer model. The winter warming is small and not significant, whereas the cooling is large and significant. Simultaneously with the warming (cooling), the polar wind weak-
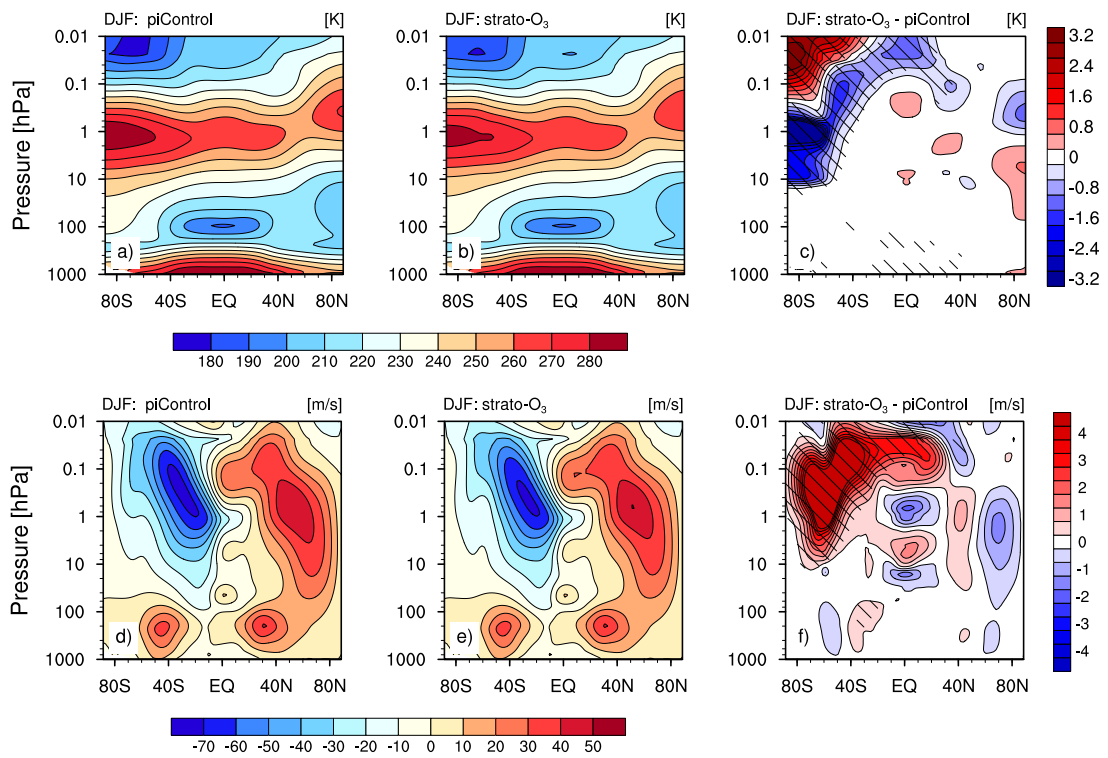
Figure 4.4. (upper row) Zonal mean temperature [K] and (lower row) zonal mean zonal wind [m/s] averaged over December - February (DJF) for the simulations (a,d) piControl, (b,e) strato-O$_3$ and (c,f) their difference. Shaded areas are statistically significant at the 95 % confidence interval.
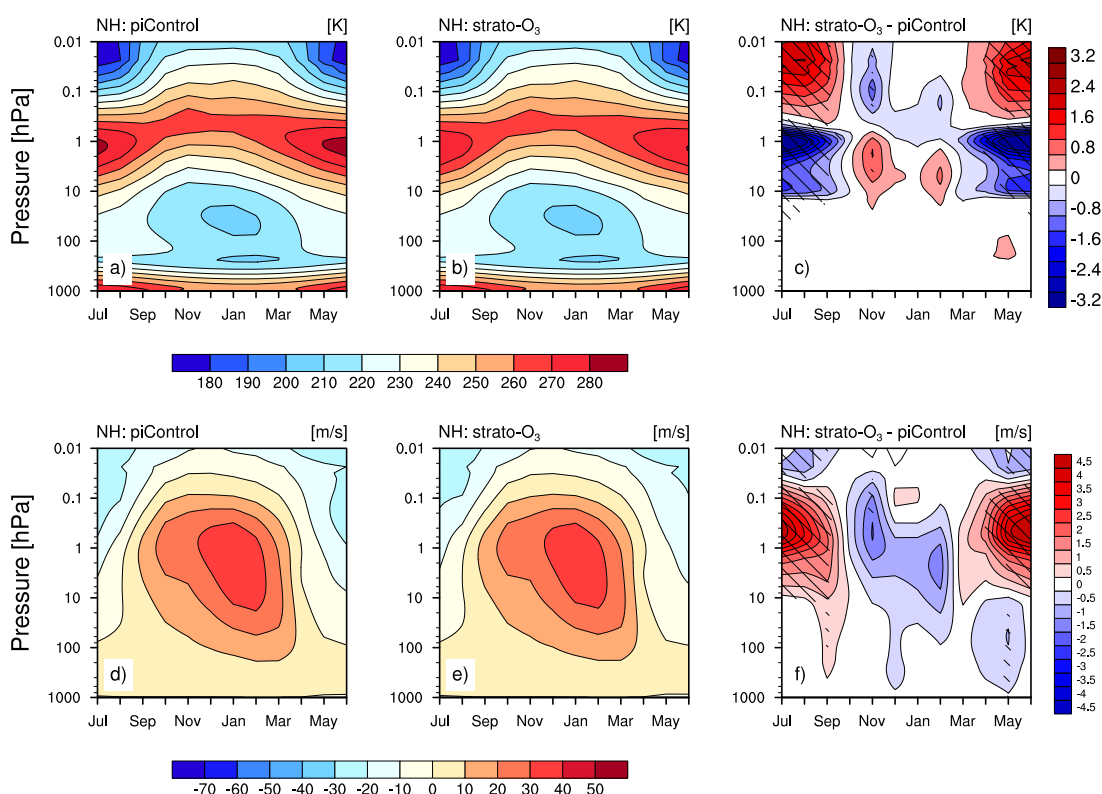
Figure 4.5. Monthly mean (upper row) temperature [K] and (lower row) zonal wind [m/s] averaged between 60° N and 90° N for the simulations (a,d) piControl, (b,e) strato-O_3 and (c,f) their difference. Shaded areas are statistically significant at the 95 % confidence interval.

ens (strengthens). Changes in the polar vortex occasionally reach the surface (e.g., the strengthening in September or the weakening in December or May). However, those changes are not significant.

Some disturbances in the polar vortex may still reach the surface and force the surface temperature (see Figure 4.6). In boreal winter, stratospheric ozone loss cools large parts of the northern high latitudes from northern Europe to Eurasia and over northern America. Over Greenland and the pole, the surface warms. This pattern is similar to a negative Northern Annual Mode response. However, most changes are small and not significant.

4.4 Summary and Conclusion

In this study, we analyzed the climate impact of a mesospheric and a stratospheric ozone loss. Although this study is motivated from the large enhancement of NO_x due to energetic particle precipitation (EPP), the results presented here could also be applied to other processes causing ozone destruction. We reduced the ozone for either
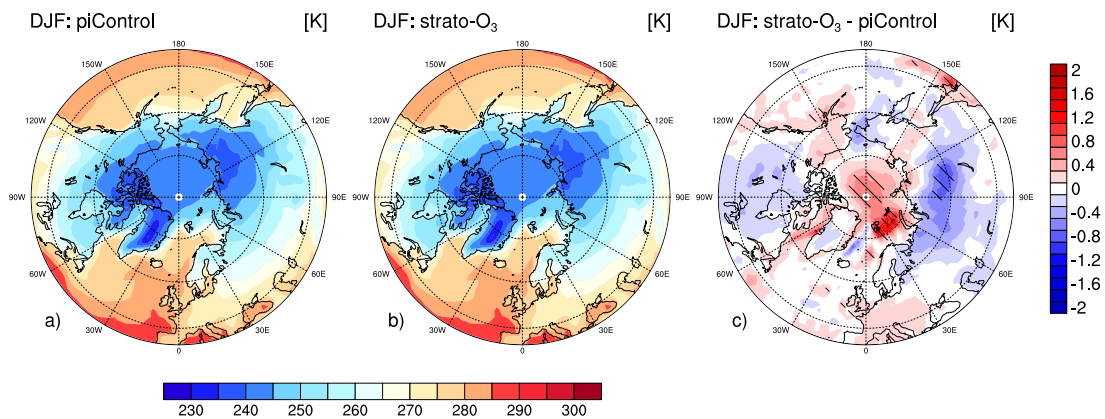
Figure 4.6. Surface temperature [K] averaged over December - February (DJF) for the simulations (a,d) piControl, (b,e) strato-O$_3$ and (c,f) their difference. Shaded areas are statistically significant at the 95 % confidence interval.

-40 % in the polar mesosphere or for -20 % in the polar stratosphere in the Max Planck Institute Earth System Model (MPI-ESM). Furthermore, the radiative forcing of ozone is calculated by the radiative transfer model PSrad.

Recently, Andersson et al. (2014) showed that the direct EPP-HO$_x$ effect induces large long-term variability in the mesospheric ozone. They suggested that these large changes may impact on the climate. Following their idea, we analyzed the atmospheric response to a mesospheric ozone loss. We found that the atmospheric changes due to a mesospheric ozone loss are negligible. This results from a very small radiative forcing of mesospheric ozone.

Several studies analyzed the climate effect of a stratospheric ozone loss due to EPP. However, those studies simulate only a few years and applied complex forcings (e.g., depletion of ozone at different times and altitudes and the involvement of transport processes), which complicates the understanding to the climate response induced by EPP. All of them reported a dynamical cooling of the winter polar stratosphere (Arsenovic et al. 2016; Baumgaertner et al. 2011; Rozanov et al. 2005). Baumgaertner et al. (2011) stated that this stratospheric cooling is caused by a decrease in the mean meridional circulation. However, it has not been shown that this dynamical feedback applies for a latitudinal confined ozone loss. Our calculations with the radiative transfer model showed that a winter polar stratospheric ozone loss should result in a warming, which our experiments reproduced, however, not significantly. Consequently, the impact on the simulated winter surface temperature is weak. In contrast to the above mentioned studies, in our experiment the dynamical feedback leading to a stratospheric cooling instead of a warming is missing. Hence, we cannot prove the suggested mechanism of the dynamical cooling for a polar ozone loss. We would like to raise the awareness that positive studies tend to be preferred over negative study

outcomes (publication bias).

Our results suggest that the climate impact of an ozone loss due to EPP is small. As the radiative forcing of mesospheric ozone loss is negligible, the climate impact of a mesospheric ozone change as suggested by Andersson et al. (2014) seems unlikely. However, we cannot rule out that not only the final ozone loss but also the downward propagation of NO_x concentrations are important. Nevertheless, EPP is an interesting research field to understand the interplay of chemistry and transport processes in the middle and upper atmosphere, because the EPP forcing is distinct and a good observational coverage exists.

Our analysis showed to treat small data sample sizes with caution. Experiments with few simulation years may present signals of apparently high statistical significance, which cannot withstand longer simulation periods due to the large variability of the polar vortex strength. We would like to point to more robust tests for significance (e.g., using the likelihood of a random occurrence of a signal).

Finally, although previous studies have shown that MPI-ESM reproduces stratospheric temperature responses to forcings reasonably well (e.g., Bittner et al. 2016), an uncertainty remains that the model's sensitivity to ozone loss is low. To address this, we would like to encourage multi-model studies on EPP climate impact as currently suggested for the third phase of the SPARC's SOLARIS-HEPPA project.

Short summary of Chapter 4:

- A mesospheric ozone loss leads to negligible atmospheric changes resulting from a small radiative forcing of mesospheric ozone.

- A stratospheric ozone loss leads to a weak stratospheric warming. No dynamical cooling is found.

- Impacts on the surface climate are weak.

Summary, Conclusions and Outlook 5

This thesis aims to enhance the understanding of the climate effects of energetic particle precipitation (EPP). Previous work suggested that energetic particles influence the winter surface temperature (e.g., Andersson et al. 2014; Seppälä et al. 2009). However, models may underestimate this effect, because EPP-induced NO_x accumulations are underestimated (B. Funke, HEPPA-II model-measurement intercomparison project: EPP indirect effects during the dynamically perturbed NH winter 2008–2009, submitted to Atmospheric Chemistry and Physics). First, I investigated the transport of NO_x from the upper to the middle atmosphere clarifying which processes are responsible for modeling realistic mesospheric NO_x concentrations. Second, the climate effects of a mesospheric and a stratospheric ozone loss are evaluated. This chapter summarizes the main findings of this thesis by answering the research questions stated in Section 1.2. An outlook presents open questions left by the work presented here.

5.1 Summary and Conclusions

Which transport mechanisms are responsible for the downward transport of nitrogen oxides induced by energetic particle precipitation from the polar thermosphere to the polar mesosphere?

Using simulations of the general circulation and chemistry model HAMMONIA, I quantified, for the first time, the contribution of the processes advection, molecular diffusion and eddy diffusion on the transport through the winter mesopause. Advection and molecular diffusion dominate transport through the mesopause. Whereas the impact of molecular diffusion rapidly decreases below the mesopause, the impact of advection increases. Eddy diffusion has a negligible impact on the transport, but could contribute substantially if eddy diffusion is enhanced as suggested by observations. Further research on the magnitude of eddy diffusion is needed. During disturbed dynamical conditions such as sudden stratospheric warmings, the transport through the mesopause is purely driven by advection.

I showed that the intra-daily variability of advection is large in the thermosphere and contributes significantly to the transport through the mesopause. In other words, a streamfunction calculated from daily means is insufficient to explain the transport in the lower thermosphere and upper mesosphere.

How sensitive is the transport of nitrogen oxides to changes of the non-orographic gravity wave sources? How can the underestimation of the NO_x concentrations in the polar mesosphere be reduced?

I investigated the impact of parameterized gravity wave sources on the transport of nitrogen oxides (NO_x). Using the general circulation and chemistry model HAMMO-NIA, I discussed differences in a homogeneous background and in a source related to tropospheric frontal activity. I found that the transport of NO_x is highly sensitive to changes in non-orographic gravity waves. Weakening the gravity wave sources (i.e., reducing the wave amplitude at launching level) enhances the downward transport. The transport is controlled by the altitude of the largest gravity wave drag and, hence, by the vertical extent of the downwelling. This strengthening of the vertical wind in the lower thermosphere and upper mesosphere is further amplified by resolved waves. Accordingly, weakening the gravity wave sources shifts the maximum in the gravity wave drag upward resulting in an enhanced transport. This results from a small wave amplitude at launching level, which favors the transition to turbulence at a high altitude.

The underestimation of the NO_x transport in earlier studies may be reduced by weakening the gravity wave sources. This might seem counterintuitive, because gravity waves mainly drive the winter mesospheric downwelling. One might assume that increased wave activity would strengthen the downwelling. However, I showed that not only the magnitude matters but also the distribution of momentum deposition with height.

What is the climate impact of a mesospheric and a stratospheric ozone loss induced by energetic particle precipitation?

The climate impacts of a mesospheric and a stratospheric ozone loss due to energetic particles are analyzed. Idealized ozone losses are applied to the Earth system model MPI-ESM. I focused on the atmospheric responses, because they are a precondition for a potential influence on the surface climate. Atmospheric changes due to a winter polar mesospheric ozone loss are negligible. This results from a very small radiative forcing of mesospheric ozone. Hence, a climate impact of a mesospheric ozone loss as suggested by Andersson et al. (2014) seems unlikely. Calculations with a radiative transfer model showed that a winter polar stratospheric ozone loss should result in a weak stratospheric warming. The MPI-ESM reproduces this warming; however, it is not statistically significant. Consequently, a winter polar stratospheric ozone loss weakly impacts on the polar surface temperature.

5.2 Research Perspectives and Outlook

This thesis advances the understanding of energetic particle precipitation in terms of relevant transport processes and climate effects. The results of this thesis are also of importance for SPARC's SOLARIS-HEPPA project, which investigates the effects of solar influence on climate.

I showed that an adequate estimate of the effects of EPP requires a realistic transport of NO_x in addition to a realistic representation of energetic particle sources. The underestimated NO_x concentrations in the mesosphere are not caused by a deficiency in the production of NO_x but by a too weak transport. I found that molecular diffusion and advection dominate the transport from the upper to the middle atmosphere. Hence, the underestimation arises from an underestimated advective transport. In particular, a proper representation of (non-orographic) gravity waves in models is needed. Based on my results, it seems unlikely that an underestimated eddy diffusion causes the too low mesospheric NO_x concentrations.

Whereas Jackman et al. (2009) showed that solar energetic protons have no long-term climate effects, the influence of magnetospheric energetic electrons (MEE) on the climate remains unclear. Previous work suggested that MEEs can alter the polar surface temperature; however, those studies applied complex forcings and simulated only a few years. To clarify the response of the climate to MEEs, I used a simplified forcing and a long integration period. My results indicate that the climate effect of MEEs is small due to the weak radiative forcing of ozone during polar night. To reduce the uncertainty remaining by this thesis, I propose a multi-model study with an idealized, stratospheric ozone loss during winter and early spring. This setup could also estimate whether an ozone loss close to the terminator can influence the climate. Furthermore, this thesis did not consider the effects arising from the downward transport of NO_x produced by medium energetic electrons. To tackle this issue, I suggest a study with a general circulation and chemistry model covering a long integration time. However, I am aware that those model runs are computationally expensive. To reduce the costs, the recommended solar forcing for the upcoming CMIP6, which includes for the first time energetic particle forcing, could be used (Matthes et al. 2016).

More in general, outcomes of this thesis could be of interest for a broader community. I showed that a proper representation of gravity waves is crucial for the dynamics in the middle and upper atmosphere. This applies not only to the polar winter downwelling, but also to the latitudinal extent of stratospheric zonal winds and for the temperature of the mesopause. However, constraining gravity wave parameterizations from observations remains a challenge (Alexander 2015). I suggest two pathways: (1) using improved attempts to observe gravity waves from satellite as suggested by Geller et al. (2013) and (2) increasing the resolution of general circulation models to ex-

plicitly resolve gravity waves. Advancing the understanding of gravity waves would also clarify the role of eddy diffusion, which highly relates to gravity waves in models. Furthermore, I have shown that intra-daily variability of advection is important in the lower thermosphere. Further work is needed on the role of advection in the thermosphere and its relation to atmospheric tides.

Bibliography

Akmaev, R. A., V. A. Yudin, and D. A. Ortland (1997). "SMLTM simulations of the diurnal tide: comparison with UARS observations". In: *Ann. Geophys.* 15.9, pp. 1187–1197. DOI: 10.1007/s00585-997-1187-7.

Alexander, M. J., M. Geller, C. McLandress, S. Polavarapu, P. Preusse, F. Sassi, K. Sato, S. Eckermann, M. Ern, A. Hertzog, Y. Kawatani, M. Pulido, T. A. Shaw, M. Sigmond, R. Vincent, and S. Watanabe (2010). "Recent developments in gravity-wave effects in climate models and the global distribution of gravity-wave momentum flux from observations and models". In: *Quarterly Journal of the Royal Meteorological Society* 136.650, pp. 1103–1124. DOI: 10.1002/qj.637.

Alexander, M. J. (2015). "Global and seasonal variations in three-dimensional gravity wave momentum flux from satellite limb-sounding temperatures". In: *Geophysical Research Letters* 42.16, 2015GL065234. DOI: 10.1002/2015GL065234.

Andersson, M. E., P. T. Verronen, C. J. Rodger, M. A. Clilverd, and A. Seppälä (2014). "Missing driver in the Sun–Earth connection from energetic electron precipitation impacts mesospheric ozone". In: *Nature Communications* 5. DOI: 10.1038/ncomms6197.

Arsenovic, P., E. Rozanov, A. Stenke, B. Funke, J. M. Wissing, K. Mursula, F. Tummon, and T. Peter (2016). "The influence of Middle Range Energy Electrons on atmospheric chemistry and regional climate". In: *Journal of Atmospheric and Solar-Terrestrial Physics*. DOI: 10.1016/j.jastp.2016.04.008.

Bailey, S. M., B. Thurairajah, C. E. Randall, L. Holt, D. E. Siskind, V. L. Harvey, K. Venkataramani, M. E. Hervig, P. Rong, and J. M. Russell (2014). "A multi tracer analysis of thermosphere to stratosphere descent triggered by the 2013 Stratospheric Sudden Warming". In: *Geophysical Research Letters* 41.14, 2014GL059860. DOI: 10.1002/2014GL059860.

Baker, D. N., R. A. Goldberg, F. A. Herrero, J. B. Blake, and L. B. Callis (1993). "Satellite and rocket studies of relativistic electrons and their influence on the middle atmosphere". In: *Journal of Atmospheric and Terrestrial Physics* 55.13, pp. 1619–1628. DOI: 10.1016/0021-9169(93)90167-W.

Baldwin, M. P. and T. J. Dunkerton (2001). "Stratospheric Harbingers of Anomalous Weather Regimes". In: *Science* 294.5542, pp. 581–584. DOI: 10.1126/science.1063315.

Banks, P. M. and G. Kockarts (1973). *Aeronomy, Part B.* Academic Press.

Baumgaertner, A. J. G., A. Seppälä, P. Jöckel, and M. A. Clilverd (2011). "Geomagnetic activity related NOx enhancements and polar surface air temperature variability in a chemistry climate model: modulation of the NAM index". In: *Atmos. Chem. Phys.* 11.9, pp. 4521–4531. DOI: 10.5194/acp-11-4521-2011.

Bender, S., M. Sinnhuber, T. von Clarmann, G. Stiller, B. Funke, M. López-Puertas, J. Urban, K. Pérot, K. A. Walker, and J. P. Burrows (2015). "Comparison of nitric oxide measurements in the mesosphere and lower thermosphere from ACE-FTS, MIPAS, SCIAMACHY, and SMR". In: *Atmos. Meas. Tech.* 8.10, pp. 4171–4195. DOI: 10.5194/amt-8-4171-2015.

Bittner, M., C. Timmreck, H. Schmidt, M. Toohey, and K. Krüger (2016). "The impact of wave-mean flow interaction on the Northern Hemisphere polar vortex after tropical volcanic eruptions". In: *Journal of Geophysical Research: Atmospheres* 121.10, 2015JD024603. DOI: 10.1002/2015JD024603.

Brasseur, G. P. and S. Solomon (2005). *Aeronomy of the Middle Atmosphere: Chemistry and Physics of the Stratosphere and Mesosphere.* Springer Science & Business Media.

Callis, L. B., M. Natarajan, and J. D. Lambeth (2001). "Solar-atmospheric coupling by electrons (SOLACE): 3. Comparisons of simulations and observations, 1979–1997, issues and implications". In: *Journal of Geophysical Research: Atmospheres* 106.D7, pp. 7523–7539. DOI: 10.1029/2000JD900615.

Chandran, A., R. L. Collins, R. R. Garcia, D. R. Marsh, V. L. Harvey, J. Yue, and L. de la Torre (2013a). "A climatology of elevated stratopause events in the whole atmosphere community climate model". In: *Journal of Geophysical Research: Atmospheres* 118.3, pp. 1234–1246. DOI: 10.1002/jgrd.50123.

Chandran, A., R. L. Collins, and V. L. Harvey (2014). "Stratosphere-mesosphere coupling during stratospheric sudden warming events". In: *Advances in Space Research* 53.9, pp. 1265–1289. DOI: 10.1016/j.asr.2014.02.005.

Chandran, A., R. R. Garcia, R. L. Collins, and L. C. Chang (2013b). "Secondary planetary waves in the middle and upper atmosphere following the stratospheric sudden warming event of January 2012". In: *Geophysical Research Letters* 40.9, pp. 1861–1867. DOI: 10.1002/grl.50373.

Charron, M. and E. Manzini (2002). "Gravity Waves from Fronts: Parameterization and Middle Atmosphere Response in a General Circulation Model". In: *Journal of the Atmospheric Sciences* 59.5, pp. 923–941. DOI: 10.1175/1520-0469(2002)059<0923:GWFFPA>2.0.CO;2.

Collins, R. L., G. A. Lehmacher, M. F. Larsen, and K. Mizutani (2011). "Estimates of vertical eddy diffusivity in the upper mesosphere in the presence of a mesospheric inversion layer". In: *Ann. Geophys.* 29.11, pp. 2019–2029. DOI: 10.5194/angeo-29-2019-2011.

Crutzen, P. J., I. S. A. Isaksen, and G. C. Reid (1975). "Solar Proton Events: Stratospheric Sources of Nitric Oxide". In: *Science* 189.4201, pp. 457–459. DOI: 10.1126/science.189.4201.457.

Dee, D. P., S. M. Uppala, A. J. Simmons, P. Berrisford, P. Poli, S. Kobayashi, U. Andrae, M. A. Balmaseda, G. Balsamo, P. Bauer, P. Bechtold, A. C. M. Beljaars, L. van de Berg, J. Bidlot, N. Bormann, C. Delsol, R. Dragani, M. Fuentes, A. J. Geer, L. Haimberger, S. B. Healy, H. Hersbach, E. V. Hólm, L. Isaksen, P. Kållberg, M. Köhler, M. Matricardi, A. P. McNally, B. M. Monge-Sanz, J.-J. Morcrette, B.-K. Park, C. Peubey, P. de Rosnay, C. Tavolato, J.-N. Thépaut, and F. Vitart (2011). "The ERA-Interim reanalysis: configuration and performance of the data assimilation system". In: *Quarterly Journal of the Royal Meteorological Society* 137.656, pp. 553–597. DOI: 10.1002/qj.828.

Dikty, S., H. Schmidt, M. Weber, C. von Savigny, and M. G. Mlynczak (2010). "Daytime ozone and temperature variations in the mesosphere: a comparison between SABER observations and HAMMONIA model". In: *Atmos. Chem. Phys.* 10.17, pp. 8331–8339. DOI: 10.5194/acp-10-8331-2010.

Emmert, J. T., M. H. Stevens, P. F. Bernath, D. P. Drob, and C. D. Boone (2012). "Observations of increasing carbon dioxide concentration in Earth's thermosphere". In: *Nature Geoscience* 5.12, pp. 868–871. DOI: 10.1038/ngeo1626.

Fischer, H., M. Birk, C. Blom, B. Carli, M. Carlotti, T. von Clarmann, L. Delbouille, A. Dudhia, D. Ehhalt, M. Endemann, J. M. Flaud, R. Gessner, A. Kleinert, R. Koopman, J. Langen, M. López-Puertas, P. Mosner, H. Nett, H. Oelhaf, G. Perron, J. Remedios, M. Ridolfi, G. Stiller, and R. Zander (2008). "MIPAS: an instrument for atmospheric and climate research". In: *Atmos. Chem. Phys.* 8.8, pp. 2151–2188. DOI: 10.5194/acp-8-2151-2008.

Funke, B., A. Baumgaertner, M. Calisto, T. Egorova, C. H. Jackman, J. Kieser, A. Krivo-lutsky, M. López-Puertas, D. R. Marsh, T. Reddmann, E. Rozanov, S.-M. Salmi, M. Sinnhuber, G. P. Stiller, P. T. Verronen, S. Versick, T. von Clarmann, T. Y. Vyushkova, N. Wieters, and J. M. Wissing (2011). "Composition changes after the "Halloween" solar proton event: the High Energy Particle Precipitation in the Atmosphere (HEPPA) model versus MIPAS data intercomparison study". In: *Atmos. Chem. Phys.* 11.17, pp. 9089–9139. DOI: 10.5194/acp-11-9089-2011.

Funke, B., M. López-Puertas, H. Fischer, G. P. Stiller, T. von Clarmann, G. Wetzel, B. Carli, and C. Belotti (2007). "Comment on "Origin of the January–April 2004 increase in stratospheric NO2 observed in northern polar latitudes" by Jean-Baptiste Renard et al." In: *Geophysical Research Letters* 34.7, p. L07813. DOI: 10.1029/2006GL027518.

Funke, B., M. López-Puertas, S. Gil-López, T. von Clarmann, G. P. Stiller, H. Fischer, and S. Kellmann (2005). "Downward transport of upper atmospheric NOx into the polar stratosphere and lower mesosphere during the Antarctic 2003 and Arctic 2002/2003 winters". In: *Journal of Geophysical Research: Atmospheres* 110.D24. DOI: 10.1029/2005JD006463.

Garcia, R. R., M. López-Puertas, B. Funke, D. R. Marsh, D. E. Kinnison, A. K. Smith, and F. González-Galindo (2014). "On the distribution of CO2 and CO in the mesosphere and lower thermosphere". In: *Journal of Geophysical Research: Atmospheres* 119.9, 2013JD021208. DOI: 10.1002/2013JD021208.

García-Comas, M., B. Funke, A. Gardini, M. López-Puertas, A. Jurado-Navarro, T. von Clarmann, G. Stiller, M. Kiefer, C. D. Boone, T. Leblanc, B. T. Marshall, M. J. Schwartz, and P. E. Sheese (2014). "MIPAS temperature from the stratosphere to the lower thermosphere: Comparison of vM21 with ACE-FTS, MLS, OSIRIS, SABER, SOFIE and lidar measurements". In: *Atmos. Meas. Tech.* 7.11, pp. 3633–3651. DOI: 10.5194/amt-7-3633-2014.

Geller, M. A., M. J. Alexander, P. T. Love, J. Bacmeister, M. Ern, A. Hertzog, E. Manzini, P. Preusse, K. Sato, A. A. Scaife, and T. Zhou (2013). "A Comparison between Gravity Wave Momentum Fluxes in Observations and Climate Models". In: *Journal of Climate* 26.17, pp. 6383–6405. DOI: 10.1175/JCLI-D-12-00545.1.

Giorgetta, M. A., J. Jungclaus, C. H. Reick, S. Legutke, J. Bader, M. Böttinger, V. Brovkin, T. Crueger, M. Esch, K. Fieg, K. Glushak, V. Gayler, H. Haak, H.-D. Hollweg, T. Ilyina, S. Kinne, L. Kornblueh, D. Matei, T. Mauritsen, U. Mikolajewicz, W. Mueller, D. Notz, F. Pithan, T. Raddatz, S. Rast, R. Redler, E. Roeckner, H. Schmidt, R. Schnur, J. Segschneider, K. D. Six, M. Stockhause, C. Timmreck, J. Wegner, H. Widmann, K.-H. Wieners, M. Claussen, J. Marotzke, and B. Stevens (2013). "Climate and carbon cycle changes from 1850 to 2100 in MPI-ESM simulations for the Coupled Model Intercomparison Project phase 5". In: *Journal of Advances in Modeling Earth Systems* 5.3, pp. 572–597. DOI: 10.1002/jame.20038.

Graf, H.-F., I. Kirchner, and J. Perlwitz (1998). "Changing lower stratospheric circulation: The role of ozone and greenhouse gases". In: *Journal of Geophysical Research: Atmospheres* 103.D10, pp. 11251–11261. DOI: 10.1029/98JD00341.

Gray, L. J., J. Beer, M. Geller, J. D. Haigh, M. Lockwood, K. Matthes, U. Cubasch, D. Fleitmann, G. Harrison, L. Hood, J. Luterbacher, G. A. Meehl, D. Shindell, B. van Geel, and W. White (2010). "Solar Influences on Climate". In: *Reviews of Geophysics* 48.4. DOI: 10.1029/2009RG000282.

Grygalashvyly, M., E. Becker, and G. R. Sonnemann (2011). "Gravity Wave Mixing and Effective Diffusivity for Minor Chemical Constituents in the Mesosphere/Lower Thermosphere". In: *Space Science Reviews* 168.1-4, pp. 333–362. DOI: 10.1007/s11214-011-9857-x.

Haigh, J. D. (1994). "The role of stratospheric ozone in modulating the solar radiative forcing of climate". In: *Nature* 370.6490, pp. 544–546. DOI: 10.1038/370544a0.

Haynes, P. H., M. E. McIntyre, T. G. Shepherd, C. J. Marks, and K. P. Shine (1991). "On the "Downward Control" of Extratropical Diabatic Circulations by Eddy-Induced Mean Zonal Forces". In: *Journal of the Atmospheric Sciences* 48.4, pp. 651–678. DOI: 10.1175/1520-0469(1991)048<0651:OTCOED>2.0.CO;2.

Herschel, W. (1801). "Observations Tending to Investigate the Nature of the Sun, in Order to Find the Causes or Symptoms of Its Variable Emission of Light and Heat; With Remarks on the Use That May Possibly Be Drawn from Solar Observations".

In: *Philosophical Transactions of the Royal Society of London* 91, pp. 265–318. DOI: 10 . 1098/rstl.1801.0015.

Hines, C. O. (1997a). "Doppler-spread parameterization of gravity-wave momentum deposition in the middle atmosphere. Part 1: Basic formulation". In: *Journal of Atmospheric and Solar-Terrestrial Physics* 59.4, pp. 371–386. DOI: 10.1016/S1364-6826(96) 00079-X.

– (1997b). "Doppler-spread parameterization of gravity-wave momentum deposition in the middle atmosphere. Part 2: Broad and quasi monochromatic spectra, and implementation". In: *Journal of Atmospheric and Solar-Terrestrial Physics* 59.4, pp. 387–400. DOI: 10.1016/S1364-6826(96)00080-6.

Hoffmann, P., M. Rapp, W. Singer, and D. Keuer (2011). "Trends of mesospheric gravity waves at northern middle latitudes during summer". In: *Journal of Geophysical Research: Atmospheres* 116.D4, D00P08. DOI: 10.1029/2011JD015717.

Holt, L. A., C. E. Randall, E. D. Peck, D. R. Marsh, A. K. Smith, and V. L. Harvey (2013). "The influence of major sudden stratospheric warming and elevated stratopause events on the effects of energetic particle precipitation in WACCM". In: *Journal of Geophysical Research: Atmospheres* 118.20, pp. 11, 636–11, 646. DOI: 10 . 1002 / 2013JD020294.

Holton, J. R., P. H. Haynes, M. E. McIntyre, A. R. Douglass, R. B. Rood, and L. Pfister (1995). "Stratosphere-troposphere exchange". In: *Reviews of Geophysics* 33.4, pp. 403–439. DOI: 10.1029/95RG02097.

Huang, T., S. Walters, G. Brasseur, D. Hauglustaine, W. Wu, S. Chabrillat, T. Xuexi, C. Granier, A. Smith, and G. Kockarts (1998). *Description of SOCRATES-a Chemical Dynamical Radiative Two-dimensional Model*. NCAR Technical Note NCAR/TN-440+EDD. Boulder, CO: NCAR, p. 94.

Iacono, M. J., J. S. Delamere, E. J. Mlawer, M. W. Shephard, S. A. Clough, and W. D. Collins (2008). "Radiative forcing by long-lived greenhouse gases: Calculations with the AER radiative transfer models". In: *Journal of Geophysical Research: Atmospheres* 113.D13, p. D13103. DOI: 10.1029/2008JD009944.

Ilyina, T., K. D. Six, J. Segschneider, E. Maier-Reimer, H. Li, and I. Núñez-Riboni (2013). "Global ocean biogeochemistry model HAMOCC: Model architecture and performance as component of the MPI-Earth system model in different CMIP5 experimen-

tal realizations". In: *Journal of Advances in Modeling Earth Systems* 5.2, pp. 287–315. DOI: 10.1029/2012MS000178.

Jackman, C. H., D. R. Marsh, D. E. Kinnison, C. J. Mertens, and E. L. Fleming (2016). "Atmospheric changes caused by galactic cosmic rays over the period 1960–2010". In: *Atmos. Chem. Phys.* 16.9, pp. 5853–5866. DOI: 10.5194/acp-16-5853-2016.

Jackman, C. H., D. R. Marsh, F. M. Vitt, R. R. Garcia, E. L. Fleming, G. J. Labow, C. E. Randall, M. López-Puertas, B. Funke, T. von Clarmann, and G. P. Stiller (2008). "Short- and medium-term atmospheric constituent effects of very large solar proton events". In: *Atmos. Chem. Phys.* 8.3, pp. 765–785. DOI: 10.5194/acp-8-765-2008.

Jackman, C. H., M. T. DeLand, G. J. Labow, E. L. Fleming, D. K. Weisenstein, M. K. W. Ko, M. Sinnhuber, and J. M. Russell (2005). "Neutral atmospheric influences of the solar proton events in October–November 2003". In: *Journal of Geophysical Research: Space Physics* 110.A9, A09S27. DOI: 10.1029/2004JA010888.

Jackman, C. H., D. R. Marsh, F. M. Vitt, R. R. Garcia, C. E. Randall, E. L. Fleming, and S. M. Frith (2009). "Long-term middle atmospheric influence of very large solar proton events". In: *Journal of Geophysical Research: Atmospheres* 114.D11. DOI: 10.1029/2008JD011415.

Jones, M., J. M. Forbes, and M. E. Hagan (2014). "Tidal-induced net transport effects on the oxygen distribution in the thermosphere". In: *Geophysical Research Letters* 41.14, pp. 5272–5279. DOI: 10.1002/2014GL060698.

Jungclaus, J. H., N. Fischer, H. Haak, K. Lohmann, J. Marotzke, D. Matei, U. Mikolajewicz, D. Notz, and J. S. von Storch (2013). "Characteristics of the ocean simulations in the Max Planck Institute Ocean Model (MPIOM) the ocean component of the MPI-Earth system model". In: *Journal of Advances in Modeling Earth Systems* 5.2, pp. 422–446. DOI: 10.1002/jame.20023.

Kieser, J. (2011). *The Influence of Precipitating Solar and Magnetospheric Energetic Charged Particles on the Entire Atmosphere Simulations with Hammonia*. Berichte zur Erdsystemforschung. Hamburg, Germany: Max-Planck-Institut für Meteorologie.

Kinnison, D. E., G. P. Brasseur, S. Walters, R. R. Garcia, D. R. Marsh, F. Sassi, V. L. Harvey, C. E. Randall, L. Emmons, J. F. Lamarque, P. Hess, J. J. Orlando, X. X. Tie, W. Randel, L. L. Pan, A. Gettelman, C. Granier, T. Diehl, U. Niemeier, and A. J. Simmons (2007). "Sensitivity of chemical tracers to meteorological parameters in the

MOZART-3 chemical transport model". In: *Journal of Geophysical Research: Atmospheres* 112.D20. DOI: 10.1029/2006JD007879.

Langematz, U., M. Kunze, K. Krüger, K. Labitzke, and G. L. Roff (2003). "Thermal and dynamical changes of the stratosphere since 1979 and their link to ozone and CO2 changes". In: *Journal of Geophysical Research: Atmospheres* 108.D1, p. 4027. DOI: 10.1029/2002JD002069.

Limpasuvan, V., Y. J. Orsolini, A. Chandran, R. R. Garcia, and A. K. Smith (2016). "On the composite response of the MLT to major sudden stratospheric warming events with elevated stratopause". In: *Journal of Geophysical Research: Atmospheres* 121.9, 2015JD024401. DOI: 10.1002/2015JD024401.

Limpasuvan, V., J. H. Richter, Y. J. Orsolini, F. Stordal, and O.-K. Kvissel (2012). "The roles of planetary and gravity waves during a major stratospheric sudden warming as characterized in WACCM". In: *Journal of Atmospheric and Solar-Terrestrial Physics*. Structure and Dynamics of Mesosphere and Lower Thermosphere 78–79, pp. 84–98. DOI: 10.1016/j.jastp.2011.03.004.

Lin, S.-J. and R. B. Rood (1996). "Multidimensional Flux-Form Semi-Lagrangian Transport Schemes". In: *Monthly Weather Review* 124.9, pp. 2046–2070. DOI: 10.1175/1520-0493(1996)124<2046:MFFSLT>2.0.CO;2.

Liu, A. Z. (2009). "Estimate eddy diffusion coefficients from gravity wave vertical momentum and heat fluxes". In: *Geophysical Research Letters* 36.8, p. L08806. DOI: 10.1029/2009GL037495.

Lott, F. and M. J. Miller (1997). "A new subgrid-scale orographic drag parametrization: Its formulation and testing". In: *Quarterly Journal of the Royal Meteorological Society* 123.537, pp. 101–127. DOI: 10.1002/qj.49712353704.

Lubis, S. W., N.-E. Omrani, K. Matthes, and S. Wahl (2016). "Impact of the Antarctic Ozone Hole on the Vertical Coupling of the Stratosphere–Mesosphere–Lower Thermosphere System". In: *Journal of the Atmospheric Sciences* 73.6, pp. 2509–2528. DOI: 10.1175/JAS-D-15-0189.1.

Lübken, F.-J. and U. von Zahn (1991). "Thermal structure of the mesopause region at polar latitudes". In: *Journal of Geophysical Research: Atmospheres* 96.D11, pp. 20841–20857. DOI: 10.1029/91JD02018.

Manney, G. L., M. J. Schwartz, K. Krüger, M. L. Santee, S. Pawson, J. N. Lee, W. H. Daffer, R. A. Fuller, and N. J. Livesey (2009). "Aura Microwave Limb Sounder observations of dynamics and transport during the record-breaking 2009 Arctic stratospheric major warming". In: *Geophysical Research Letters* 36.12. DOI: 10.1029/2009GL038586.

Manzini, E. and N. A. McFarlane (1998). "The effect of varying the source spectrum of a gravity wave parameterization in a middle atmosphere general circulation model". In: *Journal of Geophysical Research: Atmospheres* 103.D24, pp. 31523–31539. DOI: 10.1029/98JD02274.

Matthes, K., B. Funke, M. E. Anderson, L. Barnard, J. Beer, P. Charbonneau, M. A. Clilverd, T. Dudok de Wit, M. Haberreiter, A. Hendry, C. H. Jackman, M. Kretschmar, T. Kruschke, M. Kunze, U. Langematz, D. R. Marsh, A. Maycock, S. Misios, C. J. Rodger, A. A. Scaife, A. Seppälä, M. Shangguan, M. Sinnhuber, K. Tourpali, I. Usoskin, M. van de Kamp, P. T. Verronen, and S. Versick (2016). "Solar Forcing for CMIP6 (v3.1)". In: *Geoscientific Model Development Discussions*, pp. 1–82. DOI: 10.5194/gmd-2016-91.

McLandress, C., J. F. Scinocca, T. G. Shepherd, M. C. Reader, and G. L. Manney (2013). "Dynamical Control of the Mesosphere by Orographic and Nonorographic Gravity Wave Drag during the Extended Northern Winters of 2006 and 2009". In: *Journal of the Atmospheric Sciences* 70.7, pp. 2152–2169. DOI: 10.1175/JAS-D-12-0297.1.

Meraner, K. and H. Schmidt (2016). "Transport of nitrogen oxides through the winter mesopause in HAMMONIA". In: *Journal of Geophysical Research: Atmospheres* 121.6, 2015JD024136. DOI: 10.1002/2015JD024136.

Mlawer, E. J., S. J. Taubman, P. D. Brown, M. J. Iacono, and S. A. Clough (1997). "Radiative transfer for inhomogeneous atmospheres: RRTM, a validated correlated-k model for the longwave". In: *Journal of Geophysical Research: Atmospheres* 102.D14, pp. 16663–16682. DOI: 10.1029/97JD00237.

Ney, E. P. (1959). "Cosmic Radiation and the Weather". In: *Nature* 183.4659, pp. 451–452. DOI: 10.1038/183451a0.

Peck, E. D., C. E. Randall, J. C. Green, J. V. Rodriguez, and C. J. Rodger (2015). "POES MEPED differential flux retrievals and electron channel contamination correction". In: *Journal of Geophysical Research: Space Physics* 120.6, 2014JA020817. DOI: 10.1002/2014JA020817.

Pedatella, N. M., T. Fuller-Rowell, H. Wang, H. Jin, Y. Miyoshi, H. Fujiwara, H. Shinagawa, H.-L. Liu, F. Sassi, H. Schmidt, V. Matthias, and L. Goncharenko (2014). "The neutral dynamics during the 2009 sudden stratosphere warming simulated by different whole atmosphere models". In: *Journal of Geophysical Research: Space Physics* 119.2, pp. 1306–1324. DOI: 10.1002/2013JA019421.

Pincus, R. and B. Stevens (2013). "Paths to accuracy for radiation parameterizations in atmospheric models". In: *Journal of Advances in Modeling Earth Systems* 5.2, pp. 225–233. DOI: 10.1002/jame.20027.

Porter, H. S., C. H. Jackman, and A. E. S. Green (1976). "Efficiencies for production of atomic nitrogen and oxygen by relativistic proton impact in air". In: *The Journal of Chemical Physics* 65.1, pp. 154–167. DOI: 10.1063/1.432812.

Randall, C. E., V. L. Harvey, C. S. Singleton, S. M. Bailey, P. F. Bernath, M. Codrescu, H. Nakajima, and J. M. Russell (2007). "Energetic particle precipitation effects on the Southern Hemisphere stratosphere in 1992–2005". In: *Journal of Geophysical Research: Atmospheres* 112.D8, p. D08308. DOI: 10.1029/2006JD007696.

Randall, C. E., V. L. Harvey, C. S. Singleton, P. F. Bernath, C. D. Boone, and J. U. Kozyra (2006). "Enhanced NOx in 2006 linked to strong upper stratospheric Arctic vortex". In: *Geophysical Research Letters* 33.18, p. L18811. DOI: 10.1029/2006GL027160.

Randall, C. E., V. L. Harvey, D. E. Siskind, J. France, P. F. Bernath, C. D. Boone, and K. A. Walker (2009). "NOx descent in the Arctic middle atmosphere in early 2009". In: *Geophysical Research Letters* 36.18. DOI: 10.1029/2009GL039706.

Randel, W. J. and F. Wu (1999). "Cooling of the Arctic and Antarctic Polar Stratospheres due to Ozone Depletion". In: *Journal of Climate* 12.5, pp. 1467–1479. DOI: 10.1175/1520-0442(1999)012<1467:COTAAA>2.0.CO;2.

Rawal, A., S. N. Tripathi, M. Michael, A. K. Srivastava, and R. G. Harrison (2013). "Quantifying the importance of galactic cosmic rays in cloud microphysical processes". In: *Journal of Atmospheric and Solar-Terrestrial Physics* 102, pp. 243–251. DOI: 10.1016/j.jastp.2013.05.017.

Reick, C. H., T. Raddatz, V. Brovkin, and V. Gayler (2013). "Representation of natural and anthropogenic land cover change in MPI-ESM". In: *Journal of Advances in Modeling Earth Systems* 5.3, pp. 459–482. DOI: 10.1002/jame.20022.

Ren, S., S. Polavarapu, S. R. Beagley, Y. Nezlin, and Y. J. Rochon (2011). "The impact of gravity wave drag on mesospheric analyses of the 2006 stratospheric major warming". In: *Journal of Geophysical Research: Atmospheres* 116.D19, p. D19116. DOI: 10.1029/2011JD015943.

Richter, J. H., F. Sassi, and R. R. Garcia (2010). "Toward a Physically Based Gravity Wave Source Parameterization in a General Circulation Model". In: *Journal of the Atmospheric Sciences* 67.1, pp. 136–156. DOI: 10.1175/2009JAS3112.1.

Rienecker, M. M., M. J. Suarez, R. Gelaro, R. Todling, J. Bacmeister, E. Liu, M. G. Bosilovich, S. D. Schubert, L. Takacs, G.-K. Kim, S. Bloom, J. Chen, D. Collins, A. Conaty, A. da Silva, W. Gu, J. Joiner, R. D. Koster, R. Lucchesi, A. Molod, T. Owens, S. Pawson, P. Pegion, C. R. Redder, R. Reichle, F. R. Robertson, A. G. Ruddick, M. Sienkiewicz, and J. Woollen (2011). "MERRA: NASA's Modern-Era Retrospective Analysis for Research and Applications". In: *Journal of Climate* 24.14, pp. 3624–3648. DOI: 10.1175/JCLI-D-11-00015.1.

Rodger, C. J., M. A. Clilverd, J. C. Green, and M. M. Lam (2010). "Use of POES SEM-2 observations to examine radiation belt dynamics and energetic electron precipitation into the atmosphere". In: *Journal of Geophysical Research: Space Physics* 115.A4, A04202. DOI: 10.1029/2008JA014023.

Rodger, C. J., M. A. Clilverd, N. R. Thomson, R. J. Gamble, A. Seppälä, E. Turunen, N. P. Meredith, M. Parrot, J.-A. Sauvaud, and J.-J. Berthelier (2007). "Radiation belt electron precipitation into the atmosphere: Recovery from a geomagnetic storm". In: *Journal of Geophysical Research: Space Physics* 112.A11, A11307. DOI: 10.1029/2007JA012383.

Roeckner, E., R. Brokopf, M. Esch, M. Giorgetta, S. Hagemann, L. Kornblueh, E. Manzini, U. Schlese, and U. Schulzweida (2006). "Sensitivity of Simulated Climate to Horizontal and Vertical Resolution in the ECHAM5 Atmosphere Model". In: *Journal of Climate* 19.16, pp. 3771–3791. DOI: 10.1175/JCLI3824.1.

Rozanov, E., L. Callis, M. Schlesinger, F. Yang, N. Andronova, and V. Zubov (2005). "Atmospheric response to NOy source due to energetic electron precipitation". In: *Geophysical Research Letters* 32.14. DOI: 10.1029/2005GL023041.

Rusch, D., J.-C. Gérard, S. Solomon, P. Crutzen, and G. Reid (1981). "The effect of particle precipitation events on the neutral and ion chemistry of the middle atmosphere—I. Odd nitrogen". In: *Planetary and Space Science* 29.7, pp. 767–774. DOI: 10.1016/0032-0633(81)90048-9.

Salmi, S.-M., P. T. Verronen, L. Thölix, E. Kyrölä, L. Backman, A. Y. Karpechko, and A. Seppälä (2011). "Mesosphere-to-stratosphere descent of odd nitrogen in February–March 2009 after sudden stratospheric warming". In: *Atmospheric Chemistry and Physics* 11.10, pp. 4645–4655. DOI: 10.5194/acp-11-4645-2011.

Sander, S. P., R. R. Friedl, D. M. Golden, R. E. Huie, C. E. Kolb, M. J. Kurylo, G. K. Moortgat, V. L. Orkin, P. H. Wine, A. R. Ravishankara, M. J. Molina, B. J. Finlayson-Pitts, and H. Keller-Rudek (2006). *Chemical Kinetics and Photochemical Data for Use in Atmospheric Studies, Evaluation No. 15*. Pasadena.

Scaife, A. A., N. Butchart, C. D. Warner, D. Stainforth, W. Norton, and J. Austin (2000). "Realistic quasi-biennial oscillations in a simulation of the global climate". In: *Geophysical Research Letters* 27.21, pp. 3481–3484. DOI: 10.1029/2000GL011625.

Schmidt, H., G. P. Brasseur, M. Charron, E. Manzini, M. A. Giorgetta, T. Diehl, V. I. Fomichev, D. Kinnison, D. Marsh, and S. Walters (2006). "The HAMMONIA Chemistry Climate Model: Sensitivity of the Mesopause Region to the 11-Year Solar Cycle and CO_2 Doubling". In: *Journal of Climate* 19.16, pp. 3903–3931. DOI: 10.1175/JCLI3829.1.

Schmidt, H., G. P. Brasseur, and M. A. Giorgetta (2010). "Solar cycle signal in a general circulation and chemistry model with internally generated quasi-biennial oscillation". In: *Journal of Geophysical Research: Atmospheres* 115.D1, p. D00I14. DOI: 10.1029/2009JD012542.

Schmidt, H., S. Rast, F. Bunzel, M. Esch, M. Giorgetta, S. Kinne, T. Krismer, G. Stenchikov, C. Timmreck, L. Tomassini, and M. Walz (2013). "Response of the middle atmosphere to anthropogenic and natural forcings in the CMIP5 simulations with the Max Planck Institute Earth system model". In: *Journal of Advances in Modeling Earth Systems* 5.1, pp. 98–116. DOI: 10.1002/jame.20014.

Semeniuk, K., V. I. Fomichev, J. C. McConnell, C. Fu, S. M. L. Melo, and I. G. Usoskin (2011). "Middle atmosphere response to the solar cycle in irradiance and ionizing particle precipitation". In: *Atmos. Chem. Phys.* 11.10, pp. 5045–5077. DOI: 10.5194/acp-11-5045-2011.

Semeniuk, K., J. C. McConnell, and C. H. Jackman (2005). "Simulation of the October–November 2003 solar proton events in the CMAM GCM: Comparison with observations". In: *Geophysical Research Letters* 32.15. DOI: 10.1029/2005GL022392.

Seppälä, A., C. E. Randall, M. A. Clilverd, E. Rozanov, and C. J. Rodger (2009). "Geomagnetic activity and polar surface air temperature variability". In: *Journal of Geophysical Research: Space Physics* 114.A10. DOI: 10.1029/2008JA014029.

Seppälä, A. and M. A. Clilverd (2014). "Energetic particle forcing of the Northern Hemisphere winter stratosphere: comparison to solar irradiance forcing". In: *Atmospheric Science* 2, p. 25. DOI: 10.3389/fphy.2014.00025.

Shine, K. P. (1986). "On the modelled thermal response of the Antarctic stratosphere to a depletion of ozone". In: *Geophysical Research Letters* 13.12, pp. 1331–1334. DOI: 10.1029/GL013i012p01331.

Sigmond, M. and T. G. Shepherd (2014). "Compensation between Resolved Wave Driving and Parameterized Orographic Gravity Wave Driving of the Brewer–Dobson Circulation and Its Response to Climate Change". In: *Journal of Climate* 27.14, pp. 5601–5610. DOI: 10.1175/JCLI-D-13-00644.1.

Sinnhuber, M., B. Funke, T. von Clarmann, M. Lopez-Puertas, G. P. Stiller, and A. Seppälä (2014). "Variability of NOx in the polar middle atmosphere from October 2003 to March 2004: vertical transport vs. local production by energetic particles". In: *Atmos. Chem. Phys.* 14.14, pp. 7681–7692. DOI: 10.5194/acp-14-7681-2014.

Sinnhuber, M., S. Kazeminejad, and J. M. Wissing (2011). "Interannual variation of NOx from the lower thermosphere to the upper stratosphere in the years 1991–2005". In: *Journal of Geophysical Research: Space Physics* 116.A2, A02312. DOI: 10.1029/2010JA015825.

Sinnhuber, M., H. Nieder, and N. Wieters (2012). "Energetic Particle Precipitation and the Chemistry of the Mesosphere/Lower Thermosphere". In: *Surveys in Geophysics* 33.6, pp. 1281–1334. DOI: 10.1007/s10712-012-9201-3.

Siskind, D. E., L. Coy, and P. Espy (2005). "Observations of stratospheric warmings and mesospheric coolings by the TIMED SABER instrument". In: *Geophysical Research Letters* 32.9, p. L09804. DOI: 10.1029/2005GL022399.

Siskind, D. E., F. Sassi, C. E. Randall, V. L. Harvey, M. E. Hervig, and S. M. Bailey (2015). "Is a high-altitude meteorological analysis necessary to simulate thermosphere-stratosphere coupling?" In: *Geophysical Research Letters* 42.19. DOI: 10.1002/2015GL065838.

Siskind, D. E., S. D. Eckermann, L. Coy, J. P. McCormack, and C. E. Randall (2007). "On recent interannual variability of the Arctic winter mesosphere: Implications for tracer descent". In: *Geophysical Research Letters* 34.9. DOI: 10.1029/2007GL029293.

Siskind, D. E., S. D. Eckermann, J. P. McCormack, L. Coy, K. W. Hoppel, and N. L. Baker (2010). "Case studies of the mesospheric response to recent minor, major, and extended stratospheric warmings". In: *Journal of Geophysical Research: Atmospheres* 115.D3, D00N03. DOI: 10.1029/2010JD014114.

Smith, A. K. (2012). "Global Dynamics of the MLT". In: *Surveys in Geophysics* 33.6, pp. 1177–1230. DOI: 10.1007/s10712-012-9196-9.

Smith, A. K., R. R. Garcia, D. R. Marsh, and J. H. Richter (2011). "WACCM simulations of the mean circulation and trace species transport in the winter mesosphere". In: *Journal of Geophysical Research: Atmospheres* 116.D20, p. D20115. DOI: 10.1029/2011JD016083.

Solomon, S., D. W. Rusch, J. C. Gérard, G. C. Reid, and P. J. Crutzen (1981). "The effect of particle precipitation events on the neutral and ion chemistry of the middle atmosphere: II. Odd hydrogen". In: *Planetary and Space Science* 29.8, pp. 885–893. DOI: 10.1016/0032-0633(81)90078-7.

Solomon, S., P. J. Crutzen, and R. G. Roble (1982). "Photochemical coupling between the thermosphere and the lower atmosphere: 1. Odd nitrogen from 50 to 120 km". In: *Journal of Geophysical Research* 87.C9, p. 7206. DOI: 10.1029/JC087iC09p07206.

Stevens, B., M. Giorgetta, M. Esch, T. Mauritsen, T. Crueger, S. Rast, M. Salzmann, H. Schmidt, J. Bader, K. Block, R. Brokopf, I. Fast, S. Kinne, L. Kornblueh, U. Lohmann, R. Pincus, T. Reichler, and E. Roeckner (2013). "Atmospheric component of the MPI-M Earth System Model: ECHAM6". In: *Journal of Advances in Modeling Earth Systems* 5.2, pp. 146–172. DOI: 10.1002/jame.20015.

Taylor, K. E., R. J. Stouffer, and G. A. Meehl (2012). "An Overview of CMIP5 and the Experiment Design". In: *Bulletin of the American Meteorological Society* 93.4, pp. 485–498. DOI: 10.1175/BAMS-D-11-00094.1.

Tomikawa, Y., K. Sato, S. Watanabe, Y. Kawatani, K. Miyazaki, and M. Takahashi (2012). "Growth of planetary waves and the formation of an elevated stratopause after a major stratospheric sudden warming in a T213L256 GCM". In: *Journal of Geophysical Research: Atmospheres* 117.D16, p. D16101. DOI: 10.1029/2011JD017243.

Weeks, L. H., R. S. Cuikay, and J. R. Corbin (1972). "Ozone Measurements in the Mesosphere During The Solar Proton Event of 2 November 1969". In: *Journal of the Atmospheric Sciences* 29.6, pp. 1138–1142.

Wissing, J. M. and M.-B. Kallenrode (2009). "Atmospheric Ionization Module Osnabrück (AIMOS): A 3-D model to determine atmospheric ionization by energetic charged particles from different populations". In: *Journal of Geophysical Research: Space Physics* 114.A6. DOI: 10.1029/2008JA013884.

List of Figures

List of Tables

Acronyms

ACE-FTS	Atmospheric Chemistry Experiment Fourier Transform Spectrometer
AIMOS	Atmospheric Ionization Module Osnabrück
AMIP	Atmospheric Model Intercomparison Project
CMAM	Canadian Middle Atmosphere Model
CMIP	Coupled Model Intercomparison Project
ECMWF	European Centre for Medium-Range Weather Forecasts
ENVISAT	European Environmental Satellite
EP	Eliassen Palm
EPP	Energetic Particle Precipitation
GCM	General Circulation Models
GCR	Galactic Cosmic Ray
HAMMONIA	Hamburg Model of the Neutral and Ionized Atmosphere
MEE	Magnetospheric Energetic Electrons
MERRA	Modern-Era Retrospective Analysis for Research and Applications
MIPAS	Michelson Interferometer for Passive Atmospheric Sounding
MLT	Upper Mesosphere and Lower Thermosphere
MOZART	Model of Ozone and Related Tracers
MPI-ESM	Max Planck Institute Earth System Model
NAM	Northern Annual Mode
POES MEPED	Polar-orbiting Operational Environmental Satellites Medium Energy Proton/Electron Detector
RMS	Root-Mean-Square

SEP	Solar Energetic Protons
SSW	Sudden Stratospheric Warming
TEM	Transformed Eulerian Mean
TSI	Total Solar Irradiance
UV	Ultra Violet
WACCM	Whole Atmosphere Community Climate Model

Acknowledgements

Aus dieser Dissertation hervorgegangene Vorveröffentlichungen
List of Publications

Meraner, K. and H. Schmidt (2016), Transport of nitrogen oxides through the winter mesopause in HAMMONIA, J. Geophys. Res. Atmos., 121, 2556–2570, doi:10.1002/2015JD024136.

Meraner, K., H. Schmidt, E. Manzini, B. Funke, and A. Gardini (2016), Sensitivity of simulated mesospheric transport of nitrogen oxides to parameterized gravity waves, J. Geophys. Res. Atmos., 121, 12,045–12,061, doi:10.1002/2016JD025012.